NAME OF THE AUTHOR(S): OKOH PAUL
SUPERVISOR: **PÅL ØSTEBØ ANDERSEN**

DYNAMIC STORAGE CAPACITY OF CARBON DIOXIDE

Master thesis (2024)

Petroleum Engineering

Faculty of Science and Technology

Department of Energy and Petroleum Engineering

University
of Stavanger

Abstract

In this thesis, a sensitivity analysis of dynamic CO2 storage capacity is made against some reservoir parameters by using the Black Oil model (BOM) in Petrel. In this context, dynamic signifies that CO2 storage capacity varies over time as a function of the interplay between fluid low, pressure evolution and changes in reservoir geological properties. Anticline geological structure was considered as a saline aquifer. Water phase was considered brine and gas phase as CO2. The parameters studied have taken care of both permeabilities, porosity, the ratio of vertical-to-horizontal permeability, injection rates. Further studies were carried out to ascertain the impact of geological shapes on dynamic CO2 storage capacity by constructing six different geological grid structures namely anticline, circular (radial), rectangular structure with no dip angle, 10 degrees dip, 25 degrees dip and 40 degrees dip rectangular structures. An optimum CO2 sequestration scheme in saline aquifers, a key strategy process to offset greenhouse gas emissions is dependent on understanding these impacts.

It was under this premise that we conducted a suite of numerical simulations that subjected the before-mentioned parameters to modifications, to evaluate the impact on CO2 storage capacity. The results also indicate higher porosity increases the storage capacity, this is an intuitive result, because more pore space can provide a larger storage capacity of CO2. Likewise, with higher permeability comes a larger storage capacity but for different reasons. The higher permeability makes the reservoirs easier to be penetrated by CO2 and then occupy more pore spaces. This effect is more evident in the pattern of plume distribution and time for the plume to reach the spill point. The vertical to horizontal permeability ratio, impacts the timing of CO2 plume migration to the spill point rather than the overall storage capacity and plume migration pattern. This highlights the important of considering reservoir, porosity, permeability and fluid properties such as density as they determine CO2 spatial distribution and trapping mechanisms. The results obtained from the evaluation of various injection rates suggested that higher injection rates will result to higher CO2 storage capacity and a quicker time for the plume to extend to the spill point.

On the evaluation of different geologic shapes on the storage capacity, the outcome suggest that dip structures can be more efficient when the spill point is located downdip. Higher dip structures did not experience spill point throughout the injection period because the plume is structurally stored updip, rectangular structure with no dip indicated a good storage potential, followed by the radial geometry. The anticline structure surprisingly indicated the list storage capacity and shortest time to spill point when compared to other structural shapes.

We finally evaluated how porosity and injection rates impact on the reservoir pressure, since we observed that porosity and injection rates have greater impact on the dynamic storage capacity. The outcomes outline that higher porosity can buffer over

pressurisation because of the more space available for storage, while injection rate needs to be moderated considering other reservoir parameter to avoid inducing seismic.

Overall, the work done in this thesis reinforces that correct characterization and selection of parameters is essential for a successful CO2 storage operation at saline aquifers. This requires good quantification of things like reservoir porosity, permeability, vertical to horizontal permeability ratio, and injection rates. These parameters have a large impact on storage capacity, plume migration paths and the efficiency of seal mechanisms. The priority for future research should be developing dynamic models that simulates how porosity and permeability is changing over time due to the chemical reactions between CO2, brine and rock minerals. This will help with forecasting long-term storage capacity and stability.

Acknowledgement

Table of Contents

List of Figures

List of Tables

1. Introduction

Global warming is the long-term increase in Earth's average surface temperature because of greenhouse gases, such as carbon dioxide (CO_2) emissions from burning fossil fuels or other human activities, which trap heat that would otherwise escape following exposure to sunlight on our planet's surface. The main greenhouse gases produced by human activity are carbon dioxide (CO_2), methane (CH_4), nitrous oxide (N_2O), and water vapor. These gases act as a blanket; capturing the sun's heat warming the earth, over time. Absent of the greenhouse impact, Earth would be chilling to a great degree cold. However, over certain limit, these gases will heat the earth too much for its residents. These gases in the atmosphere are on the constant rise as we, human population is growing and indulging in different activities. Evidently clear that at this time of geological history, too much anthropogenic gases were being fixed into ecosystems, posing more danger to life sustainability. Therein is the challenging aspect, a human struggle to find an answer on how to mitigate the amount of these gases been released to the atmosphere. To provide a reducing solution, various ways have been approached. Overall, CO_2 is the single largest source of greenhouse gases. People have come up with many strategies, recommendations, research and tests to take carbon out of the atmosphere. These include techniques like afforestation, reforestation, improved industrial energy efficiency, scrubbings and other influences on the source of chemical conversions of CO_2 to useful products and complete sequestration underground. The most attractive seems to be the geological carbon storage, an option that can store large volume of CO_2 under the rock (AlRassas et al., 2021). The core processes of geological CO_2 storage include collection and separation of the CO_2 from locality sources, and injection of the extracted CO_2 into pore space underground for long-term sequestration.

Options including oil and gas reservoirs, deep coal seams, deep ocean, salt caverns, and deep saline aquifers have all been investigated for CO_2 storage with some currently used (Voormeij & Simandl, 2004). The global frequency of saline aquifers makes them promising candidate due to the potential of much larger storage volume than other geologic options such as, oil and gas reservoir which is only available in few areas across the world (Hatzignatiou et al., 2011). Static and dynamic concepts of hydraulic properties have been used for the evaluation of CO_2 storage capacity in geological reservoirs. We will examine possible geological alternative of CO_2 storage in saline aquifers, in dynamic conditions.

1.1. The notion of CO2 static and dynamic storage capacity.

Dynamic storage capacity refers to the time-varying ability of a geological formation or a reservoir to store and retain CO2, in response to changes induced by dynamic processes (e.g., injection, migration, trapping, dissolution and mineralization). Dynamic storage capacity studies aim to estimate the volume of CO2 that can be safely and efficiently stored under different operating conditions and over the life of the project. Static storage capacity of the geological feature and dynamic storage capacity need to be distinguished.

Static CO2 storage capacity is the theoretical maximum amount of CO2 that a geological formation can store under optimum conditions. This value abstracts away the fluid flow dynamics, random pressure fluctuations and all other factors that really affect how much you can store in a specific place.

Static capacity is generally calculated through Volumetric method which consists of:

- Reservoir rock volume calculation.
- Approximation of rock porosity (CO2 storage percentage within rock voids).
- Estimation of CO2 density at reservoir conditions.
- Using a storage efficiency factor (that fraction of pore space in which CO2 can be stored.

The meaning of static capacity refers to the theoretical volume available for CO2 storage without accounting for any dynamic factors. This dynamic factor can include fluid dynamics and pressure impact. Static capacity evaluation is usually done during pre-selection among potential storage places.

In the aspect of Dynamic CO2 storage capacity, this stands for the amount of CO2 that can be contained in a geological formation over time considering the dynamic behaviour of the fluid within the reservoir. This parameter includes the details of injection, liquid movement, pressure modifications and various other factors that associate with storage. Dynamic storage assessment is evaluated using more sophisticated modelling and simulation methods such as reservoir simulation. These methods include:

- Fluid dynamics (Multiphase flow models)
- Pressure fluctuations and build-up before and after injection.
- Trapping mechanism, this includes both the structural, residual, solubility and mineral trapping mechanisms of CO2.
- Variability in the reservoir (differences in rock properties).
- Boundary and operations constraint s(e.g., injection rates, aquifers, well location and type).

To realize this goal, it is essential to determine the static and dynamic CO2 storage capacity. Whilst static capacity gives an initial measure of a potential basin suitable for CO2 storage, dynamic capacity which is the variation in the amount of CO2 that can be stored overtime provides a more comprehensive and practical appraisal necessary for successful implementation and operation of CO2 injection and storage activities. The methodology for characterising CO2 storage sites covers the economic aspects, political features, reservoir properties, seal properties, safety and data coverage (Anthonsen et al., 2014). Some characterisation does not consider the economic and political criteria for above-mentioned reason since the economic and political situation differ from region to region.

Here are few essential elements central to measuring the success of CO2 storage in geological formations:

- **Quantifying Storage Potential:** Storage capacity assessments consider the reservoir porosity, permeability, thickness and area to calculate how much CO2 could be trapped in the reservoir. It is one of the important considerations for making up site decisions and development planning.

- **Migration and Trapping Mechanisms Assessment:** Accurately predicting the transient behaviour of CO2 within the reservoir is crucial for assessing storage capacity in the long term. Dynamic estimates of storage capacities - assessment of migratory paths, trapping mechanisms (e.g., structural trapping, residual trapping and solubility trapping) and traps homogeneity, continuity as well effectiveness in retaining CO2 within the reservoir with time (Zhang & Song, 2014). This knowledge is important for predicting CO2 plume mobility, assessing containment integrity, and minimizing the risk of CO2 leakage or migration into overlying formations.

- **Rates and Pressures:** Estimates the injection rates and pressures that can be used to inject CO2 into the reservoir without exceeding safe thresholds of formation pressure or avoid inducing seismicity. Injecting CO2 at different rates and pressures can help operators tailor injection strategies to minimize reservoir overpressure/leak issues. The fracture pressure gradient should be in the range of 130 % to 180 % of the hydraulic pressure gradient (Zhou et al., 2008), however for safe operations, the pressure should not be more than 90 % of the fracture pressure gradient (Benson & Cole, 2008; Gibson-Poole et al., 2008; Oldenburg et al., 2014).

- **Predictive Simulation of Storage Capacity**: Numerical simulation models are employed to predict the performance of CO2 storage projects under different operating scenarios and geological conditions. A numerical model allows us to simulate how CO2 moves within a formation being injected; this kind of dynamic, spatial computer-based reservoir engineering or modelling can be used to estimate in detail the storage capacity at a potential site. Such models simulate

the injection of CO2, with its migration and trapping through time, so that operators can assess the performance of storage, estimate storage capacity and clarify issues surrounding uncertainty.

1.2. Objectives and scope

The behaviour of CO2 in the subsurface has been extensively studied with a lot of literature dedicated to understanding various aspects of CO2 storage available. These contributions encompass a wide range of approaches, including field observations, laboratory experiments, and simulations conducted at different scales. Although much has been done on these contributions, more still needs to be addressed because of the need in optimizing CO2 storage in the subsurface through further research, monitoring, and verification to fully understand the long-term CO2 plume behaviour in the existing projects. This thesis aims to bridge this gap by providing a comprehensive overview and conducting a detail sensitivity analysis of the dynamic storage capacity of CO2 in the target saline aquifer prior to the spill point using the Black Oil Model (BOM) in Petrel

This research investigates the impact of various reservoir parameters on CO2 storage capacity and plume migration prior to reaching the spill point. By enhancing the understanding of CO2 injection and geological storage dynamics in saline aquifers, this work contributes to the advancement of knowledge in carbon capture storage practice. This following were investigated:

- The influence of porosity on carbon dioxide plume distribution and storage volume over time.

- The influence of permeability, vertical to horizontal permeability ratio (k_v/k_h) on carbon dioxide plume distribution and storage volume over time.

- Examination of CO2 storage volume and plume distribution due to varying injection rate because high injection rate can result to a pressure higher than the formation fracture pressure if not monitored.

- Volume capacity of injected CO2 on different geological shapes.

- Finally, the influence of porosity and injection rates on reservoir pressure within the injection period of CO2 in the aquifer.

The thesis is organized as follows:

Chapter 1: Gave introduction to the work and objectives of the thesis.

Chapter 2: Explored the fundamental concepts of geological CO2 storage.

Chapter 3: Distinguished some methods of estimating static and dynamic CO2 storage capacity and gave insight on some properties that impact storage capacity.

Chapter 4: Presented the study design and methodology utilized in this work.

Chapter 5: Presented the results and findings from implementation of chapter 4 methodology.

Finally, Chapter 6: summarized and gave recommendations for future research in this field.

2. Fundamental Concepts of geological CO2 Storage

Subsurface CO2 migration involves the vertical and lateral flow of carbon dioxide (CO2) already in the nature in a series of geological formation, as for example sedimentary basins, saline aquifers, oil and gas reservoirs. It is also relevant to projects for the storage of CO2 (carbon capture and sequestration) underground as a method to mitigate climate change.

The flowing subchapters present important features and processes controlling CO2 migration in the subsurface.

2.1. Injection and storage

CO2 migration usually starts with the injection of CO2 into a subsurface reservoir, such as a saline aquifer or a depleted oil or gas reserve. CO2 can naturally travel from deep geological formations to shallower depths via faults, fractures, and other channels. CO2 is typically injected into the reservoir in a supercritical state, at a temperature and pressure above its critical point (31.1°C and 73.8 bar). See Figure 2-1 showing pressure and temperature of supercritical CO2.
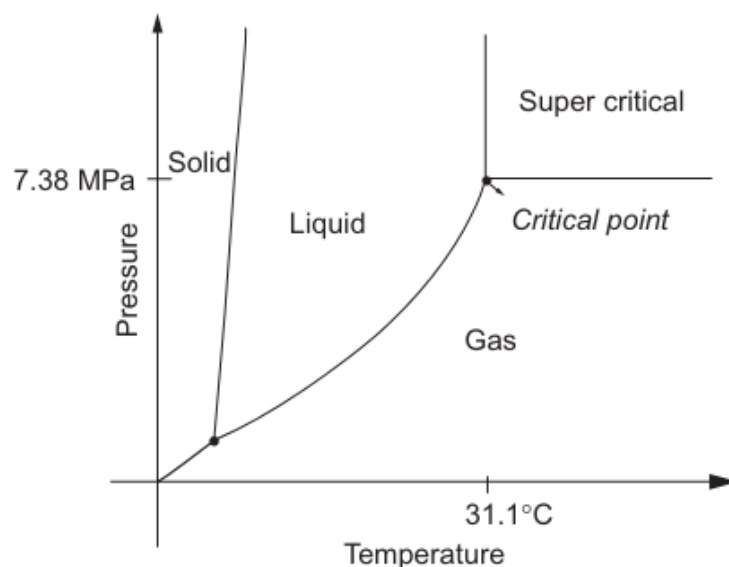
Figure 2-1: Graph of pressure versus temperature of supercritical CO2 (Gopalakrishnan et al., 2019; Weibel & Ober, 2003).

CO2 under such supercritical conditions is a dense fluid that possesses the characteristics of both a gas and a liquid, capturing those properties to better fill pore spaces than gaseous CO2, resulting in larger storage capacities. When subjected to a supercritical state, it could inhibit buoyant migration thus enhancing stability of storage (Metz et al., 2005). In the reservoir, after CO2 injection ceases and the well shut-in, the pressure built up from the injected CO2 begins to slowly decrease into the formation. This change in the regime arises due to the reduced viscous forces near the well and allows advection to take place when fluid phases are brought into equilibrium with each other inside of the porous media as they follow gravitational and capillary forces (Nordbotten et al., 2005). The upper part of the CO2 plume spreads laterally below the caprock. Such imbibition of the in situ brine reverses the quick-drainage as CO2 would naturally rise due to gravitational forces (Nordbotten et al., 2005). Like the water saturation that is irreducible, the imbibition process does not displace all CO2, leading a portion of it trapped in pores by capillary forces known as residual trapping (Metz & Intergovernmental Panel on Climate Change, 2005). Progression is stopped vertically by the sealing caprock on top of an uplift. However, CO2 is not immobilised and slowly spreads up-slope under the cap rock (hydrodynamic trapping). While migrating upwards, parts of the CO2 might be trapped permanently in local pockets, sealed fault blocks or salt domes along this path; a process called structural trapping (Nordbotten et al., 2005). If there are unconformities or changes in rock type within the storage this type of trapping mechanism can also be present and is called stratigraphic trapping.

2.2. CO2 flow and trapping mechanisms

Following its injection, CO2 migrates through the subsurface primarily through fluid flow processes driven by pressure gradients, buoyancy forces and strong reservoir characterisation such as porosity and permeability. Even after being injected underground in the form of supercritical CO2, the CO2 can still migrate vertically within or between zones, laterally within layers, or move preferentially along fractures and other flow paths within a reservoir.

The following are the trapping mechanisms of CO2 storage.

2.2.1. Structural Trapping

Trapping in geological strata: structural features (like fractures, folds, and stratigraphic traps) can make rocks porous enough for fluids to flow through them; but with the correct shapes (and sometimes containing salt or another barrier), these same pores can trap CO2 within them. Structural trapping occurs when impermeable barriers, such a sealing faults or low-permeability rock layers, prevent the CO2 from migrating anywhere further and trapped in the in-situ reservoir. The trapping mechanism that this seal creates is called a structural trap or stratigraphic trap, in case the underlying geology of the reservoir is controlled by differences in the density between the target sands and the surrounding

rocks. This process is especially important as it is a requirement of all storage sites, preventing the escape of CO2 from the caprock during the time that other trapping processes take effect (Bachu et al., 1994). The volume of pore space and the homogeneity of the reservoir also significantly affect hydrodynamic trapping, as demonstrated by previous work on saline aquifers where millions of years were required for a deep hydrodynamic trap to release buoyantly driven CO2 (Gunter et al., 2004). See Figure 2-2 indicating structural trapping. From the top, CO2 is trapped under a dome and cannot migrate laterally or to the surface. The lower image shows that the CO2 is capped on its vertical flow by overlying seal rock and a fault located right of the CO2.
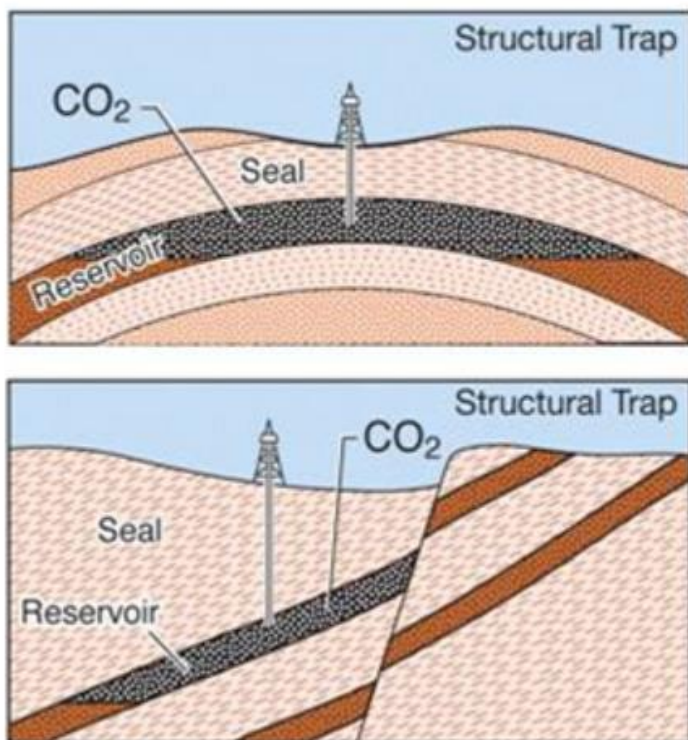
*Figure 2-2: Depicting two examples of structural trapping (*National Energy Technology Laboratory - Carbon Storage FAQs*, n.d.)*

Structural trapping is the first, most ephemeral type of trapping and one that is essential to even get CO2 injected into the ground. Shales or evaporites may seal the CO2 within the reservoir when they occur as caprocks (Benson & Cole, 2008).

2.2.2. Solubility and mineralization

Another is dissolution of carbon dioxide into formation fluids (for example brine or connate water), which is particularly relevant for saline aquifers. Furthermore, dissolved CO2 in brine may react with resident minerals of the reservoir rock resulting in carbonate mineral precipitation (mineralization) but this is a slow process that requires thousands of years to completely dissolve the CO2 (Lindeberg & Wessel-Berg, 1997). The solubility of CO2 in water does depend on the salinity, pressure and temperature of the formation

waters (Chang et al., 1998). The movement of CO2 in brine on molecular scale influenced by diffusion, this led to the enhanced dissolution of diffused CO2 in the water, which increased the density of aqueous CO2 to around 1 % with reference to the formation brine (Kumar et al., 2005). The buoyancy difference is too small to overcome gravity segregation, which displaces the heavier dissolved CO2 in brine in convective downward flow. The entire process is referred to as dissolution-diffusion- convection (DDC) and resists CO2 storage capacity with issues in the time and length scales of the resulting convection (Pruess & Zhang, 2008). Mineralization process, on the other hand, is the atomic conversion of a gas phase into solid mineral through chemical reactions that happens within the formation minerals and organic materials. The injected CO2 will eventually dissolve into the formation water adjacent to it and that leads to variety of geochemical processes. Some of these reactions could prove beneficial to retaining CO2 as dissolved species or in new carbonate minerals (being essentially a chemical containment or "trap"), while others may be harmful, facilitating the migration of CO2. To understand the net impact of these two opposing processes is crucial. These processes will be dependent on the nature of the lithologies involved with likely interplay with mineralogical and hydrogeological characteristics (Rochelle et al., 2004). Figure 2-3 below from the left shows at the interface between CO2 and brine water, some of the CO2 molecules are dissolved into the brine water in the pore spaces of the rock. Then, some of that CO2 dissolves into available hydrogen atoms, forming HCO3 while on the right the Figure 2-3 shows how minerals are formed over the surface of a rock grain reacting with dissolved CO2 in brine water. The magnesium present in the mineral grain reacts with the CO3 in water to create MgCO3 on its surface.
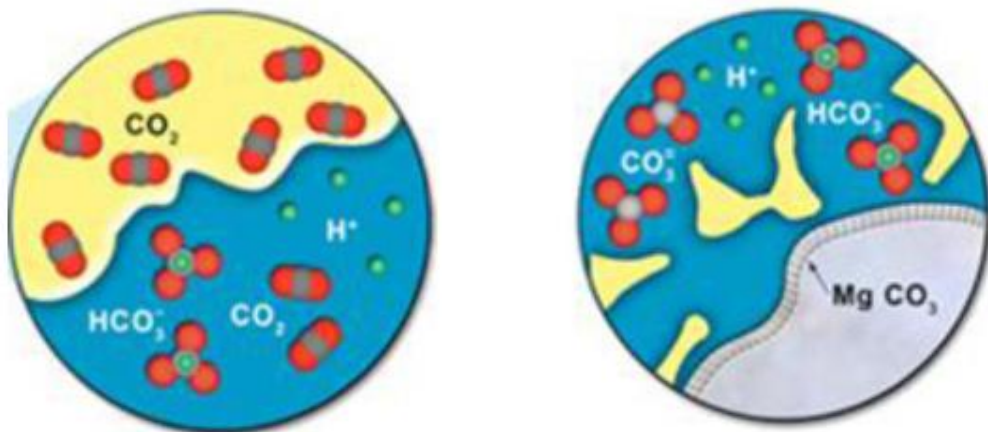
*Figure 2-3: Depicting solubility trapping at the left and mineral trapping on the right (*National Energy Technology Laboratory - Carbon Storage FAQs*, n.d.).*

Mineral trapping is the most irreversible form of trapping and can last over geological timescales. CO2 is converted to solid by the process of mineral trapping which removes it from the fluid phase (Gunter et al., 2004).

2.2.3.   Residual trapping / Capillary trapping

If regions of high initial CO2 saturation contain remaining liquid CO2 after the injection phase, This liquid will exist as an isolated residual or surviving phase within the pore space which may be only a few percent of the total volume of the resident fluid, in part due to capillary and interfacial trapping effects (Juanes et al., 2006). This trapping process involves brine displacement in the piston or leaky piston sense initially. Yet, once the well is shut in, counter-current flow of brine below and CO2 above occurs due to a density difference between CO2 and the brine. In this way, the wetting-phase (the brine) flows into the pores through the non-wetting phase (the CO2). During this process, brine displaces CO2 leading to a significant saturation of CO2 that gets confined into tiny pore clusters. The unbound CO2 is subsequently sequestered and stored in place (Zhang & Song, 2014). Residual trapping helps ensure the long-term integrity and security of CO2 storage, mitigating any risk of leaking to the surface or overlying formations. Capillary trapping is also observed in the neighbouring rock and therefore prevents CO2 movement in terms of storage security. Figure 2-4 illustrating small pockets of residually trapped CO2 in the pore space as it migrates to the right through openings between rock grain blocks.
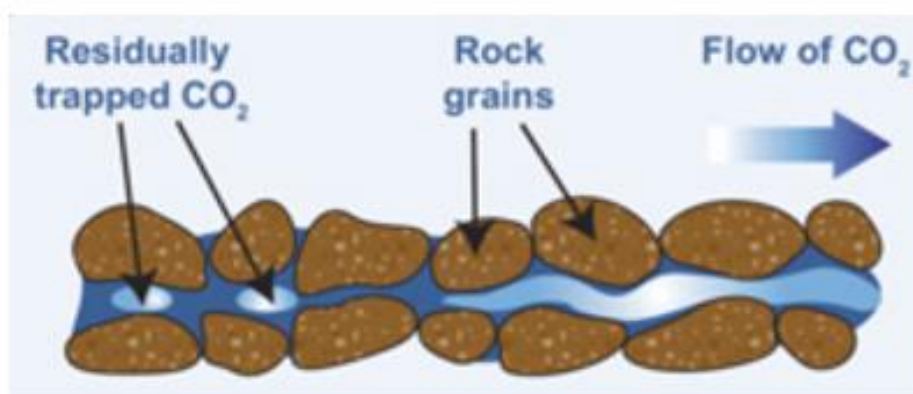
*Figure 2-4: Depicting residual trapping (*National Energy Technology Laboratory - Carbon Storage FAQs*, n.d.)*

Experimental and numerical modelling results also suggest that the mechanisms of capillary trapping have a strong influence on the migration and distribution of CO2, hence regulating the efficiency of other trapping mechanisms (Suekane et al., 2008).

Figure 2-5 below shows time evolution of the processes of CO2 trapping. Structural and mineral trapping come first and last respectively in the CO2 trapping process.
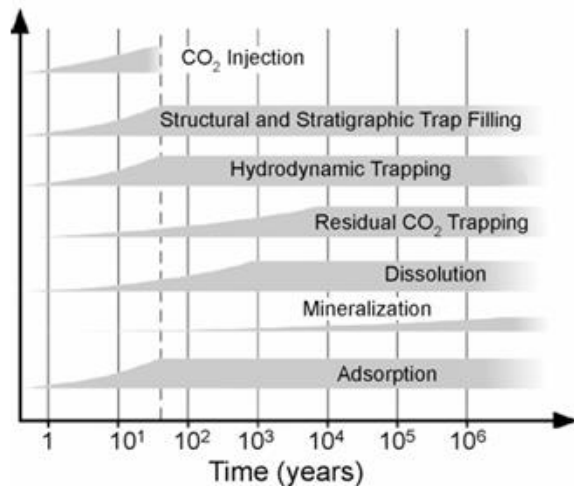
Figure 2-5: Time dependency of processes involved in CO2 geological storage modified from (Bachu et al., 2007).

To sum up, the CO2 migration in subsurface is a complex mechanism influenced by various factors together from reservoir parameters, fluid properties to injection strategies and geological conditions. Knowledge of the mechanisms and reasons for CO2 migration is essential not only to estimate whether a given CO2 storage project would be appropriate, sustainable, and efficient, but also to design mitigation measures which include carbon capture with CO2 storage technologies.

3. Methods for Estimating CO2 Storage in Saline Reservoirs and Reservoir properties affecting CO2 storage capacity.

This chapter visited the different techniques for CO2 geological storage capacity assessment and as well as reservoir characteristics governing CO2 storage capacity. Some insight was gained by doing a bit of literature research on the various work being done with CO2 sequestration.

Storage capacity: The amount of CO2 that it is estimated could be stored commercially in a particular geologic formation under current or anticipated policies (Frailey & Finley, 2009). In general, for CO2 storage, the subsurface volume calculations are either made using static approaches or dynamic approaches. Whether to use it in the CO2 storage volume calculation or not depends on both the assessment domain and available data, plus its accuracy. The static technique relies on unchanged fluid and rock properties over time. Dynamic is the term denoted entity that the parameters of contrast are time dependent. More information about the static and dynamic approach for storage capacity evaluation are covered in Section 3.1 and 3.2 respectively. The equation for the

evaluation of different storage capacity is similar to five different production and injection methods employed and tested over the past several decades using fluids in vertical porous permeable formation in a coordinate system. Although CO2 geologic sequestration in saline aquifer is not identical, the processes are similar which makes it relevant to come up with equivalent approaches and equations for modelling CO2 sequestration(Frailey, 2009).

The methods of CO2 storage capacity evaluation listed in Table 3-1 below is outlined and described in this chapter.

Table 3-1: Summary table of methods of assessing CO2 storage capacity modified from (Pickup, 2013)

Approach	Methods	Remark
Static	Volumetric	- Calculate formation pore volume - Assume a storage efficiency - Simple approach
	Pressure build-up	- Assume a closed system - Estimate the maximum allowable pressure build-up - Calculate CO2 volume from total compressibility and pressure increase
Dynamic	Semi-closed	Similar to the pressure build-up method, but allows water to leak through the seals
	Pressure build-up at wells	- Assumes pressure at injection well is the limiting factor. - Uses an analytical formula to estimate the injection pressure
	Material balance	Similar to the pressure build-up method, but update calculations with time
	Decline curve analysis	- Monitor pressure build-up in a CO2 injection site - Opposite of decline curve analysis in hydrocarbon reservoir
	Reservoir simulation	- Construct a detailed geological model - Perform fluid flow simulations

Section 3.3 discussed on the geological and reservoir features that influence the dynamic storage capacity of CO2 in underground formations.

3.1. Static Methods for Estimating CO2 Storage in Saline Reservoirs.

This static version of CO2 storage is not as difficult as in the dynamic case, where the variables are time-varying. At first a comprehensive review on how to measure static storage capacity obtained by (Frailey, 2009). He divided the methods into volumetric and compressibility approaches and outlined some of them.

3.1.1. Volumetric Method

The National Atlas I and II, which was created by the US Department of Energy, estimate CO2 resources using a volumetric method. This formulation makes use of Equation (3.1) which includes porosity (φ), area (A), and thickness (h), multiplied by storage efficiency (E), the fraction of connected pore volume expected to be in contact with injected CO2. This volumetric method is common in the early stages of oil-and-gas exploration when little, if any, site-specific data are available.

$$G_{co2} = Ah\phi E \qquad\qquad (3.1)$$

where G_{co2} is the estimated CO2 storage amount. Assigning average values to every parameter might be literally the only thing you can do in situations where data is very scarce Still, where specific information on thickness or porosity of layers is available at the injection site, it might be applied individually for that layer more specifically. The trapezoid or pyramid rules are often applied for the calculations in the case where linkage between an area and height can be established (Frailey, 2009).

The area multiply by thickness (height) calculates the bulk volume of a formation's unit for which we consider. The pore volume is calculated by the area, thickness and porosity of pores. In contrast, effective porosity ignores the meso- and macro-scale interconnected pore spaces, resulting in a total pore volume that is less than that yielded by total porosity. It only considers the effective pore volume to estimate the storage accurately. Storage efficiency (E) will depend on what you define to be your area (A) and how thick it is in the taken reference frame (h). If, for example, (h) is the total thickness, then (E) must account for the net-to-total relationship of thickness. Likewise, for total porosity one should convert (E) into the ratio between effective and total porosity. Storage efficiency will become expected level of CO2 saturation (the fraction of pore volume you expect to be filled with CO2).

3.1.2. Compressibility Method

CO2 storage estimation In saline aquifer can be achieved using rock and fluid Compressibility. This method requires an understanding of how the compressibility of the fluid and pore space in the reservoir affect storage of CO2 (Frailey, 2009). The method of compressibility is based on the fact that the higher the pressure due to CO2 injection, the

smaller will be volume of water in the reservoir. Decreased water volume increases the pore space for CO2 storage. Fluids with nearly constant total compressibility (C_t) over some range of initial pressure (P$_0$) down to a final pressure (P) may be analysed using the compressibility method. The sum of the compressibility of the fluid (C_f) and the formation pore space (C_m) is called the total compressibility.

$$C_t = C_f + C_m \tag{3.2}$$

The material balance equation for the corresponding volume will be written as Equation (3.3) due to the compressibility and pressure change:

$$\Delta V_w = V_{wo} C_t (P - P_o) \tag{3.3}$$

Injecting CO2 into a saline aquifer produces two coexistent phases (CO2 and brine). For CO2 storage using the compressibility method, water phase is highly important. There will be pressure increase (P) from the original pressure (P$_0$) causing the original water volume (V_{wo}) to change by fluid and rock compression. The volume change (ΔV_w) is the available volume for CO2 storage.

The capacity for CO2 storage ($G_{co2(capacity)}$) is represented as the available volume of CO2 at the current state of compressibility in the system:

$$G_{co2(capacity)} = \Delta V_w = V_{wo} C_t (P - P_0) \tag{3.4}$$

3.2. Dynamic Methods for Estimating CO2 Storage in Saline Reservoirs.

Dynamic Modelling based CO2 storage capacity assessment methods offer a comprehensive, consistent and detailed view of the storage process. The static method are ill-suited because of time and pressure response of petrophysical parameters, therefore accurate result cannot simply be derived from static state estimations. The dynamic approach require vast amounts of data, heavy computational resources and rigorous calibration. The use of reservoir simulation (to model long-term behaviours, and estimate ultimate effectiveness at sequestering CO2 in saline aquifers), analytical models, semi-analytical approaches, geochemical modelling and coupled process models enable improvement made in understanding the long-term behaviour of CO2 storability (Bachu et al., 2007). Within dynamic CO2 storage capacity evaluation techniques, we shall explore varied options to assess the quantity of CO2 that can be stored securely and effectively in a geological formation over time. A comprehensive examination of the most applied methods in this field is shown here.

3.2.1.   Decline Curve Analysis

Decline Curve Analyses (DCA) for estimating CO2 storage potential in saline reservoirs This method offers a very simple way to estimate future performance by looking at calibrated solution flow coefficients developed from history matching operation(Netto et al., 2003) and applying some expected decline models. Nevertheless, DCA must be used in concert with other reservoir modelling techniques to improve the accuracy and reliability of projections (Frailey, 2009). DCA has been used in the oil industry for the forecasting oil rates and final production. An analogy for CO2 injection rate (q_{co2}) has been presented using an exponential function of time, determined by an initial injection rate (q_{co2i}) and a decline coefficient (D) that reflects the formation's flow characteristics. The general form of this equation is presented by (Frailey, 2009) as follows:

$$q_{co2} = q_{co2i}e^{-Dt} \tag{3.5}$$

The flow equation is used in oil industry under steady state but the situation where injection rate changes with time because of pseudo-steady state then formation pressure goes up with injection rate falling at a suitable rate. A version of this formulation is in preparation for injection at constant rates under time dependent pressures. The Exponential Decline Equation is solved to obtain the decline factor (D), from injection rate history. Where q versus t is a semi-log plot of declining exponential pass, so this downdip coefficient is found from the slope of ln q versus t. The cumulative injection volume of CO2 between rates where an abandonment or minimum economic injection rate (q_{co2A}), is defined and is then associated with the ultimate storage volume. The Calculation of the estimated CO2 capacity (G_{co2}) is expressed as (Frailey, 2009).

$$G_{co2(capacity)} = \frac{(q_{co2i}-q_{co2A})}{D} \tag{3.6}$$

3.2.2.   Material Balance

The integral material balance equation considers the cumulative CO2 injected history at different times essentially due to pore pressure (p). The important fluid properties like CO2 compressibility (z) and the gas formation volume factor(B_g), etc. This is rather similar to the p/z plot for CO2 containment in saline formations as seen in natural gas reservoirs or underground gas storage reservoirs:

$$p/z = (1 - G_p/G)(p_i/z_i) \tag{3.7}$$

This method relies solely on historical cumulative and may or may not consider initial conditions (upper right volume of gas initially in place before production). For site applications an aquifer influx or efflux term can be added, which requires parameters

such water and formation compressibility. A similar formulation can be applied to the material balance equation for sequestration:

$$p/z = \left(1 - G_{inj-co2}/G_{co2}\right)(p_a/z_a)$$

<div align="right">*(3.8)*</div>

This leads to a cumulative gas injection equation, a plot of the above equation vs p/z (where z is the CO2 z-factor calculated at pressure p) that would result in a straight line for gas production from a reservoir where pressure is decreasing; however, during sequestration, with increasing gas pressure over time and associated aquifer efflux as brine water leaves the injection zone around the well, this straight-line assumption breaks down. When we include (W_e), this results in a nonlinear relationship. The general form in the B_g format is:

$$G_{co2}\left(B_g - B_{ga}\right) + W_e = G_{co2-inj}B_g$$

<div align="right">*(3.9)*</div>

This identifies the cumulative subsurface volume of CO2 injected ($G_{co2-inj}B_g$); A concept closely related to volume that describes the space the final CO2 storage volume $G_{co2}(B_g - B_{ga})$ would occupy at current pressure (p). The term '' W_e'' has a relationship to the injected gas. We can find out G_{co2} capacity using the decline curve methodology that we discussed earlier. Conversely, one limitation of the material balance equation is that net pore pressure rise must be felt as cumulative injection moving into a detectable average pore pressure rise and that this term must assessed on its own (Frailey, 2009).

3.2.3.   Flow Simulator

This is the most advanced approach to predicting storage for volume, depositional and fluid properties considering all flow mechanisms and geologic units differentially. Nevertheless, when it comes to accuracy, this technology totally relies on the availability of data. Flow simulation uses the conservation of material balance, compressibility and volumetric equations to create a detailed grid-cell-by-grid-cell model of a geological unit. It is an advanced method as various geological descriptions, fluid properties and the relative configurations of injection/production wells are included. It can also visualize different development scenarios like vertical / horizontal wells and perforations at various locations. It could simulate some behaviours (for forecast purposes) or provide a comparison to actual field/pilot performance. Essentially only the basic equations might give similar storage estimates when used just for design purposes. As mentioned above, integrating history-matching with actual field or pilot injection and pressure data will provide more reliable prediction of CO2 storage. The most resource intensive technique to simulate hydrodynamics is the flow simulation noticed here, which requires measurements at a year scale and is not suitable except for reservoir scale even in those cases this method demands more precision data neither for the formation nor basin scales.

- **Reservoir Simulation:** Numerical reservoir simulation models (i.e. black oil, and/or compositional, or in the more complex cases dual-porosity models), which are widely used to simulate fluid flow and CO_2 migration in underground reservoirs. These models use conservation equations for mass, momentum and energy in combination with reservoir parameters, fluid behaviour and injection processes. They enable the forecasting of spatial and temporal CO_2 plume migration, storage capacity, and trapping.
- **Geomechanical Coupling:** Advances in some of the numerical modelling techniques use geomechanically coupling to incorporate the impact of CO_2 injection into a formation on reservoir deformation, stress changes, and induced seismicity. These are analysed using geomechanically models of risk such as reservoir overpressure, caprock integrity and induced fractures development in the CO_2 injection operations.

Instead, it is the cost-effective one of a kind complement for assessing other approaches for CO_2 storage capacity calculation in different geological settings, project scales and operational conditions. Combining different methodologies in combination with new technology options enhances the reliability and accuracy of estimates of dynamic storage capacity, which is a key requirement of informed decision making and successful implementation of CO_2 storage projects.

Various codes for simulating CO_2 injection is presented in (Class et al., 2009).

3.3. Geological and Reservoir Characteristics Affecting CO_2 Storage Capacity.

Dynamic storage capacity in underground formations is controlled by both geological and reservoir features of the rock. These features collectively provide the basis for assessing the feasibility and performance of CO_2 storage systems. Full Review of Key Geology and Reservoir Characteristics Affecting Dynamic CO_2 Storage Capacity

3.3.1. Porosity and Permeability

Porosity is the ratio of void space to total volume in a rock formation, whereas permeability, I will simply state that it is a measure of a rock formation to transport fluids. High Porosity and permeability could help your fluid flow, as well as the CO_2 migration and consequently enhance the storage capacity and injection efficiency. Low porosity and permeability reservoirs have limited capacity for storage, requiring injection improvements or engineering of the reservoir itself.

3.3.2. Caprock Integrity

The integrity of a caprock is the effectiveness for the upper barrier to seal, which is usually composed of impermeable rock layers such as shale or mudstone. Inferior caprocks allow CO_2 leakage, while a well-performing caprock prevents CO_2 from migrating within

or out of the reservoir. Reservoirs with fault fissures, poor-fault seal potential or erosional relief such that the caprock integrity is weakened lead to potential act as leakage pathways and hence the CO2 storage will be less effective, and the risk of CO2 may migrate into unintended strata. Table 3-2 indicates the seal criteria for co2 system.

Table 3-2: Characterisation and ranking criteria for seal properties modified from (Anthonsen et al., 2014).

Seal properties	Preferred	Questionable	Hazardous
Thickness	>50m	20-50m	<20m
Lithology of the primary seal	Homogeneous clay, mud or evaporites	Chalk	High content of silt or sand
Fault intensity	Low No mapped faults through reservoir or seal	Moderate Minor faults through reservoir or seal	High Large faults through reservoir and/or seal. Bounding faults
Lateral extend	Continuous	Unsure about existence of a continuous seal. Seal locally thinner than 20 meters	Not continuous
Multiple seals	More than one	Only one	Unsure if a seal exists

3.3.3.   Reservoir Heterogeneity

Reservoir heterogeneity is the presence of variations in the reservoir such as lithology, grain size and sedimentary facies (Tucker & Wright, 1990). When heterogeneous, the reservoirs may have spatial variability that affects porosity permeability and fluid flow that in turn impacts the distribution of CO2 and trapping processes, among other things affecting storage capacity. Proper reservoir characterisation and dynamic storage capacity estimate require a detailed understanding of reservoir heterogeneity.

3.3.4.   Depth and Pressure Conditions

CO2 behaviours and storage capacity are influenced by the depth and pressure conditions in the subsurface(Benson & Cole, 2008; *National Energy Technology Laboratory - Carbon Storage FAQs*, n.d.). The deep subsurface with higher pressures and temperatures acts as a reservoir that enhances the generation of supercritical CO2,

which is denser and more soluble than a gaseous state of CO2. It offers higher storage efficiency, especially in deep underground formations and saline aquifers, whilst its supercritical state makes it less bulky. This shallow geological reservoir may have a very high trapping efficiency but can store relatively limited amounts without further compression or densification to ensure long-term containment due to its low-pressure conditions.

3.3.5.   Rock and Fluid Properties

These factors in turn control the CO2-brine-rock interactions, trapping mechanisms and storage behaviour. CO2 can react with minerals known as carbonates, and clays, which can stabilize CO2 in a mineralized form for thousands to millions of years that it cannot escape back into the atmosphere. CO2 sequestration, storage characteristics and adsorption operations are affected, in some cases significantly, by the salinity or mineral content of the reservoir fluids. Knowing these attributes helps to understand how people store things and what kind of geochemical reactions may reasonably be stored. Rock and fluid properties can also determine the level of CO2 plume distributions.

3.3.6.   Structural Features

A description of CO2 migration pathways and reservoir compartmentalization, which are controlled by faults, fractures, folds and strata traps within the reservoir. Faults and fractures can act as conduits or barriers for CO2 movement, affecting reservoir connectivity and containment Stratigraphic traps (e.g. anticlines or pinch-outs) provide enhanced storage capacity by serving as structural closure and trapping mechanism for CO2

3.3.7.   Seismicity and Tectonics

Seismic and other processes operating in the region can affect reservoir stability, caprock integrity and hence risk to CO2 storage efforts. Seismicity induced by CO2 injection in geologically active regions can either pose a direct threat to storage integrity or increase the risk of leakage due to reactivation of faults (17). Knowledge of area seismic hazards and tectonic setting is important when assessing the suitability of storage sites and managing risks associated with CO2 injection. Table 3-3 below indicates the criteria for safety properties under seismicity considerations (Anthonsen et al., 2014).

Table 3-3: Characterisation and ranking criteria for safety properties modified from (Anthonsen et al., 2014).

Safety	Preferred	Questionable	Hazardous	Remarks
Seismicity	Low	Moderate	High	Both frequency and magnitude. Subjective, give argument for this category if moderate or high is chosen.
Risk of contamination of groundwater	No	Unsure	Yes	Risk of contamination of groundwater

Considering these geological and reservoir characteristics, the CO2 storage operators can easily assess the storage potential, locate suitable storage sites and enhance injection developments to optimise injection performance to achieve maximum storage capacity along with benefiting long-term CO2 retention. An understanding of the characteristics of a reservoir and dynamic storage capacity estimations are needed to minimise risks and ensure safety, thus they are key for management and implementation of CO2 storage programs. Characterizing criteria according to reservoir properties are summarized in Table 3-4 (Anthonsen et al., 2014; Lothe & Bergmo, 2014).

Table 3-4: Characterisation and ranking criteria for reservoir properties.

Reservoir properties	Preferred	Questionable	Hazardous	Remarks
Depth	>800m-2500m	600-800m	<600m	Case specific depending on temperature gradient in the area
Porosity	>20%	10-20%	<10%	
Permeability	>100 mD	10-100 mD or extrapolated from closest well drilled	<10 mD or no data	Indicate gas or fluid measurements

	through the reservoir			
Heterogeneity	Low N/G>0.4 Existents of uniform high porosity layers with thickness above 5 meter	Moderate N/G 0.1-0.4 Alternating high/low porosity layers. Layer thickness below 5 meter	High N/G <0.1 Highly alternating thin high/low porosity layers or channel sands with low connectivity.	Since heterogeneity is hard to quantify it advisable to give a remark about interpreted depositional environment and if the area has known diagenesis
Pore pressure	Hydrostatic or lower		Overpressure	
Thickness (Net sand)	>50m	15-50m	<15m	

4. Study Design and Methodology

Black oil model (BOM) was used for sensitivity study of various parameters impacting the CO_2 dynamic storage capacity. A black oil model is a partial differential equation -based reservoir simulation model that is used in the oil and gas sector to predict fluid behaviour in hydrocarbon reserves. This black oil terminology is for crude oil as a three-phase mixture of (black) oil, (oil dissolved gas) gas, and water in the reservoir. Its application eliminates much of the hydrocarbon fluids' complex phase behaviour yet fully captures fluid properties, the phase behaviour including single- and two-phase flow equations, and reservoir dynamics. A Black Oil model is faster to run and evaluate reservoir uncertainty and development sensitivity than a compositional model. However, judging and understanding the subsurface geological environment is always uncertainty-filled, even if for a relatively simple region of ubiquitous saline aquifer that can be more or less characterised with some level of heterogeneity (because most geological saline aquifer for CO_2 storage are not confined), so picking out a segment within an aquifer with well-known lithofacies series for CO_2 storage will certainly be the best place on storage potential because it would help prevent CO_2 leakage to underlying drinking water table(s) or over to underestimated part of the zone of interest with poor prospectivity simply

20

because abnormal pore fluid pressure much greater than normal hydrostatic pressure have been documented in many sedimentary basins around the world (Muggeridge et al., 2004).

4.1. Concept of black oil simulator

In a black oil simulator, like that used in Petrel, the basic equations describing the flow of fluids (oil, water and gas) in a porous media are derived from mass conservation and Darcy's Law. The BOM consists in a set of PDEs that model the conservation of mass balance equations, Darcy laws for pressure and saturation, capillary pressure for phase change, and equation of states (EOS) for fluid phases.

Each phase (oil, water, gas) mass conservation is shown in Equation (4.1)

$$\frac{\partial(\phi S_o \rho_o)}{\partial t} + \nabla(\rho_o v_o) = q_o \tag{4.1}$$

$$\frac{\partial(\phi S_w \rho_w)}{\partial t} + \nabla(\rho_w v_w) = q_w \tag{4.2}$$

$$\frac{\partial(\phi S_g \rho_g)}{\partial t} + \nabla(\rho_g v_g) = q_o \tag{4.3}$$

Where:

ϕ - represents the porosity of the rock.

S_o, S_w, S_g – represents the saturation of oil, water and gas respectively.

ρ_o, ρ_w, ρ_g - represents the densities of oil, water and gas respectively.

v_o, v_w, v_g - represents the Darcy velocities of oil, water and gas respectively.

q_o, q_w, q_g – The source/sink terms for oil, water and gas respectively corresponding to injection or production rates.

The Darcy's law which describes the flow of each phase (oil, water, gas) through the porous medium is given as:

$$v_o = -\frac{k}{\mu_o}(\nabla P_o - \rho_o g) \tag{4.4}$$

$$v_w = -\frac{k}{\mu_w}(\nabla P_w - \rho_w g) \tag{4.5}$$

$$v_g = -\frac{k}{\mu_g}(\nabla P_g - \rho_g g) \tag{4.6}$$

Where:

k – is the permeability of the rock.

μ_o, μ_w, μ_g – represent the viscosities of oil, water and gas respectively.

P_o, P_w, P_g - represent the pressures of oil, water and gas respectively.

g - represents the acceleration due to gravity.

Black oil model uses simplified equations of states to relates fluid properties to pressure while assuming isothermal condition. The following equations are used for the representation of formation volume factors and solution gas-oil ratio.

$$B_o = \frac{V_{o,res}}{V_{o,surf}} \tag{4.7}$$

$$R_s = \frac{V_{g,dissolved}}{V_{o,surf}} \tag{4.8}$$

$$B_w = \frac{V_{w,res}}{V_{w,surf}} \tag{4.9}$$

$$B_g = \frac{V_{g,res}}{V_{g,surf}} \tag{4.10}$$

Where:

B_o, B_w, B_g – represent the formation volume factor for oil, water and gas respectively.

$V_{o,res}, V_{o,surf}$ - represents the volume of oil at the reservoir and surface conditions respectively.

$V_{w,res}, V_{w,surf}$ - represents the volume of water at the reservoir and surface conditions respectively.

$V_{g,res}, V_{g,surf}$ - represents the volume of gas at the reservoir and surface conditions respectively.

Then the capillary pressure between phases is given by the following equations:

$$P_{cow} = P_o - P_w \tag{4.11}$$

$$P_{cgo} = P_g - P_o \tag{4.12}$$

The series of equations above are discretised and implemented in Petrel black oil simulator via a grid-based method and simulation is carried out as followings,

- **Grid generation**: The reservoir is discretized into a number of grid cells, and parameters such as porosity, permeability, and fluid saturation are assigned. It can be either homogenous or non-homogenous condition.
- **Initialization:** use geology and reservoir data to establish initial conditions for pressure, saturation and fluid properties.

- **Simulation setup:** Definition of limits, boundary conditions, inlets and outlets among other operating constraints. It achieved by employing a Petrel reservoir simulation development strategy.
- **Numerical Solution:** The simulator solves conservation equations at each of its timesteps in combination with the application of Darcy's Law using iterative numerical methods to update pressures and saturations in grid cells.
- Results and analysis: In this phase, the results are displayed to compare them and predict future behaviour of the reservoir which helps in controlling production or injection flows.

Petrel's black oil simulator can model reservoir dynamic behaviours using these basic equations and techniques, across several production and injection scenarios. We used the methods presented above to perform simulation of dynamic storage of CO2 in a saline aquifer Chapter 5 presents the result and analysis.

4.2. Developing model grid and simulation runs for sensitivity studies using black oil simulator

The model was built using two-dimensional 1 x 41 x 20-metre grid blocks in the I, J and Z directions. We selected black oil model as the simulator in petrel. Gas was selected to represent CO2, while water phase was used for brine. We tried to use oil phase instead of water phase to represent the brine but we recorded a high dissolution of gas in the oil, maybe because of the saturation pressure of the oil (the result not included in this work), due to high solution gas oil ratio we obtained initially, we reverted and made use of gas phase as pure CO2 and water as brine throughout the simulation cases. Closed systems would be ideal for CO2 storage because of high sealing surfaces that would prohibit leakage from the target formation. Since displaced brine cannot escape, the capacity for CO2 storage may be rather small (Zhou et al., 2007). To mitigate this effect, we incorporated two regions in our model, the first region is the main CO2 storage region (Region-1) while the second region (Region-2) is the spill region which incorporate open boundary effect at the bottom of the structure for pressure and saline water displacement buffer. In our model, the starting point of Region-2 with assumed level of uncertainties is referred to as the Spill point. To study the dynamic CO2 storage capacity, we utilized the advantage of the incorporated regions in the static grid model where Region-1 is assumed to be a good potential for CO2 storage while Region-2 is assumed to be uncertain for CO2 storage because it might be characterized by fault lines, inactivated fracture networks, low capillary entry sealing pressure. CO2 injection well was placed in the centre of Region-1 and above the Region-2 with CO2 being injected for couple of years from 2024 to 2900 while we observe how much volume of CO2 stored and how long it will take before the plume breaks into the Region-2 (Spill point).

We ran sensitivity analysis by varying reservoir parameters, such as porosity, permeability, ratio of vertical to horizontal permeability (k_v/k_h), injection rates to understand how they effect on the plume migration during injection period without focusing on CO2 dissolution in the aquifer or other trapping mechanisms like residual, capillary, mineral, solubility trapping mechanisms of CO2 in the aquifer.

We further considered how different geological shapes can affect the dynamic CO2 storage before the spill point and we finally evaluated the impact of porosity and injection rates on the reservoir pressure as the reservoir pressure is very critical for CO2 storage because over pressurization of the storage reservoir can fracture the seal and results to unintended leak from the storage region.

4.2.1. Grid Dimensions

We developed six geometrical shaped grid models (rectangular structure with no dip angle, 10 degrees dip rectangular structure, 25 degrees dip rectangular structure, 40 degrees dip rectangular structure, circular structure and anticline structure) for our analysis. The rectangular grid structure with no dip and the anticline structure are two-dimensional models built using 8000 x 4000 x 300 – metre with 1 x 41-metre grid blocks increment in the I and J directions, k direction of 300 metres (thickness) was divided into 15 layers of proportional division. The 300 m thickness was also designated into two regions, where 67 % of the thickness as region-1 (1000 m – 1200 m TVD), while the remaining 33 % of the thickness as region-2 (1201 m – 1300 m TVD). The assigned region-1 is the storage capacity with well define parameters and suitable for CO2 storage while region-2 is assumed to lack some required information and uncertain to be classified as a good CO2 storage site, which also offers formation water displacement buffer. This means during injection of CO2 into the subsurface when the plume spread beyond region-1 to any point in region-2, we identified that as a spill point or spill region.

For the circular structure, we used the radius of 3192 m and thickness of 300 m because we also wanted to maintain the same bulk volume (9.6 billion cubic meters) for all the structures. We incorporated the same method for layers and regions as in rectangular no dip and anticline structures. The three dip angle rectangular structures have the same size but because of the dip from the horizontal axis, the k-direction dip beyond 1000 m – 1300 m as it is in the anticline structure, circular and no dip rectangular grid structures. Below Table 4-1 gave the depth description of the dip structures.

Table 4-1: True vertical depths associated with the dip rectangular structures

Dip Structures	Top surface	Base surface	Well perforation interval	Region-1	Region-2
10 degrees dip rectangular	1000 m – 1700 m	1300 m – 2000 m	1454 m – 1504 m	1000 m - 1670 m	1671 m – 2000 m
25 degrees dip rectangular	1000 m – 2845.30 m	1300 m – 3145.3 m	2033 m – 2083 m	1000 m – 2437.3 m	-2437.3 m - 3145.3 m
40 degrees dip rectangular	1000 m – 4300 m	1300 m – 4600 m	2900 m – 2950 m	1000 m – 3412 m	3412 m – 4600 m

The depths as captured in Table 4-1 are taken with reference to the z direction.

The following are the images of geological grid structures developed for the purpose of this study.
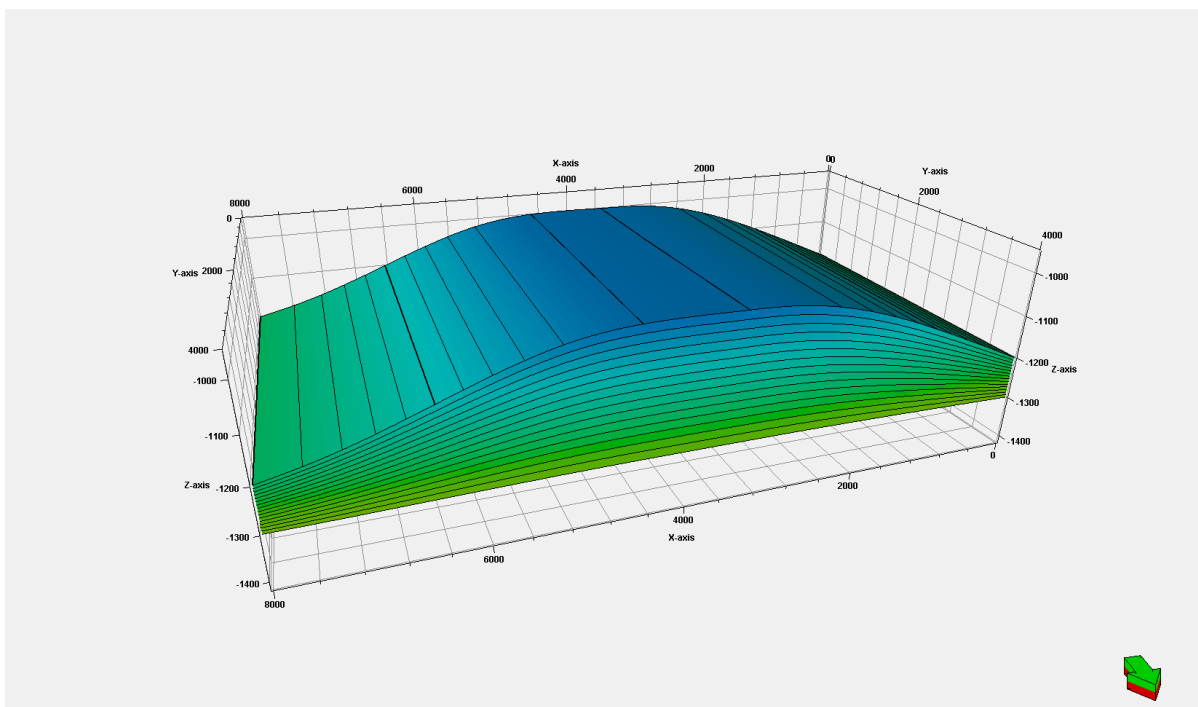
Figure 4-1: Anticline geological grid structure
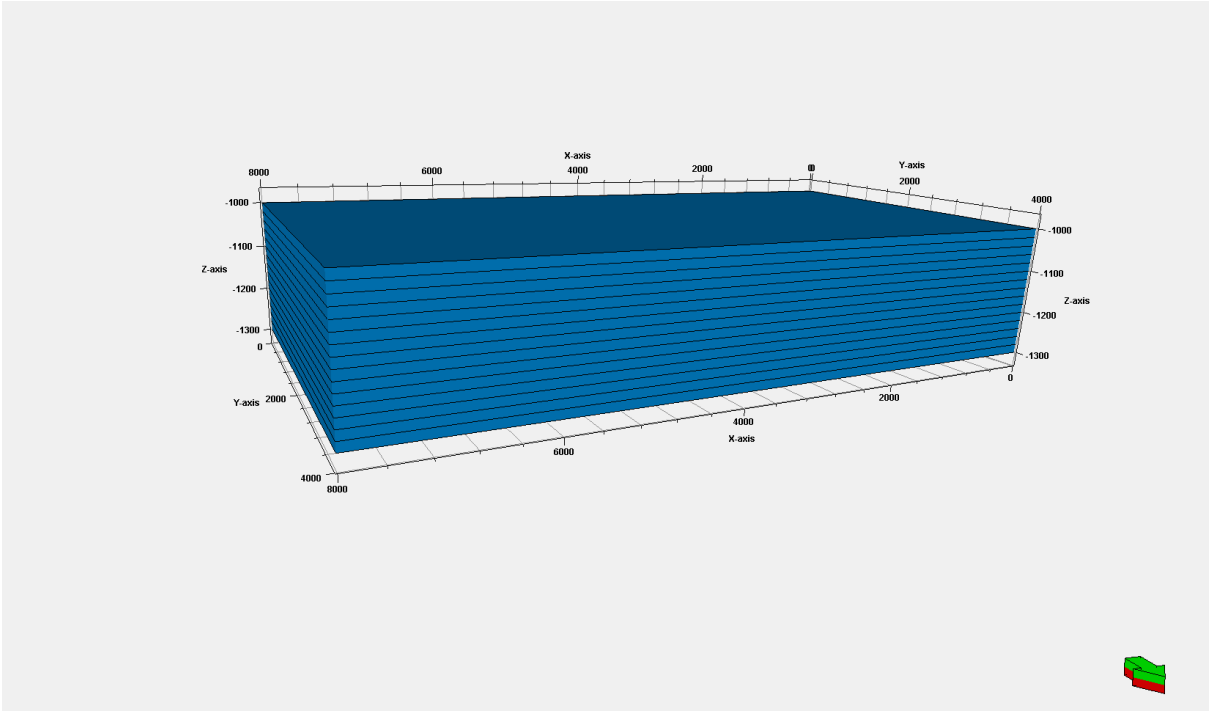
Figure 4-2: Rectangular geological grid structure with no dip
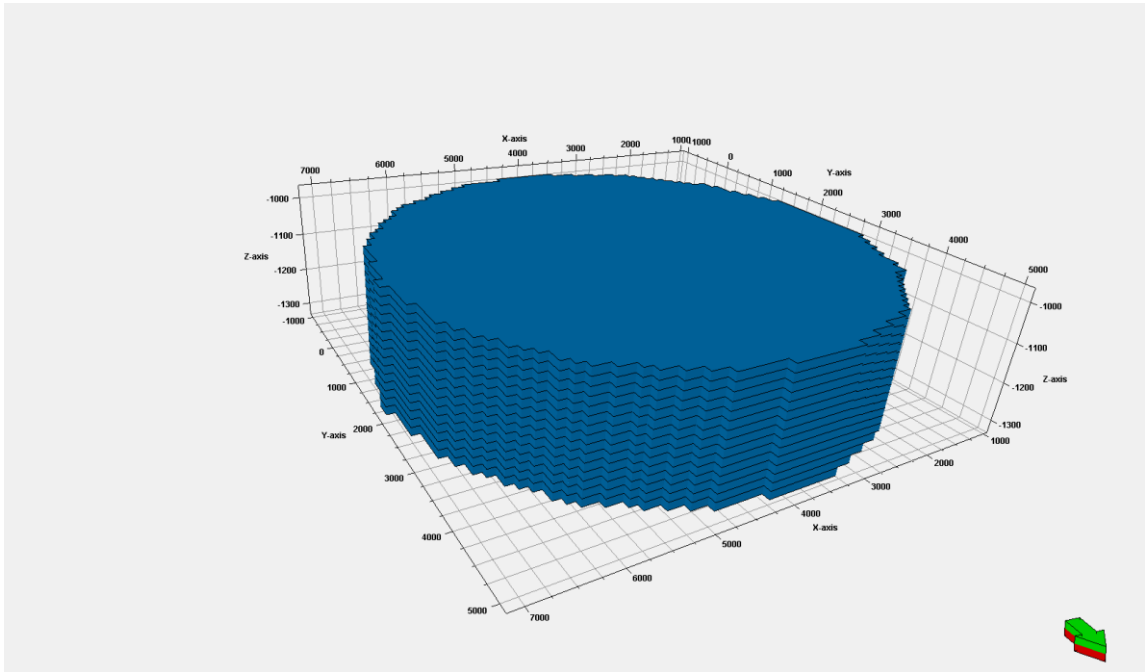
Figure 4-3: Circular (radial) geological grid structure
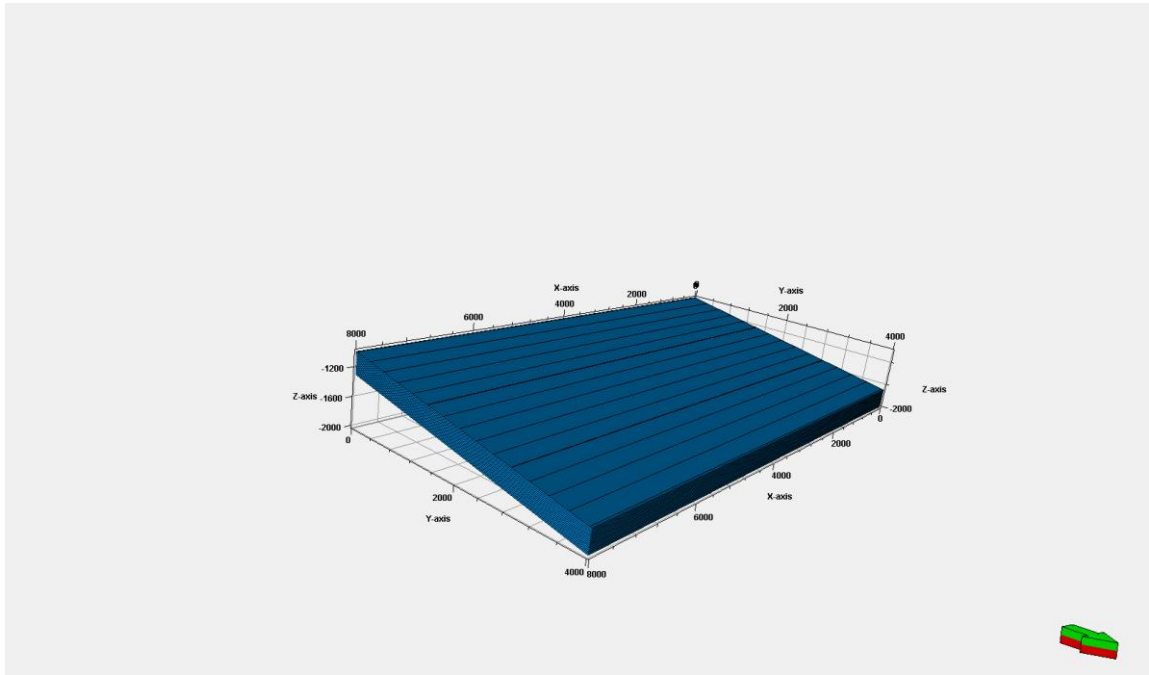
Figure 4-4: 10 degrees dip rectangular geological grid structure
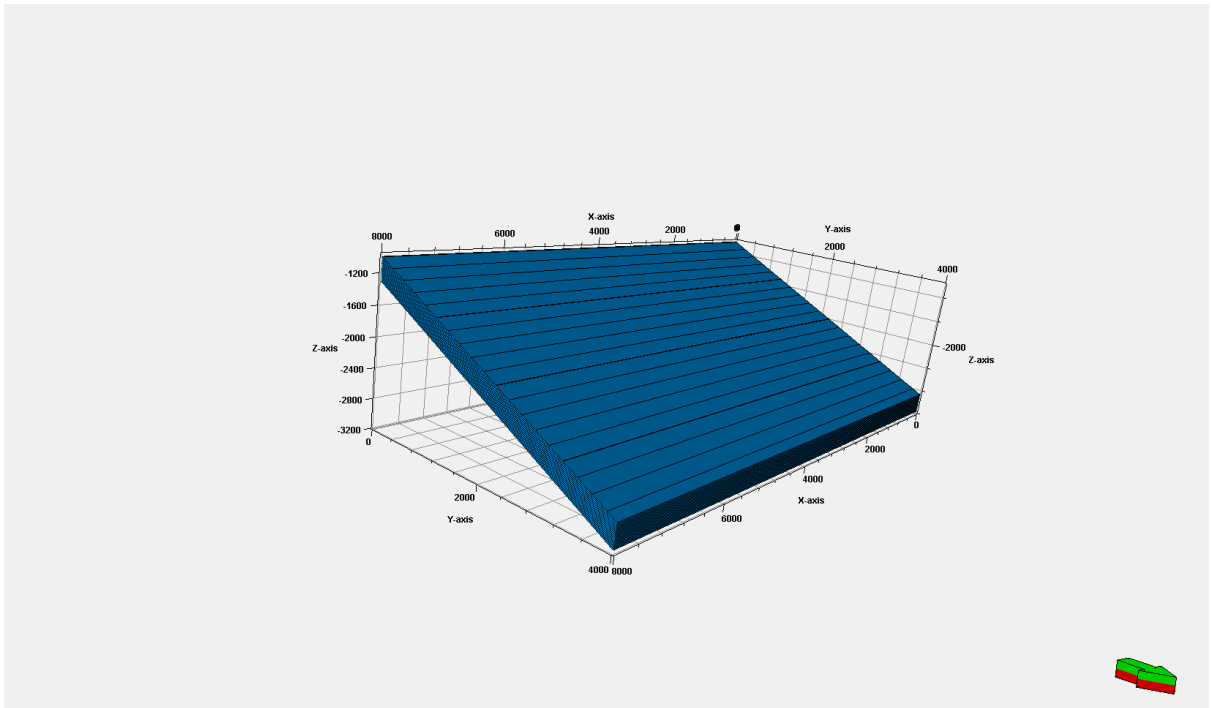
Figure 4-5: 25 degrees dip rectangular geological grid structure
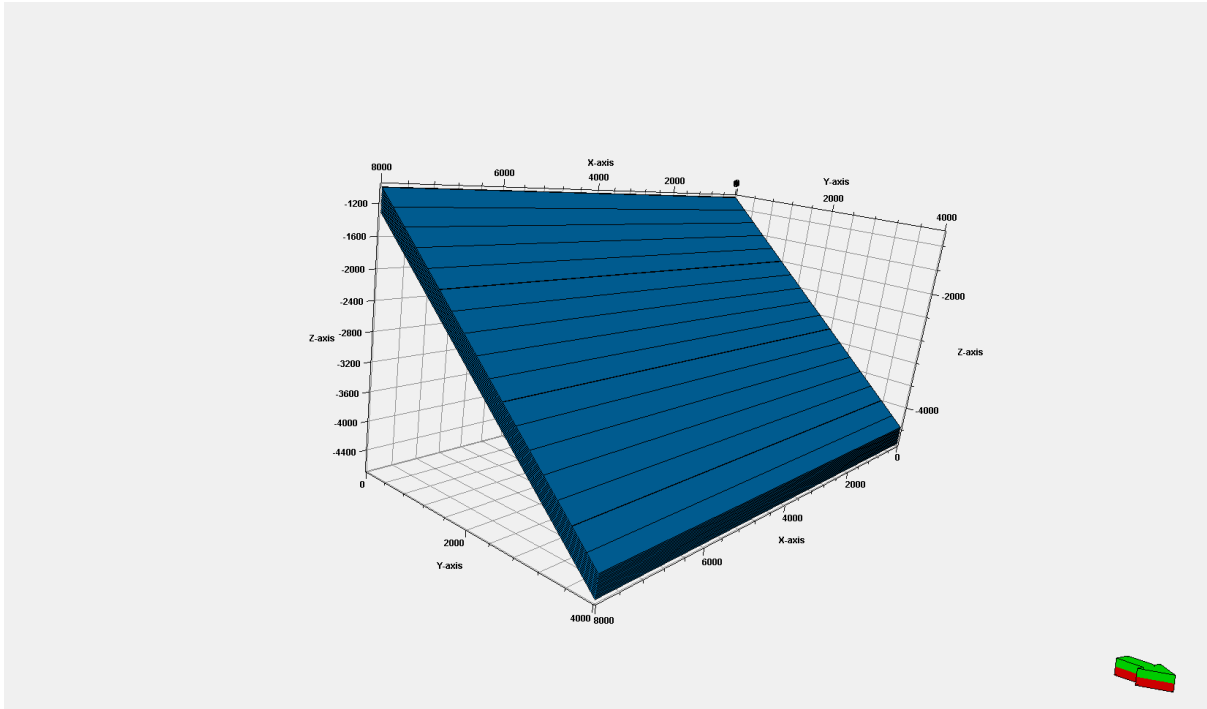
Figure 4-6: 40 degrees dip rectangular geological grid structure

4.2.2.   Data Initialisation

The rock and fluid data used in the based case is data from Sleipner CO_2 storage project in Norway. The data was obtained from the publication 'the modelling of CO_2 plume behaviour calibrated against monitoring data from Sleipner Norway' where black oil model and invasion percolation simulation methods were used to study CO_2 plume behaviour (Singh et al., 2010). Invasion Percolation Simulation is a technique to simulate fluid displacement processes in porous media, such that a fluid-phase (CO_2 phase) displaces another (brine) due to capillary forces at pore-scale level. Sleipner was the world's first commercial carbon storage project. The natural gas generated from the Sleipner West field includes up to 9% CO_2, although this must be reduced to a limit of 2.5% to meet export regulations and customer needs. CO_2 is extracted from hydrocarbons produced at an offshore platform and injected back into the earth. If this method had not been implemented and the CO_2 produced had been allowed to escape into the atmosphere, the Sleipner West field licensees would have been required to pay NOK 1 million per day in Norwegian CO_2 taxes. Equinor operates this field and had stored more than 10 million tons of CO_2 by May 2008 (*Carbon Capture and Sequestration Technologies @ MIT,* n.d.). We used Fluid properties in Table 4-2 and rock properties of Utsira formation in Appendix A1 to generate data used in our model for the purpose of depicting a known saline aquifer characteristic. Static model shape, sizes and layers were synthetically generated to enable simple structural grids for the sensitivity studies.

4.2.3. Defining Simulation Case

The development strategy for this simulated instance is to inject 2 million standard cubic meters of CO2 daily for the period of 876 years. The long injection period allows for the CO2 to get to the spill point, since the spill point is located at Region-2 which is the lower part of the geological grid. After 876 years of injection, the well is shut off from the surface and the injected CO2 is monitored for another 50 years, then bringing the total simulation time to 926 years. Total simulation period is from arbitrary period of 1st January 2024 to 1st January 2950.

The Base case is defined in Table 4-2 below.

Table 4-2: Base parameters used in defining the simulation case in Petrel.

Properties	Descriptions	Values
Fluid Properties	Temperature	45 degrees centigrade
	Density of brine	1022 kg/m3
	Gas gravity of CO2	0.6636 sg
	Salinity	33500 ppm
Rock Property	Net to gross ratio	98 %
	Rock type	Unconsolidated Sandstone
	Porosity	36 %
	Permeability	2000 mD
	Vertical Permeability	200 mD
Saturation	S_{gcr}	0.02
	Corey gas	2.8
	$k_{rg}@S_{wmin}$	0.75
	S_{wmin}	0.11
	S_{wcr}	0.386
	Corey water	2.8
	$k_{rw}@S_{grw}$	0.54
	$k_{rw}@S_{wint}$	1
Injection Rate	Dry CO2 injection rate	2 million sm3 /day
	Maximum Bottom hole pressure constraint	500 bars

Injection starts and end date	1/1/2024 to 10/1/2900	
Total Simulation Start and end date	1/1/2024 to 10/1/2950	

4.3. Sensitivity analysis

We conducted sensitivity analyses to determine the effects of critical parameters on CO2 storage performance, such as porosity, permeability, vertical to horizontal permeability ratio (k_v/k_h), injection rates, different geological shapes, impact of porosity and injection rates on the reservoir pressure. We utilized Petrel's black oil model (BOM) to examine corresponding stored CO2 volume scenarios over time.

The results and the discussions have been explicitly presented in chapter five.

5. Results and Findings

This chapter covers the results and findings of the simulations studies carried out for CO2 dynamic storage capacity using a black oil model. In the subchapters, we have discussed how porosity, permeability, (k_v/k_h), injection rates, geological shapes affect dynamic storage capacity and further evaluated porosity and injection rates effects on the reservoir pressure over simulation period.

5.1. Analysis of Porosity Sensitivity in CO_2 Dynamic Storage Simulations

The porosity of a reservoir rock is an important element in dynamic CO_2 storage simulation studies. It directly affects the storage capacity and behavior of CO_2 inside the subsurface. Porosity affects the amount of pore space available for CO_2 storage, impacting both short-term and long-term sequestration capacity. This subchapter discusses the results of porosity sensitivity assessments in CO_2 dynamic storage models. We performed sensitivity studies on porosity effect on dynamic CO2 storage capacity by creating simulation cases for anticline structure, where porosity of 36 % were used as base data while we kept base parameters of the model as shown in Table 4-2 constant, we ran a sensitivity study by varying the porosity values 36 %, 10%, 20 %, and 40 % respectively at different simulation case to see how they affect the amount of CO2 that the anticline could store before it reaches the spill point (Region-2). Figure 5-1 below is the static grid model of the anticline at the initial condition when brine saturation was 1 (Sw=1).
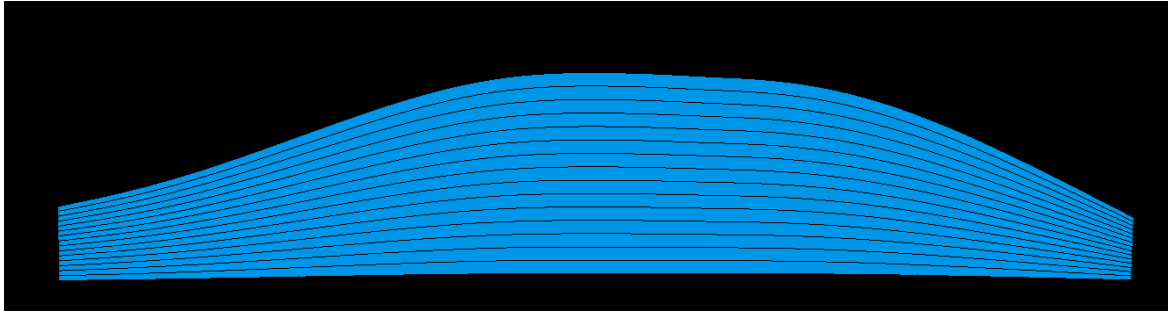
Figure 5-1: Static model of Anticline structure showing the initial water saturation of 1 (sw=1).

The dynamic simulation was carried out for nine hundred and twenty-six years which is broken down into eight hundred and seventy-six years of CO2 injection and fifty years of post-monitoring. The injection started on arbitrary date of 01/01/2024 and end on 01/01/2900, while post-injection lasted till 01701/2950.

The plume migration pattern is shown in Figure 5-2, Figure 5-3, Figure 5-4, and Figure 5-5 below with respect to different porosity values. In all cases we considered a homogenous system.
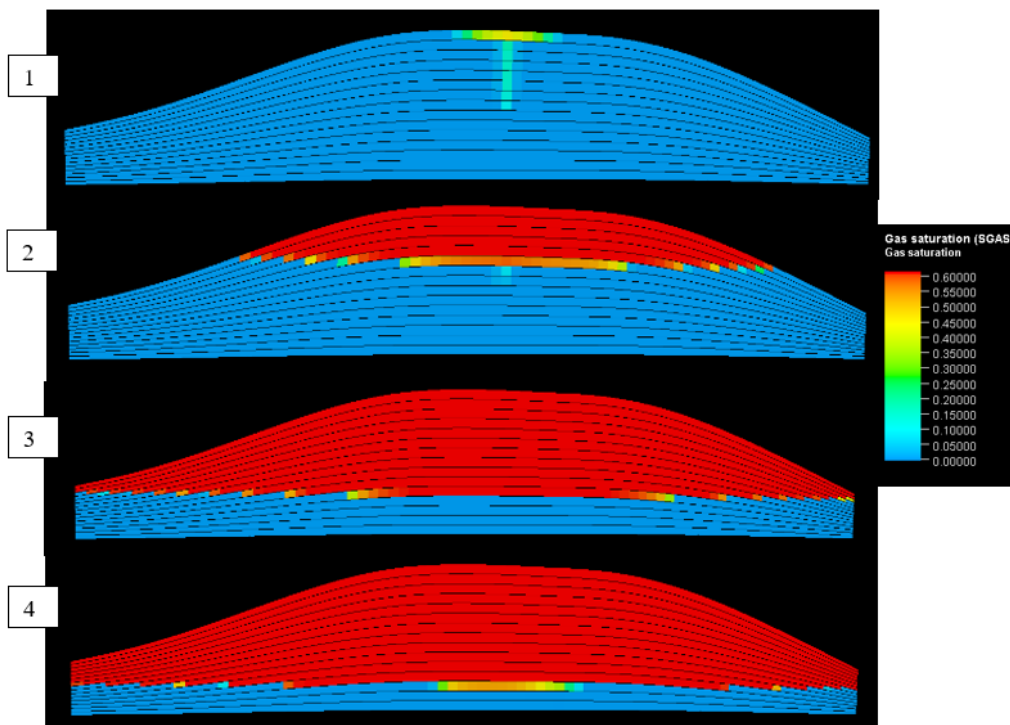
Figure 5-2: Showing 36% Porosity effect on plume distribution in the anticline structure, notation 1-depicts plume distribution after one year of injection (2025), 2 depicts plume distribution after seventy-six years of injection (2100), 3- depicts plume distribution after four hundred and seventy-six years of injection (2500), and 4-depicts plume distribution fifty years after injection (year 2950).
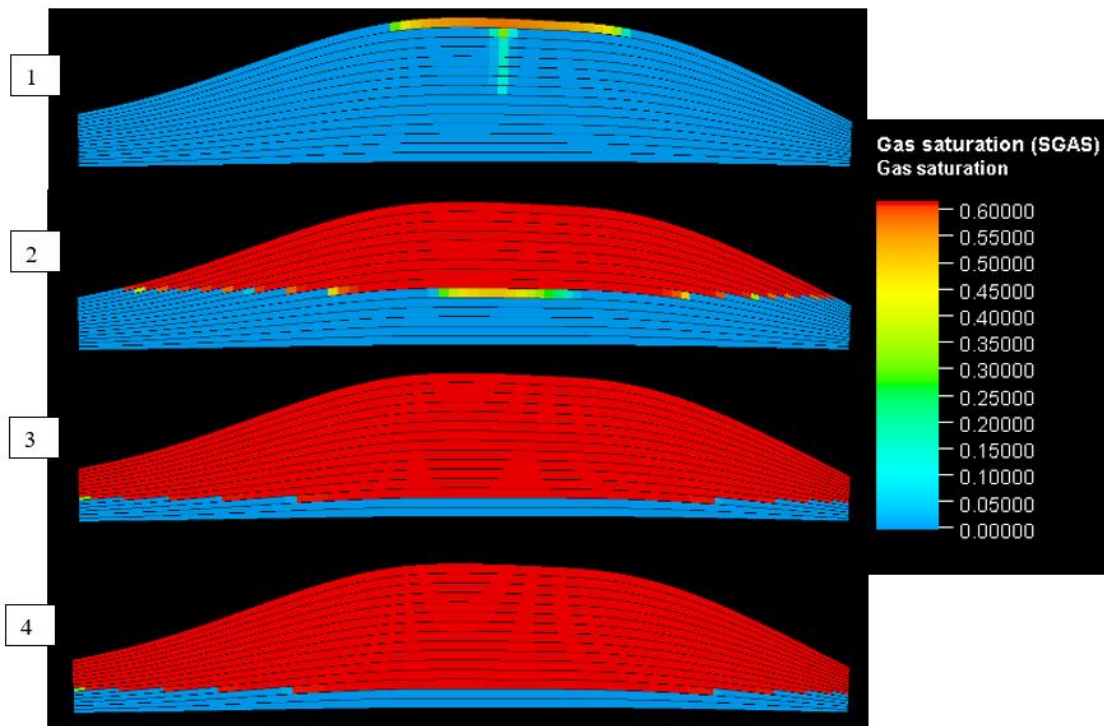
Figure 5-3: Showing 10% Porosity effect on plume distribution in the anticline structure, notation 1-depicts plume distribution after one year of injection (2025), 2-depicts plume distribution after seventy-six years of injection (2100), 3-depicts plume distribution after four hundred and seventy-six years of injection (2500), and 4-depicts plume distribution at fifty years of post-injection (year 2950).
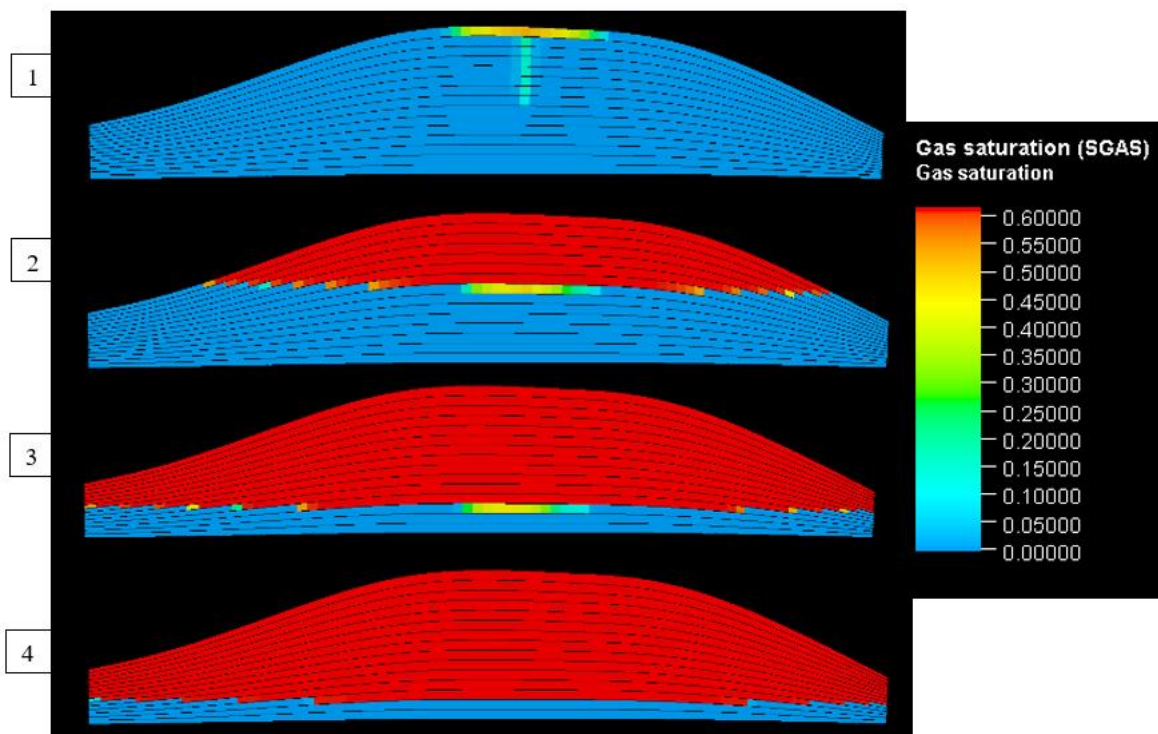
Figure 5-4: Showing 20% Porosity effect on plume distribution in the anticline structure, notation 1-depicts plume distribution after one year of injection (2025), 2-depicts plume distribution after seventy-six years of injection (2100), 3-depicts plume distribution after four hundred and seventy-six years of injection (2500), and 4 depicts plume distribution after fifty years post-injection (year 2950).

Figure 5-5: Showing 40% Porosity effect on plume distribution in the anticline structure, notation 1-depicts plume distribution after one year of injection (2025), 2-depicts plume distribution after seventy-six years of injection (2100), 3-depicts plume distribution after four hundred and seventy-six years of injection (2500), and 4-depicts plume distribution fifty years of post-injection (year 2950).

From Figure 5-2, Figure 5-3, figure 5-4 above we can see clearly that gravity flow dominates, but the CO2 plume distribution follows a particular pattern for all the porosity values considered. The advective force was initially observed at the onset of injection and overwhelmed immediately by continues gravity dominated flow until the plume reached to the top seal. On getting to the top seal, the plume spread laterally following the pattern of the top sealing structure. This confirms that structural trapping is the most dominating mechanism for CO2 storage at least for some couple of years before onset of mineralization. If the aquifer is an open boundary storage system, the CO2 plume will continue to spread laterally from the top seal to the base until it encounters a spill point which can expose the plume into escaping to other regions of the aquifer with storage potential uncertainties. In the case where the top seal integrity is questionable, the CO2 can escape the storage structure. CO2 can migrate to the top sealing surface so quickly unless encountered heterogeneity on the vertical migrating pathway.

To quantify this observed porosity effect, we investigated how different porosity values affect the storage capacity by carefully observing how much CO2 volume can be stored before a spill point and how long it will take on each porosity value for the plume distribution to reach the spill point.

The result of this capacity investigation is represented in the plots on the Figure 5.6 and Figure 5.7 which indicates effect of varying porosity values on the CO2 stored volume

versus time to reach the Spill point and effect of varying porosity on the Storage capacity of the saline aquifer respectively. At high porosity values the aquifer was able to structurally trap more volume of CO2 compared to a lower value of porosity. The same is also observed with the time to spill point. At the porosity value of 40% it took a longer time to reach to the spill point followed by 36% porosity, 20% porosity and lastly 10% porosity which reaches the spill point faster than the other porosity values. Table 5-1 shows the CO2 storage capacity and time before reaching the spill region for each porosity value.
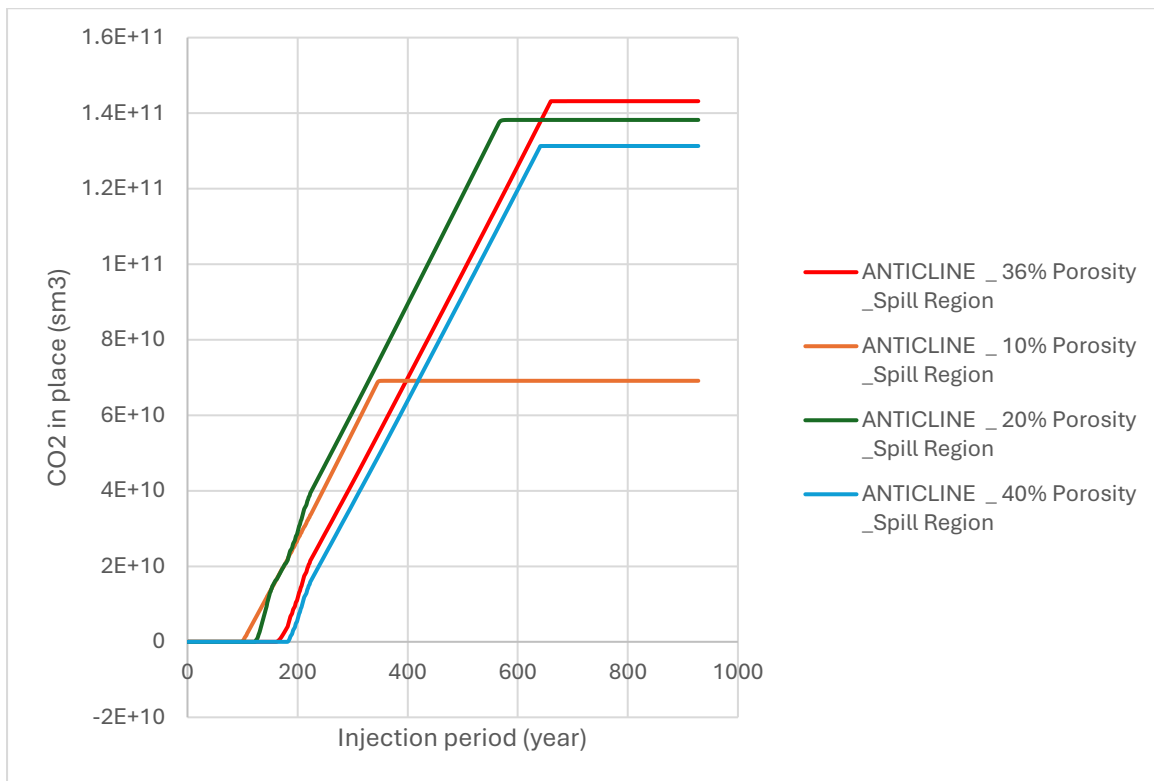
Figure 5-6: Effect of varying porosity values on the CO2 stored volume versus time to reach the Spill point.

Spill point represents the start point of Region-2 (spill region). From Figure 5-6, it can be seen that there was no CO2 in place in Region-2 for some couple of years during injection period, this is because the injected CO2 is still in the Region-1 (storage region), on continuous injection CO2 continue to saturate the formation until CO2 plume reaches the spill region (Region-2). In the CO2 volume versus time plot we are only interested in observing at what injection period does the CO2 in place stop being zero, at that point we considered it the spill time for the attributed parameter. Different porosity values have contributed to varying time for the CO2 to break to the spill point. Higher porosity values tend to delay time to spill point and encourage higher storage capacity when compared to lower porosity values. Figure 5-7 captures how the porosity contributes to the storage capacity. Change in porosity value has a great impact on the breakthrough time and capacity.
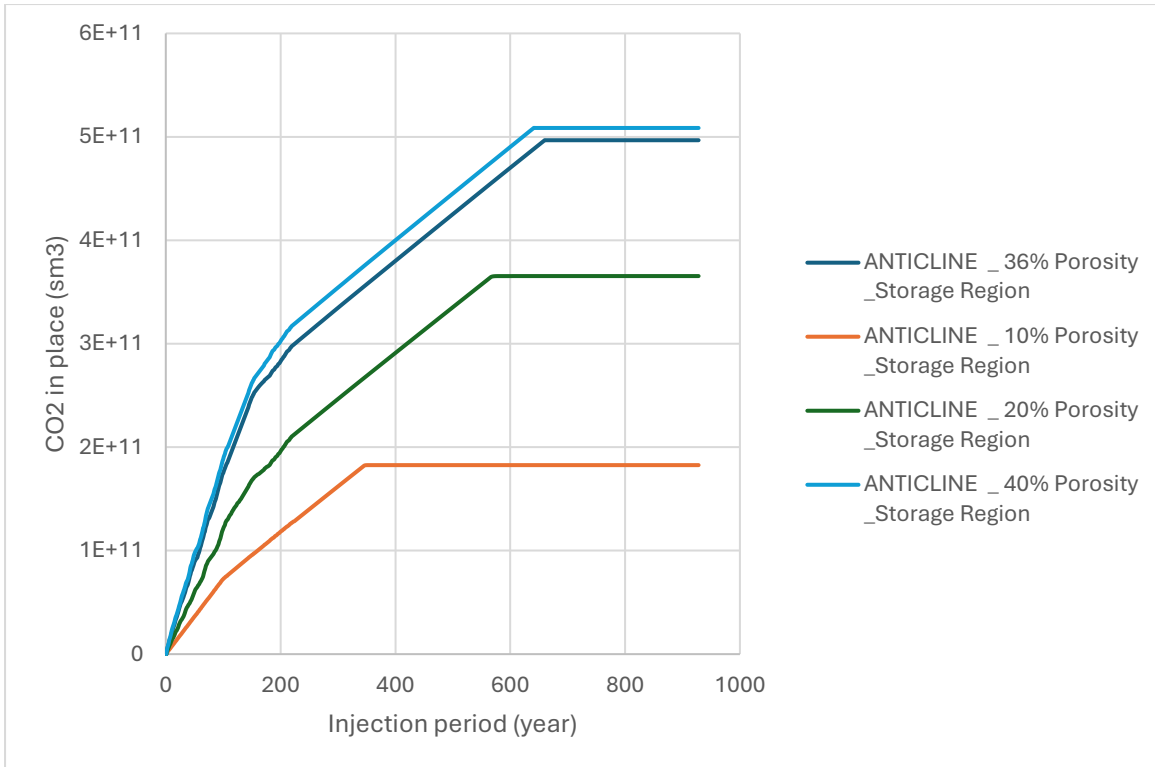
Figure 5-7: Effect of varying porosity on the Storage capacity of the saline aquifer.

From Table 5-1 below it can be seen that higher porosity values support higher storage capacity and delayed spill time. That can be said that higher pore volumes offer more space for CO2 to be stored.

Table 5-1: Storage capacity attributed to varying porosity value in a homogenous anticline reservoir before the spill point.

Porosity values	CO2 storage capacity before spill point	Time to spill point
10%	72.035 billion sm3 (134.9 M tonnes)	2024 - 2122 (98 years)
20%	143.177 billion sm3 (268.1 M tonnes)	2024 - 2145 (121 years)
36%	257.866 billion sm3 (482.9 M tonnes)	2024 - 2184 (160 years)
40%	282.709 billion sm3 (529.4 M tonnes)	2024 - 2204 (180 years)

In summary, porosity sensitivity analysis in CO_2 dynamic storage simulations relies on the advantages of obtaining an accurate characterisation of the porosities to select potential storage sites. Reservoirs have good porosity, which is suitable for large CO2 sequestration projects with the advantage of a high storage capacity and excellent CO2 diffusion as well as powerful trapping mechanisms (structural trapping). The optimization of injection tactics, the assurance of operational safety and an

economically valid CO_2 disposal can be realized on a case-by-case basis in consideration to specific reservoir characteristics

This high porosity makes it easier for the CO_2 plume to move within a single reservoir, possibly providing a mechanism by which CO_2 can diverge away from an injection well or be widely distributed in long multiple-layered storage system during course of time. That helps to spread CO_2 more evenly and keep from creating pockets of high pressure that could stress out the reservoir. The high pocket porosity values offers reduced time to spill point.

5.2. Analysis of Permeability Sensitivity in CO_2 Dynamic Storage Simulations.

To investigate the effect of permeability on the dynamic storage capacity, we applied the same method used in subchapter 5.1 for porosity sensitivity analysis, but this time we kept other parameters constant while varying the permeability values. The $k_v/k_h = 0.1$ was kept constant. We observed the plume migration pattern as seen in Figure 5-8, Figure 5-9, Figure 5-10 and Figure 5-11 below for different injection intervals and different permeability values. In all cases we considered a homogenous system.
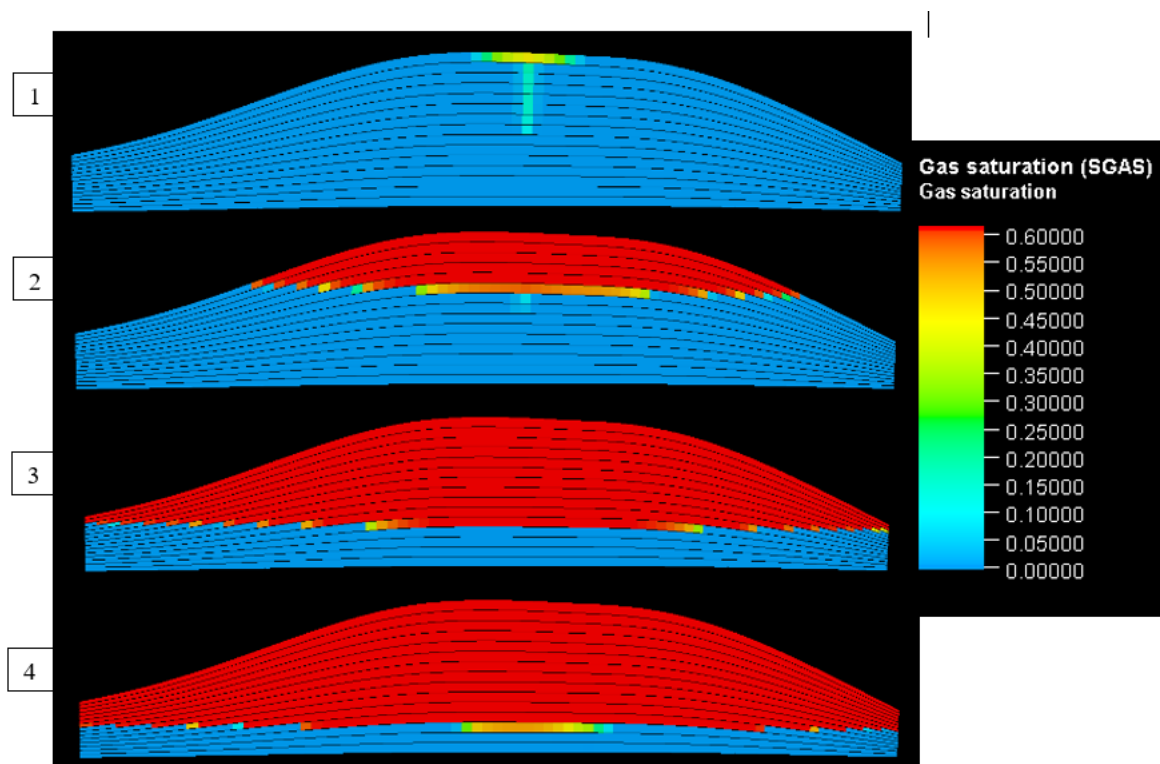
Figure 5-8: Showing 2000mD permeability effect on plume distribution in the anticline structure, notation 1-depicts plume distribution after one year of injection (2025), 2-depicts plume distribution after seventy-six years of injection (2100), 3-depicts plume distribution after four hundred and seventy-six years of injection (2500), and 4-depicts plume distribution at fifty years of post-injection (year 2950).
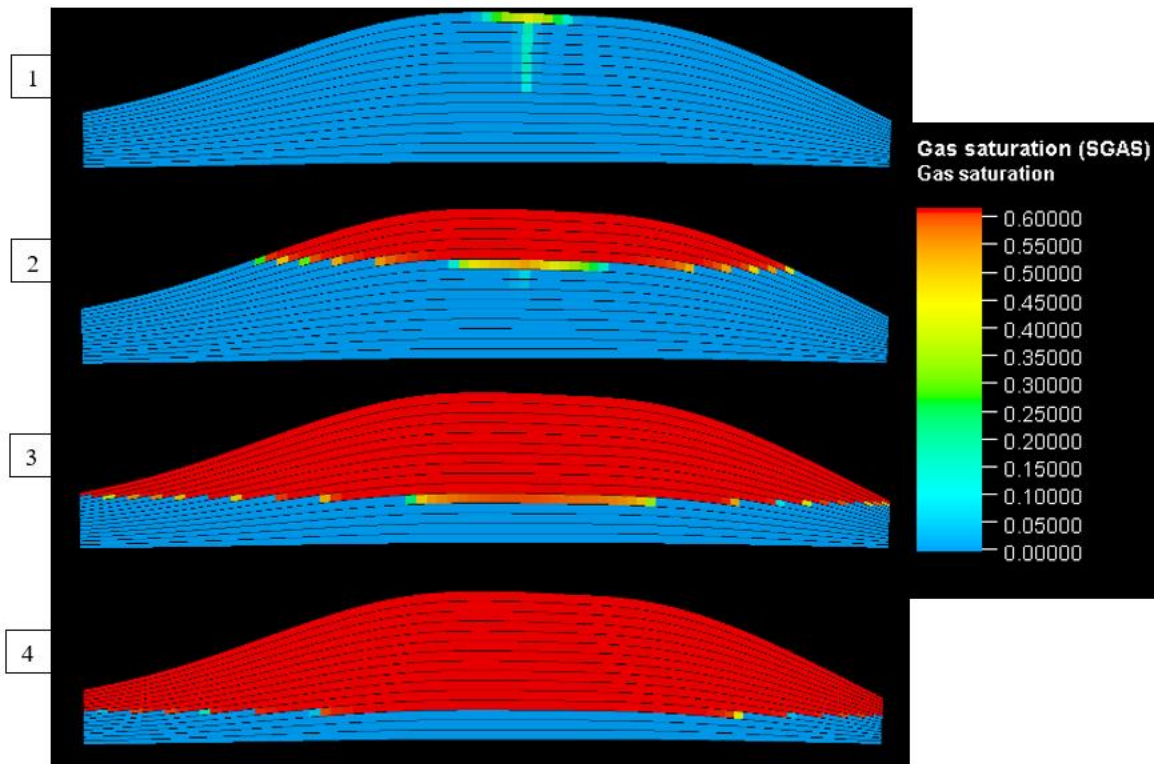
Figure 5-9: Showing 100mD permeability effect on plume distribution in the anticline structure, notation 1-depicts plume distribution after one year of injection (2025), 2-depicts plume distribution after seventy-six years of injection (2100), 3-depicts plume distribution after four hundred and seventy-six years of injection (2500), and 4-depicts plume distribution at fifty years after injection (year 2950).

Figure 5-10: Showing 800mD permeability effect on plume distribution in the anticline structure, notation 1-depicts plume distribution after one year of injection (2025), 2-depicts plume distribution after seventy-six years of injection (2100), 3-depicts plume distribution after four hundred and seventy-six years of injection (2500), and 4-depicts plume distribution fifty years after injection (year 2950).

Figure 5-11: Showing 2500mD permeability effect on plume distribution in the anticline structure, notation 1-depicts plume distribution after one year of injection (2025), 2-depicts plume distribution after seventy-six years of injection (2100), 3-depicts plume distribution after four hundred and seventy-six years of injection (2500), and 4-depicts plume distribution fifty years after injection (year 2950).

Unlike in the porosity sensitivity where the advective force was initially observed at the onset of injection and overwhelmed immediately by continues gravity dominated flow until the plume reached to the top seal, rather there was more advective dominated flow at the onset of injection for lower permeability of 100 mD and 800 mD than in the 2000 mD and 2500 mD permeability values as seen in Figure 5-8, Figure 5-9, Figure 5-10, and Figure 5-11 above. The CO_2 plume distribution follows a particular pattern vertical migration to the top seal and followed by lateral migration for all the cases considered. This shows that permeability affects the pattern of plume distributions more than porosity. On getting to the top seal, the plume spread laterally following the pattern of the top sealing structure. If the aquifer is an open boundary storage system, the CO_2 plume will continue to spread laterally from the top seal to the base until it encounters a spill point on the condition that it does not encounter heterogeneity or very low permeability structure along the distribution pattern.

We also investigated how different permeability values affect the storage capacity by carefully observing how much CO_2 volume can be stored before a spill point and how long it will take on each permeability values for the plume distribution to reach the spill point.

The result of this capacity investigation is represented in the plots on the Figure 5-12 and Figure 5-13 where effect of varying permeability values on the CO_2 stored volume versus

time to reach the Spill point and effect of varying permeability on the Storage capacity of the saline aquifer were represented respectively. Unlike in porosity sensitivity, where higher porosity values indicate high storage capacity, the effect of permeability is more significant on the time for the plume to reach the spill point. The aquifer was able to store nearly the same CO_2 capacity but on a different time interval. The same is also observed with the time to spill point, at permeability value of 2500 mD, a longer time to reach to the spill point was observed, followed by permeability of 2000 mD, 800 mD and lastly 100 mD permeability with a shorter time to spill region.
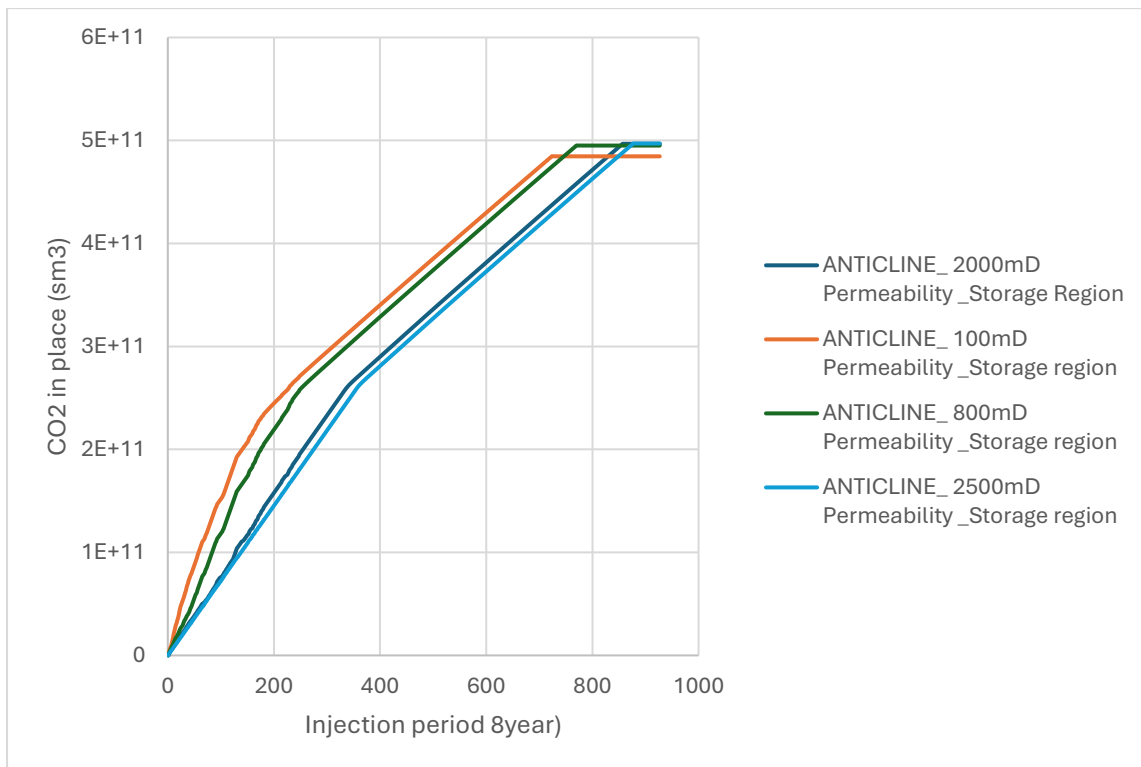
Figure 5-12: Effect of varying permeability values on the Storage capacity of the saline aquifer.
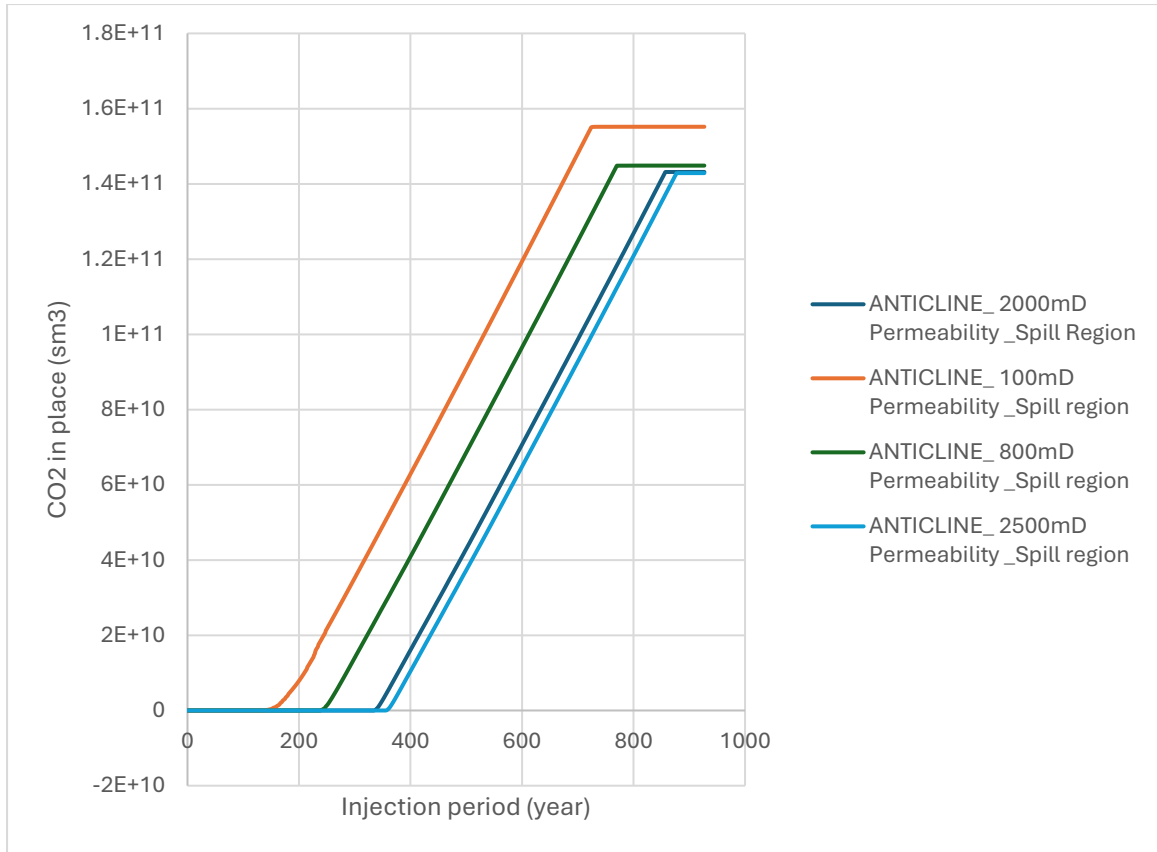
Figure 5-13: Effect of varying permeability values on the Spill time of the saline aquifer.

The Table 5-2 below gave the CO2 storage capacity and time before reaching the spill region for each permeability value.

Table 5-2: Storage capacity attributed to varying permeability value in a homogenous anticline reservoir before the spill point.

Permeability values	CO2 storage capacity before spill point	Time to spill point
100 mD	195.635 billion sm3 (366.4 M tonnes)	2024 - 2157 (133 years)
800 mD	250.544 billion sm3 (469.1 M tonnes)	2024 - 2261 (237 years)
2000 mD	257.866 billion sm3 (482.9 M tonnes)	2024 - 2357 (333 years)
2500 mD	259.319 billion sm3 (485.6 M tonnes)	2024 - 2379 (355 years)

In summary, from the capacity evaluation of geological CO2 storage by analysing the footprint of CO2 plume and storage-capacity-assigned to different permeability value at which time occurs into spoil region. In the distribution of CO2 saturation following injection and post-injection intervals from a prior viewing of figures The findings show that

the CO2 plumes are confined in space nearby their injection sites but buoyantly driven to upflow. The lack of geological barriers to vertical flow within the storage formation is a benefit in that it tends to increase upward migration. The CO2 plume is met with buoyancy on the top layer (pushing up due to significant density difference) as more and more pressure perturbation occurs during injection while post-injection, the interaction lacks any change significant change.

5.3. Sensitivity Analysis on Vertical to Horizontal Permeability Ratio on CO_2 Dynamic Storage.

We employed the same method as utilized in both porosity and permeability sensitivity studies, by keeping every other parameter constant while varying k_v/k_h values. By varying k_v/k_h ratio (0.1, 0.3, 0.1 and 1) the vertical permeability changed to (200 mD, 600 mD, 800 mD and 2000 mD) respectively while the horizontal permeability was kept constant at 2000 mD. See Figure 5-14, Figure 5-15, Figure 5-16 and Figure 5-17 for the plume distribution pattern at varying k_v/k_h values.
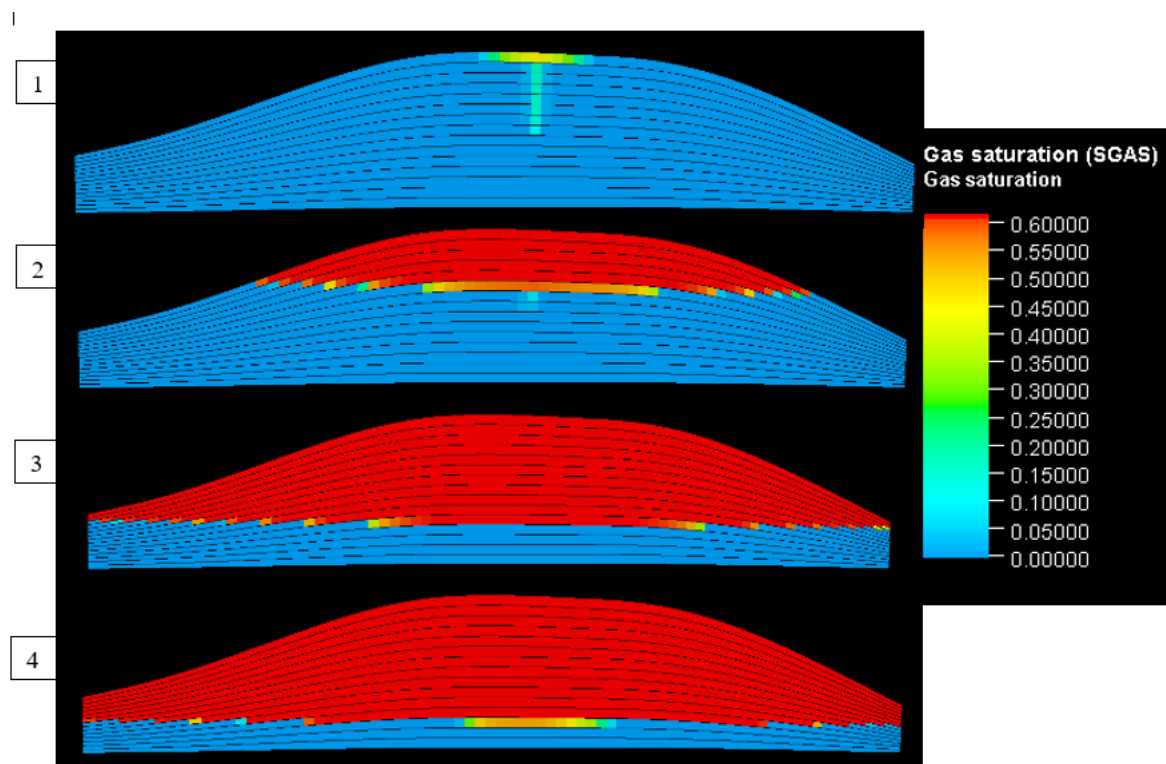
Figure 5-14: Showing Vertical to horizontal permeability ratio ($k_v/k_h = 0.1$) effect on plume distribution in the anticline structure, where notation 1-depicts plume distribution after one year of injection (2025), 2-depicts plume distribution after seventy-six years of injection (2100), 3-depicts plume distribution after four hundred and seventy-six years of injection (2500), and 4-depicts plume distribution fifty years after injection (year 2950).
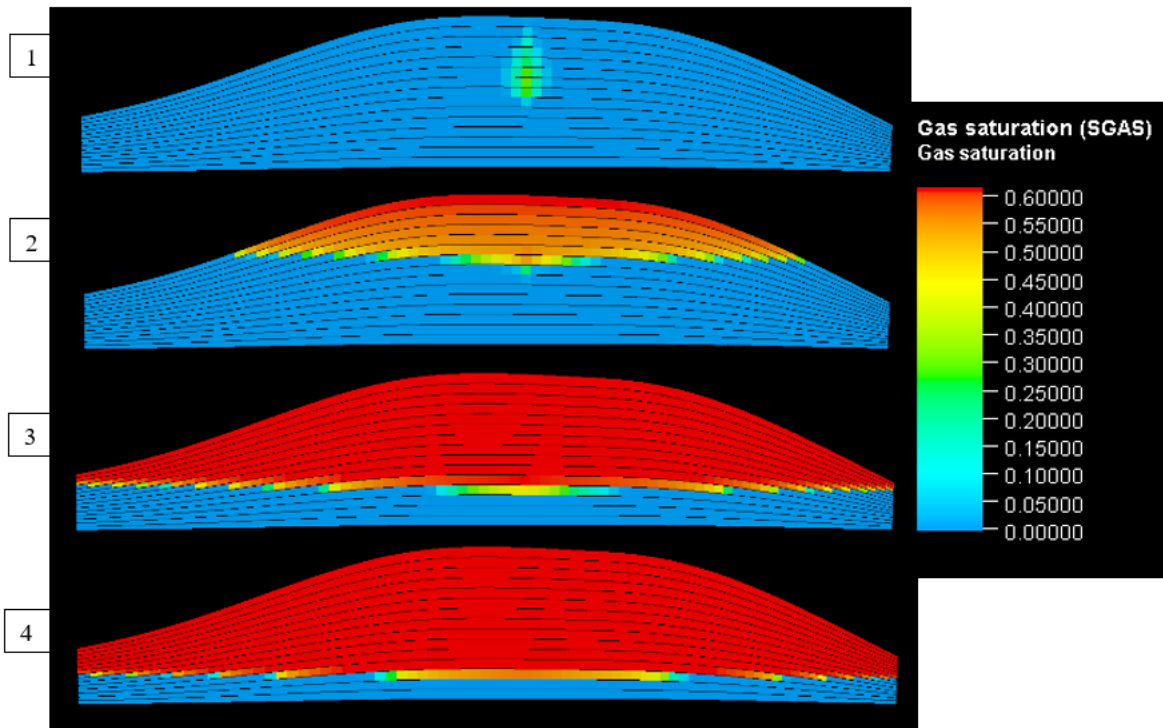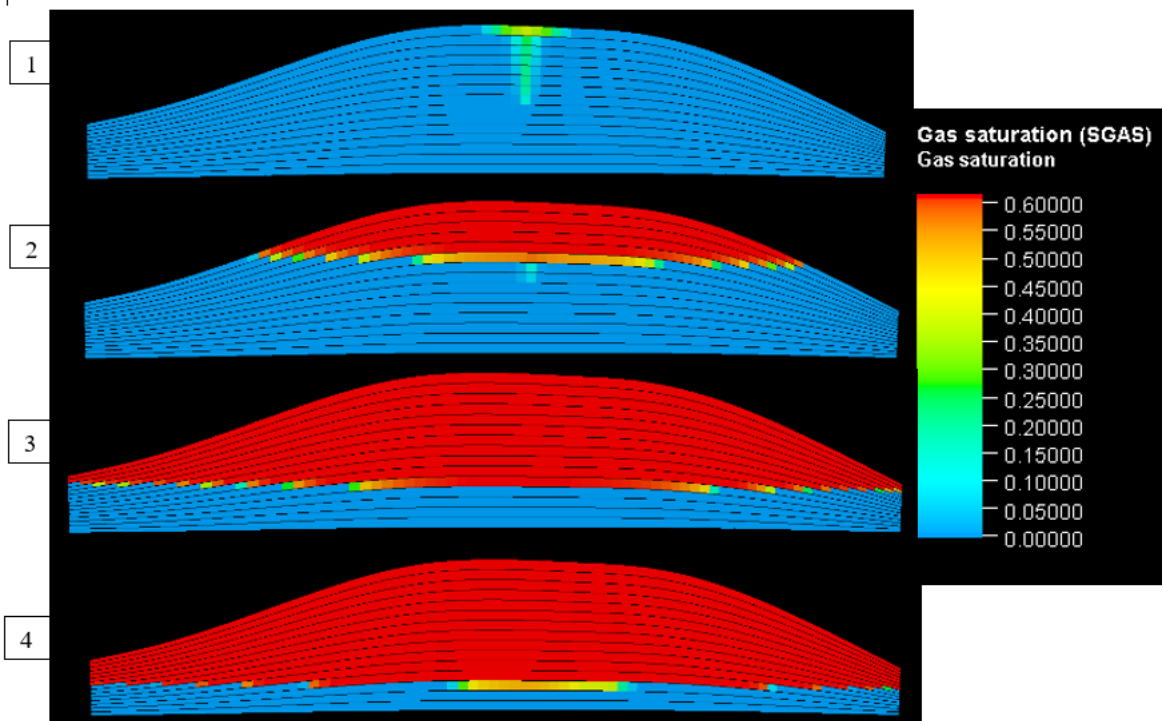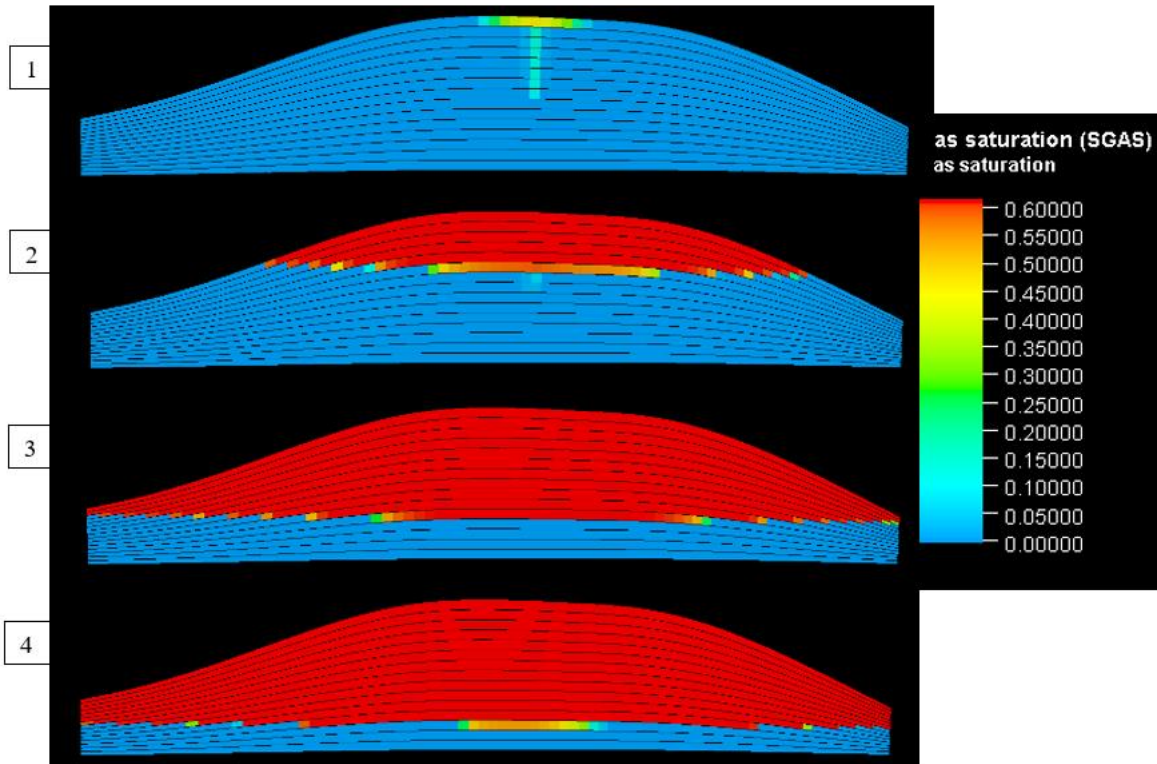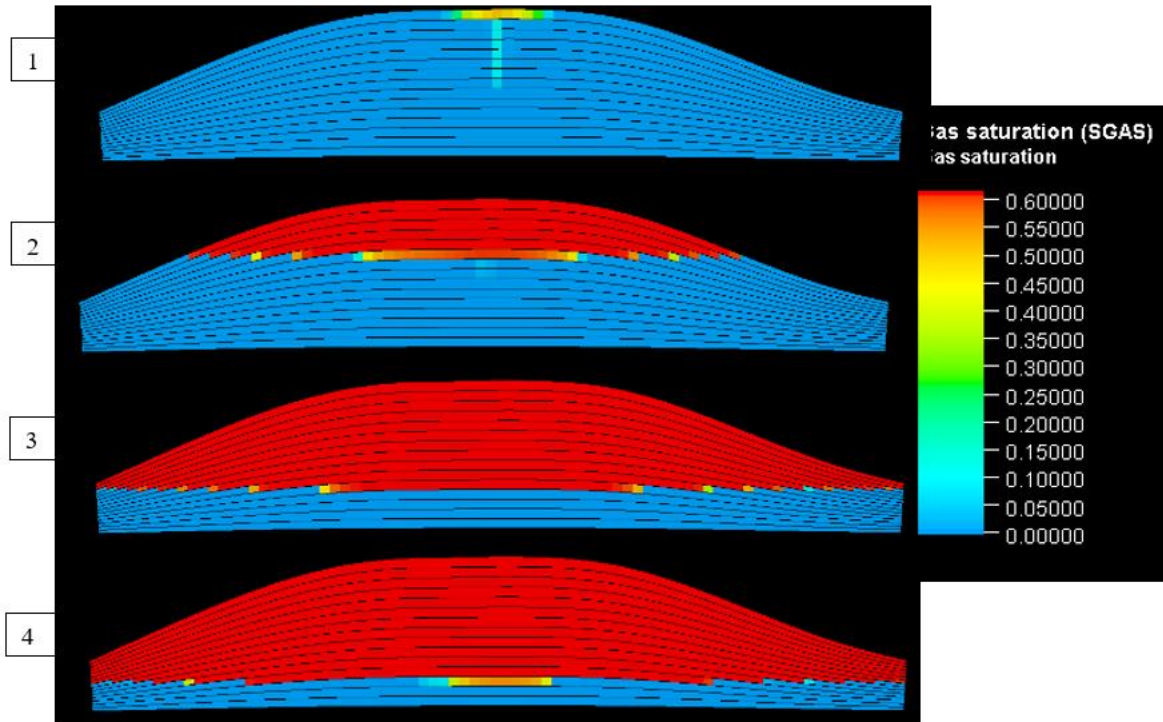
Figure 5-15: Showing Vertical to horizontal permeability ratio ($k_v/k_h = 0.3$) effect on plume distribution in the anticline structure, where notation 1-depicts plume distribution after one year of injection (2025), 2-depicts plume distribution after seventy-six years of injection (2100), 3-depicts plume distribution after four hundred and seventy-six years of injection (2500), and 4-depicts plume distribution fifty years after injection (year 2950).
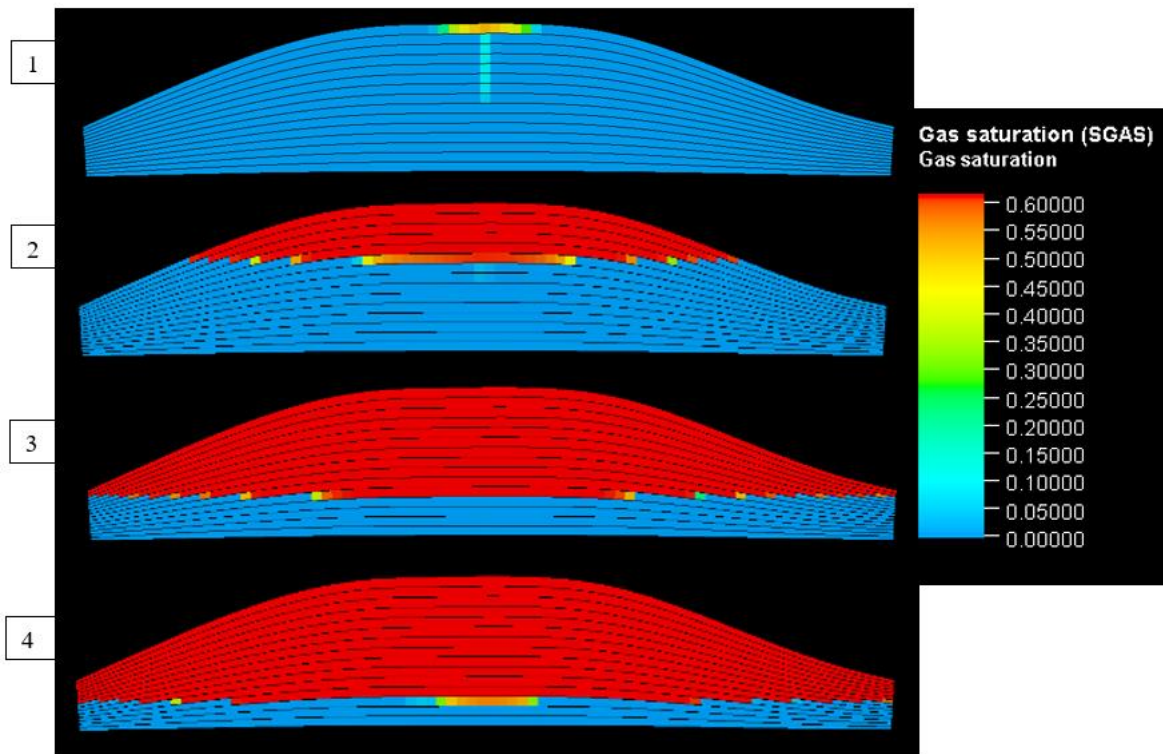
Figure 5-16: Showing Vertical to horizontal permeability ratio ($k_v/k_h = 0.4$)effect on plume distribution in the anticline structure, where notation 1-depicts plume distribution after one year of injection (2025), 2-depicts plume distribution after seventy-six years of injection (2100), 3-depicts plume distribution after four hundred and seventy-six years of injection (2500), and 4-depicts plume distribution fifty years after injection (year 2950).
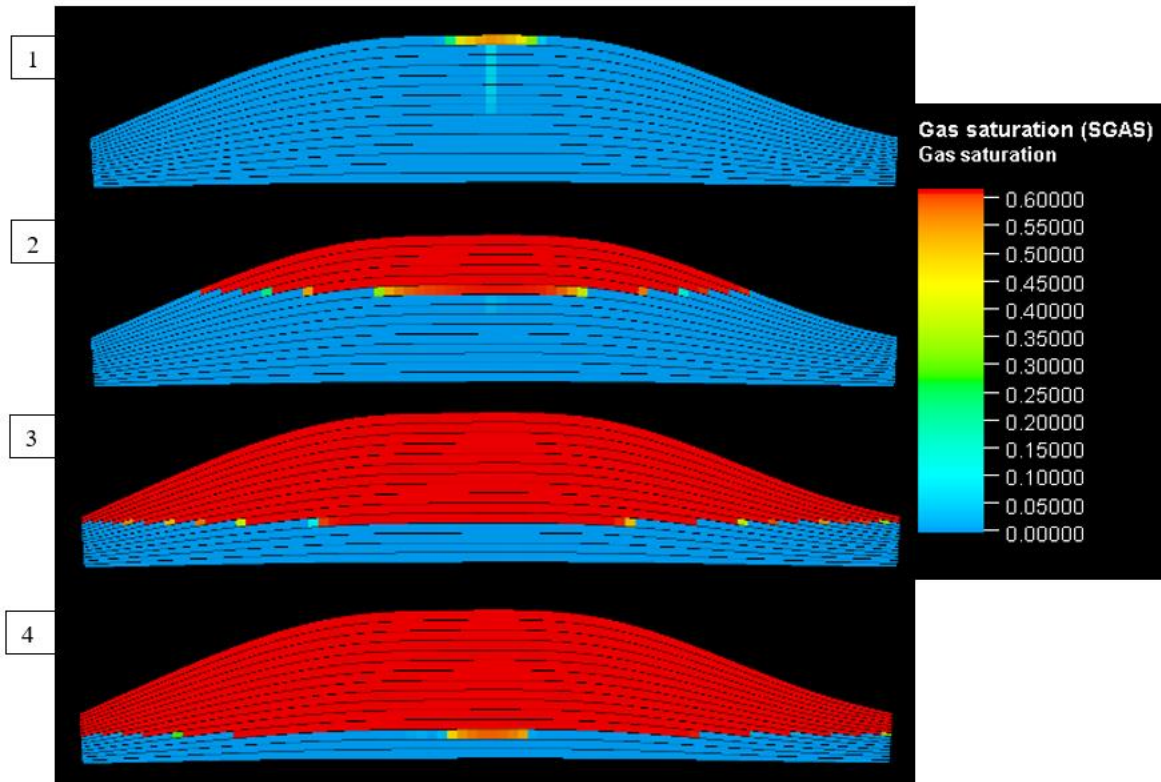
Figure 5-17: Showing Vertical to horizontal permeability ratio ($k_v/k_h = 1$) effect on plume distribution in the anticline structure, where notation 1-depicts plume distribution after one year of injection (2025), 2-depicts plume distribution after seventy-six years of injection (2100), 3-depicts plume distribution after four hundred and seventy-six years of injection (2500), and 4-depicts plume distribution fifty years after injection (year 2950).

The pattern of plume distribution with respect of varying vertical to horizontal permeability values did not show significant change, likely because the natural dominance flow pattern for CO2 in the subsurface is gravity flow, where density difference come into play. This signifies that the injection fluid property is more significant than k_v/k_h with respect to plume distribution and at high reservoir permeability. Maybe at lower reservoir permeability (permeability less than 50 mD), the effect of k_v/k_h can be more evident.

Figure 5-18 shows that all the values of k_v/k_h considered can accommodate almost the same CO2 capacity but at varying time to reach maximum capacity. This is more revealed in the Figure 5-19 where higher values of k_v/k_h show delayed time to spill point with the lower values showing quicker breakthrough time to the spill point.
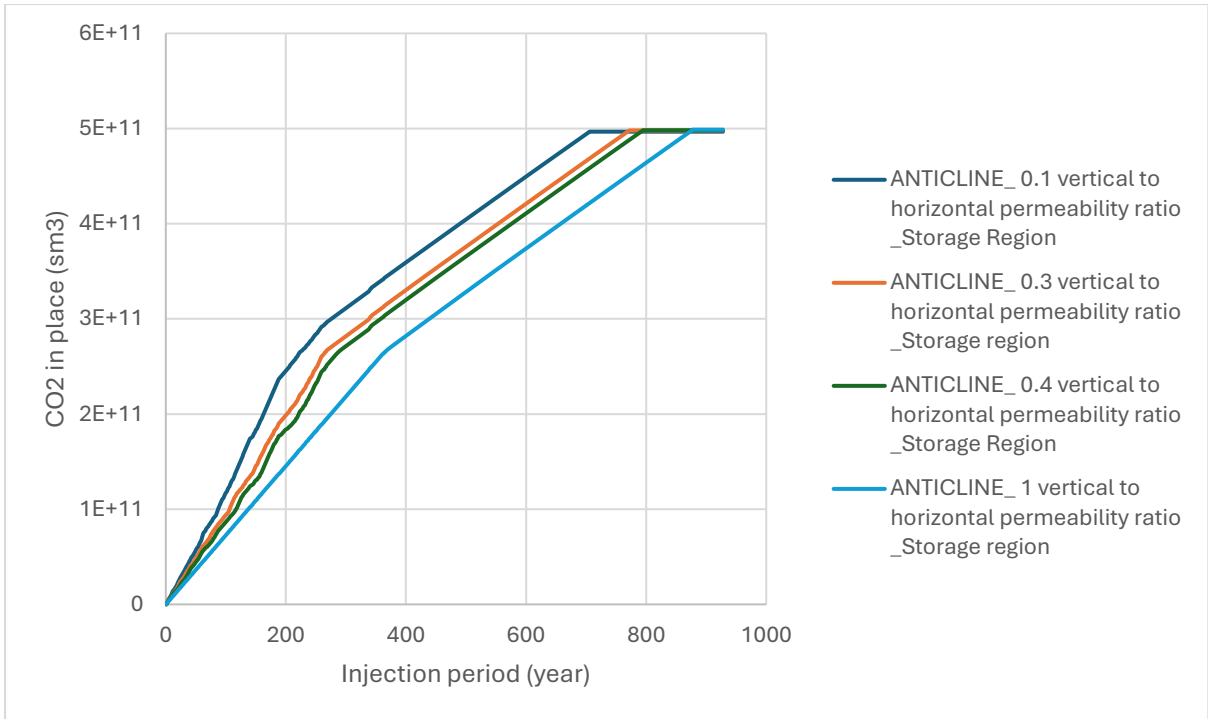
Figure 5-18: Effect of varying vertical to horizontal permeability ratio on the Storage capacity of the saline aquifer.
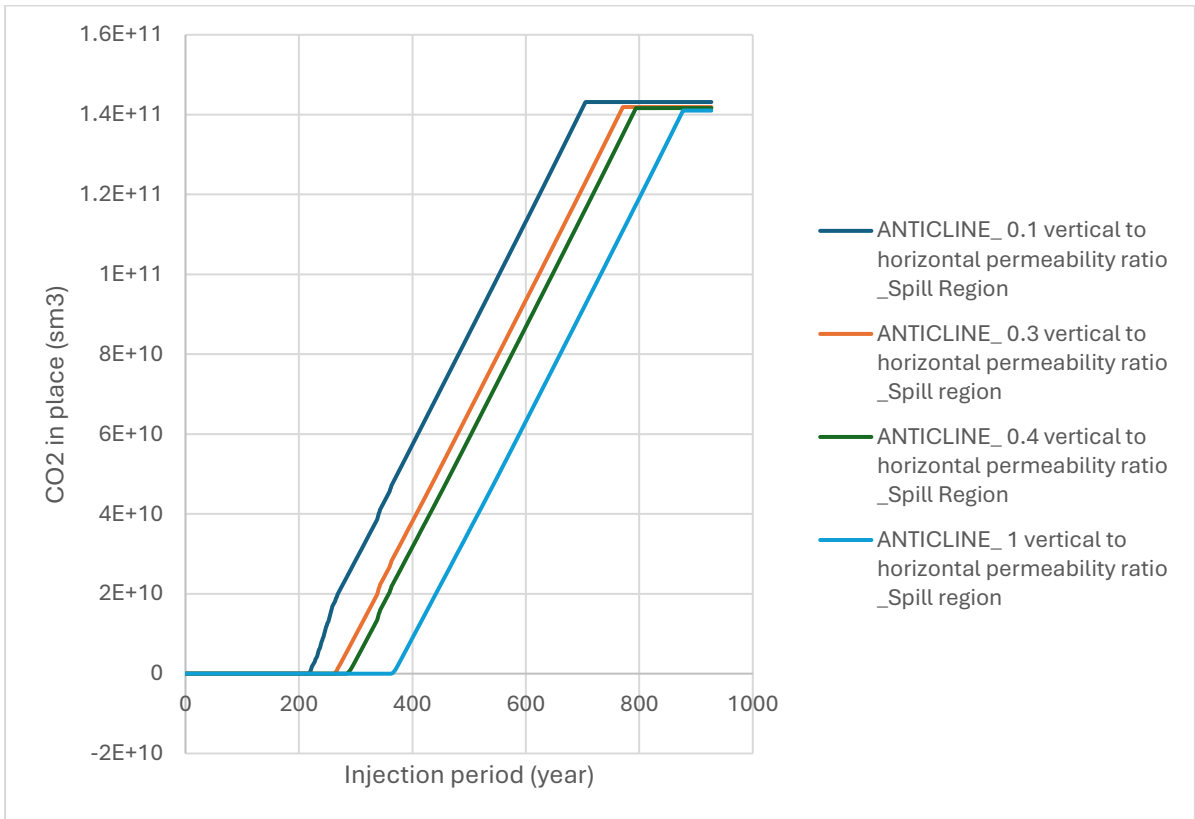
Figure 5-19: Effect of varying vertical to horizontal permeability ratio on the Spill time of the saline aquifer.

In the Table 5-3 below, we enumerated the storage capacity attributed to each vertical to horizontal permeability ratio.

Table 5-3: Storage capacity attributed to varying vertical to horizontal permeability ratio in the anticline reservoir.

Kv/kh values	CO2 storage capacity before spill point	Time to spill point
0.1	257.866 billion sm3 (482.9 M tonnes)	2024 - 2239 (215 years)
0.3	262.218 billion sm3 (491.0 M tonnes)	2024 - 2285 (261 years)
0.4	262.952 billion sm3 (492.4 M tonnes)	2024 - 2307 (283 years)
1	264.780 billion sm3 (495.8 M tonnes)	2024 - 2386 (362 years)

To conclude, the only functional correlation is between k_v/k_h ratio and how quickly CO2 takes to migrate into a plume over to the spill point rather than storage capacity. This stresses the significance of accounting for reservoir permeability and fluid nature in dynamic CO2 storage evaluations.

5.4. Sensitivity result of Injection rate on CO_2 Dynamic Storage Simulations

Injection rate is an important factor which affect the flow dynamics of CO2 storage in a saline reservoir. It directly affects the pressure build-up, plume migration and storage efficiency in general. These are some general observations on the impact of injection rate upon dynamic storage capacity for CO2 evaluated.

Faster reservoir pressure increases due to higher injection rates which can lead to a rapid migration of the plume CO2 and raise potential risks like caprock fracture if pressures exceed, e.g., the capillary entry pressure. On the other hand, lower injection rates mean a slower pressure buildup and eventually less risk of failure. High rates of injection also make the CO2 plume spread faster, which made the plume to reach the spill region quickly. Lower injection rates are consistent with a slower moving plume and tend to stabilise the flow and encourages for storage capacity. Although slower injection rates can reduce early time breakthrough, they may also result in lower initial storage volumes, but it suggests to improves the architecture of slow trapping processes by allowing a long time to ensures that the injected CO2 dissolves into formation brine and reacts with minerals, for more secure storage in the longer term.

Though, a quicker injection rate could give CO2 lower operational time in the process of having to be injected which then can help reduce short term operating costs. Nevertheless, it could be made up by the added risk of storage failure and more monitoring. In contrast, lower injection rates result in longer injection durations that could increase operational costs but may mitigate the extent of long-term leakage liability.

From Figure 5-20 to Figure 5-23, it can be seen that higher injection rate indicates more rapid spready of the plume while initiating higher capacity at the early stage of injection but induced a the shortest time to the spill point. The smallest injection rates indicated a good compromise between capacity and time to spill point. With 500 thousand standard cubic meters per day injection rate, the plume will not get to the spill region throughout the injection and simulation period. See Table 5-4 for the capacity associated with each injection rate before the plume extends to the spill region.
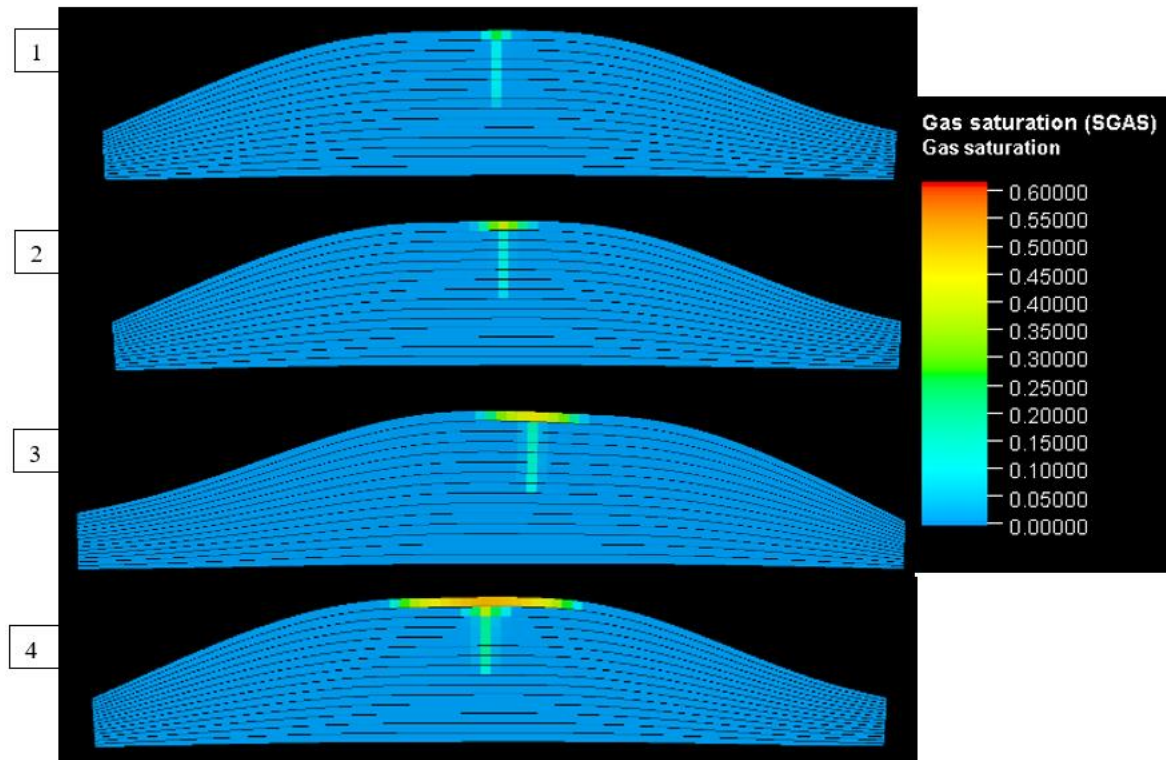
Figure 5-20: Showing Effect of injection rate on plume distribution in the anticline structure after one year (year 2025) of injection, where notation 1 depicts plume distribution due to 0.5 million sm3/day of injected CO2, 2 depicts plume distribution due to 1 million sm3/day of injected CO2, 3 depicts plume distribution due to 2 million sm3/day of injected CO2, and 4 depicts plume distribution due to 5 million sm3/day of injected CO2.

Figure 5-21: Showing Effect of injection rate on plume distribution in the anticline structure after seventy-six years (year 2100) of injection, where notation 1 depicts plume distribution due to 0.5 million sm3/day of injected CO2, 2 depicts plume distribution due to 1 million sm3/day of injected CO2, 3 depicts plume distribution due to 2 million sm3/day of injected CO2, and 4 depicts plume distribution due to 5 million sm3/day of injected CO2.

Figure 5-22: Showing Effect of injection rate on plume distribution in the anticline structure after four hundred and seventy six years (year 2500) of injection, where notation 1 depicts plume distribution due to 0.5 million sm3/day of injected CO2, 2 depicts plume distribution due to 1 million sm3/day of injected CO2, 3 depicts plume distribution due to 2 million sm3/day of injected CO2, and 4 depicts plume distribution due to 5 million sm3/day of injected CO2.

47

Figure 5-23: Showing Effect of injection rate on plume distribution in the anticline structure after 50 year (year 2950) of post injection, where notation 1 depicts plume distribution due to 0.5 million sm3/day of injected CO2, 2 depicts plume distribution due to 1 million sm3/day of injected CO2, 3 depicts plume distribution due to 2 million sm3/day of injected CO2, and 4 depicts plume distribution due to 5 million sm3/day of injected CO2.
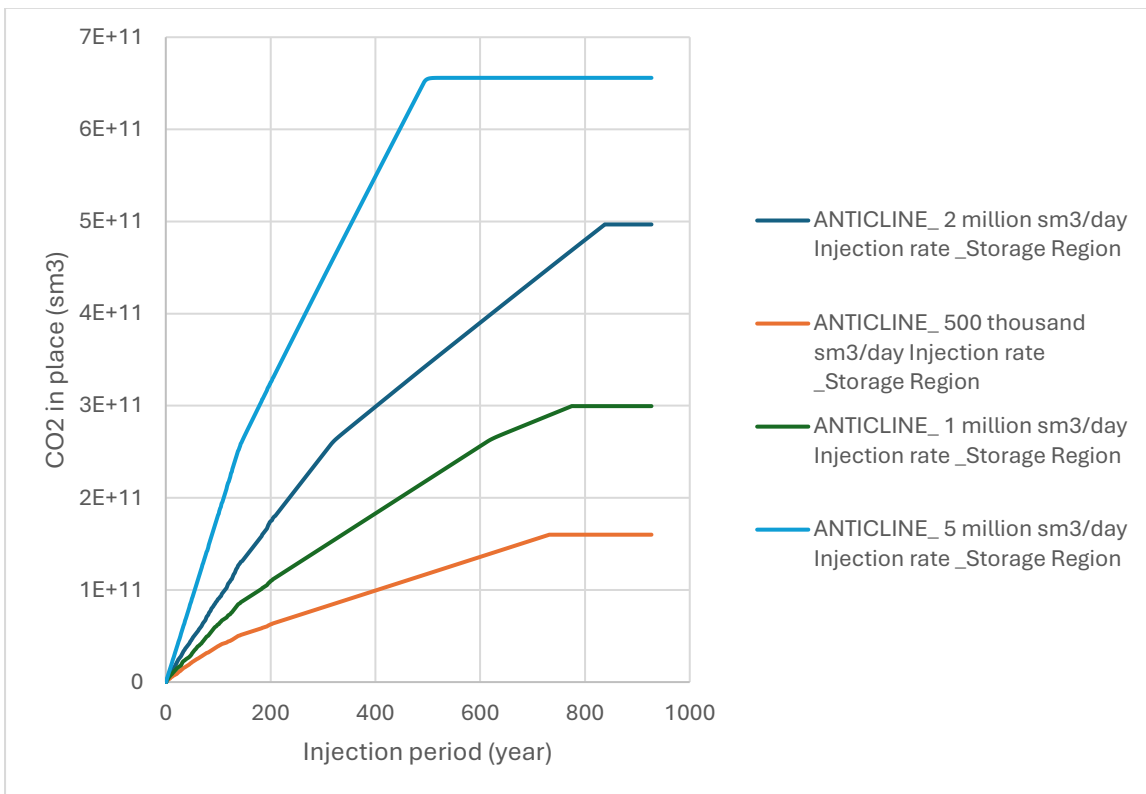
Figure 5-24: Effect of different injection rates on the Storage capacity of the anticline saline aquifer.

The Figure 5-24 above confirms how high capacity is attributed to higher injection while below Figure 5-25 shows though higher injection rates contributes to higher capacity initially but resulted to shortest time to the spill region. The lowest injection rate offered the capacity that never extends to the spill point.
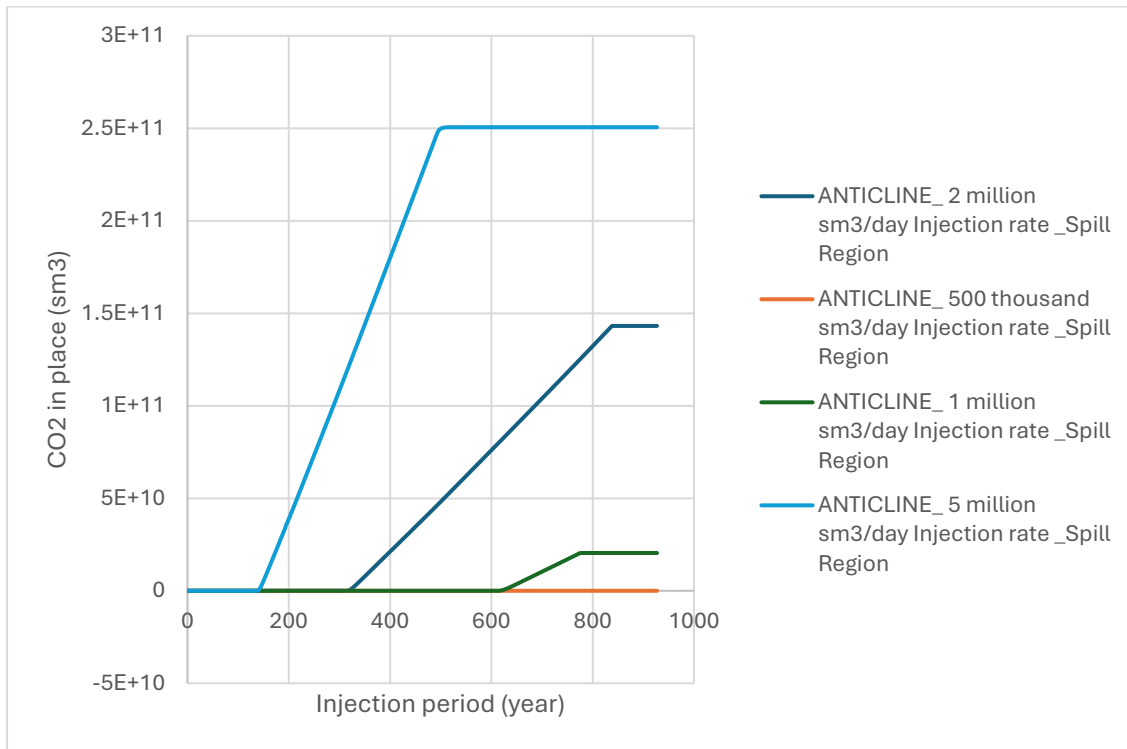
Figure 5-25: Effect of different injection rates on the Spill time of the anticline saline aquifer.

Table 5-4: Storage capacity attributed to varying injection rate in the anticline reservoir before the spill point.

Injection rate	CO2 storage capacity before spill point	Time to spill point
0.5 million sm3/day	> 159.985 billion sm3 (482.9 Mt)	> 876 years
1 million sm3/day	265.382 billion sm3 (496.9 Mt)	2024 - 2652 (628 years)
2 million sm3/day	257.866 billion sm3 (482.9 Mt)	2024 - 2357 (333 years)
5 million sm3/day	255.090 billion sm3 (477.7 Mt)	2024 - 2189 (165 years)

In summary, the injection rate is a key parameter in CO2 dynamic storage process in saline aquifers. This directly impacts overpressure, plume migration, entrapment efficiency and the performance of different trap types. The CO2 storage assessment needs to address both short and long-term performance, so a reasonable balance of high

efficiency for operation in the close future as well as permanent secure storing could be established.

5.5. Analysis of effect of different Geological Structure on storage capacity.

To carry out these studies we developed six static models of different structures, such as, circular structure (radial), rectangular structure with no dip angle, rectangular structure with 10-degree dip, rectangular structure with 25-degree dip, rectangular structure with 40-degree dip, and an anticline structure. We excluded the effect of aquifer in this simulation by excluding aquifer in the simulation case, rather we introduced a pressure constraint of 500 bars, which stops the injection once the reservoir pressure builds up to 500 bars making effect of geological shape on dynamic CO_2 capacity storage a close boundary system. We used the base case parameters to develop the dynamic model with CO_2 injection period from year 2024 to year 2900 with extra 50 years of monitoring (2950). We observed the plume distribution over the simulation and shut-in period and compare the time taken for the plume to reach the spill point in each geological structure. All the structures have 9.6 billion cubic meters reservoir volume with 67 % of the volume designated for the storage region (Region-1) and the remaining 33 % assigned as the spill region (Region-2). The CO_2 injector is placed at the middle of all the models within Region-1 and above Region-2, with 50 m perforation. See Figure 5.32, figure 5.6, figure 5.7 below indicating effect of structural shape on plume distribution after one year (year 2025), seventy-six years (year 2100), four hundred and seventy-six years (year 2500) of injection, and fifty years (year 2950) of post injection.
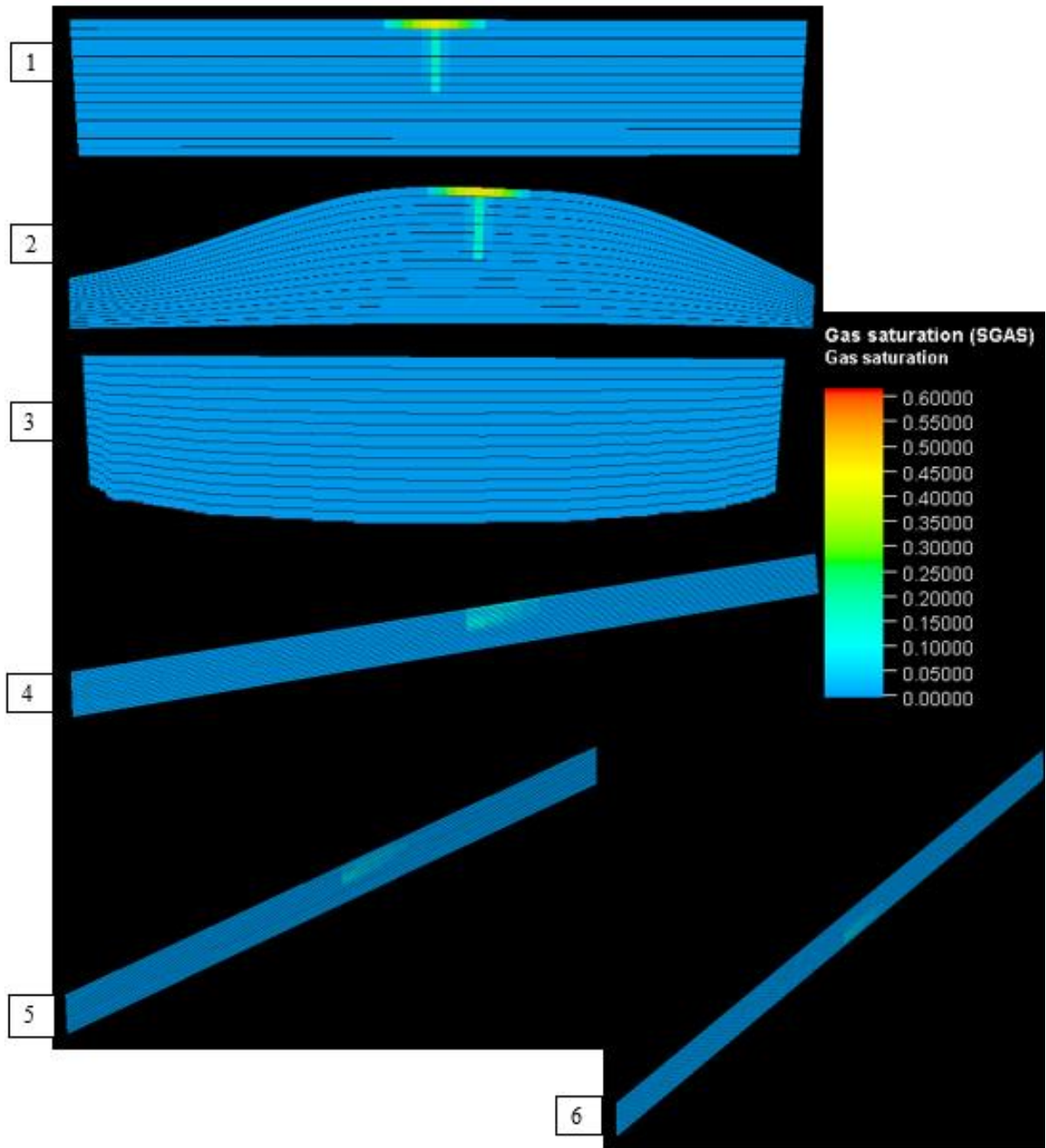
Figure 5-26: Showing Effect of structural shape on plume distribution after one year (year 2025) of injection, where notation 1 depicts plume distribution in rectangular structure with no dip, 2 depicts plume distribution in anticline structure, 3 depicts plume distribution in radial structure, 4 depicts plume distribution in rectangular structure having 10 dip angle, 5 depicts plume distribution in rectangular structure having 25 dip angle, and 6 depicts plume distribution in rectangular structure having 40 dip angle.
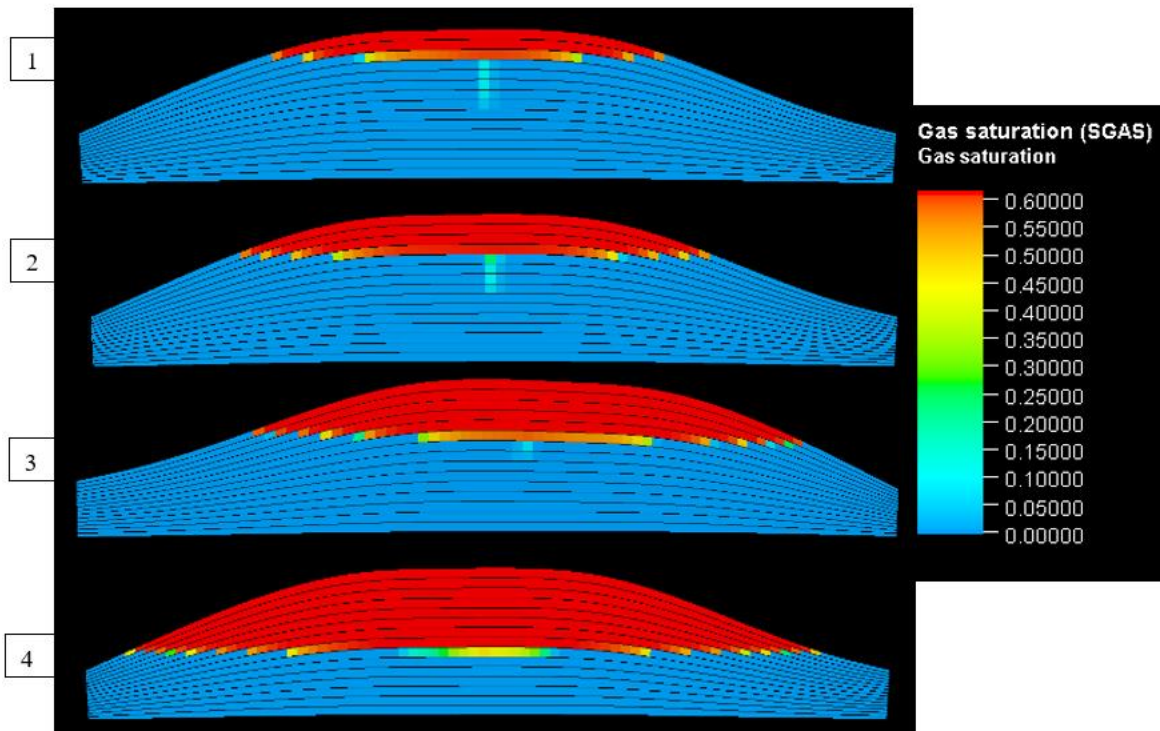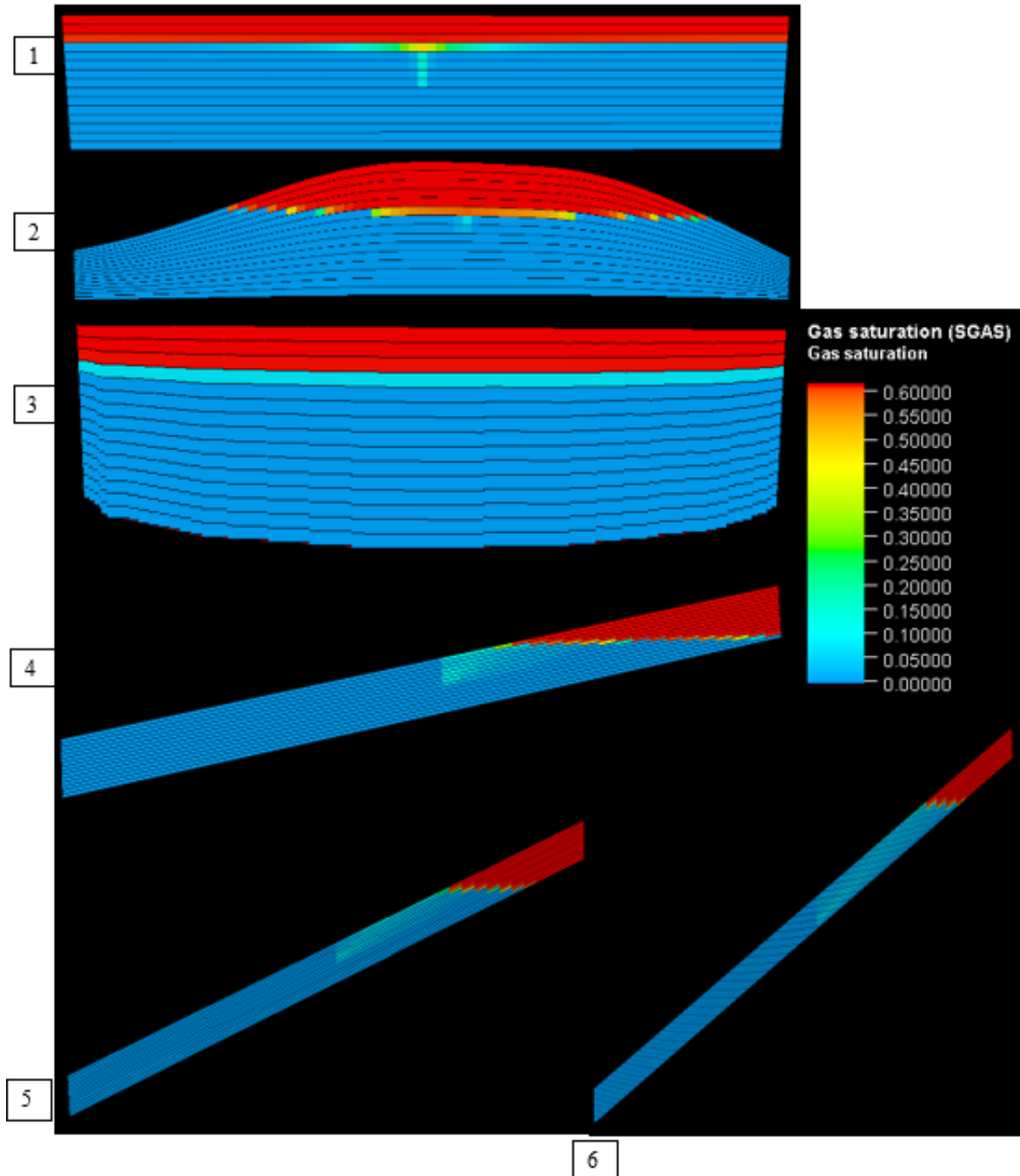
Figure 5-27: Showing Effect of structural shape on plume distribution in the anticline structure after seventy six years (year 2100) of injection, where notation 1 depicts plume distribution in rectangular structure with no dip, 2 depicts plume distribution in anticline structure, 3 depicts plume distribution in radial structure, 4 depicts plume distribution in rectangular structure having 10 dip angle, 5 depicts plume distribution in rectangular structure having 25 dip angle, and 6 depicts plume distribution in rectangular structure having 40 dip angle.
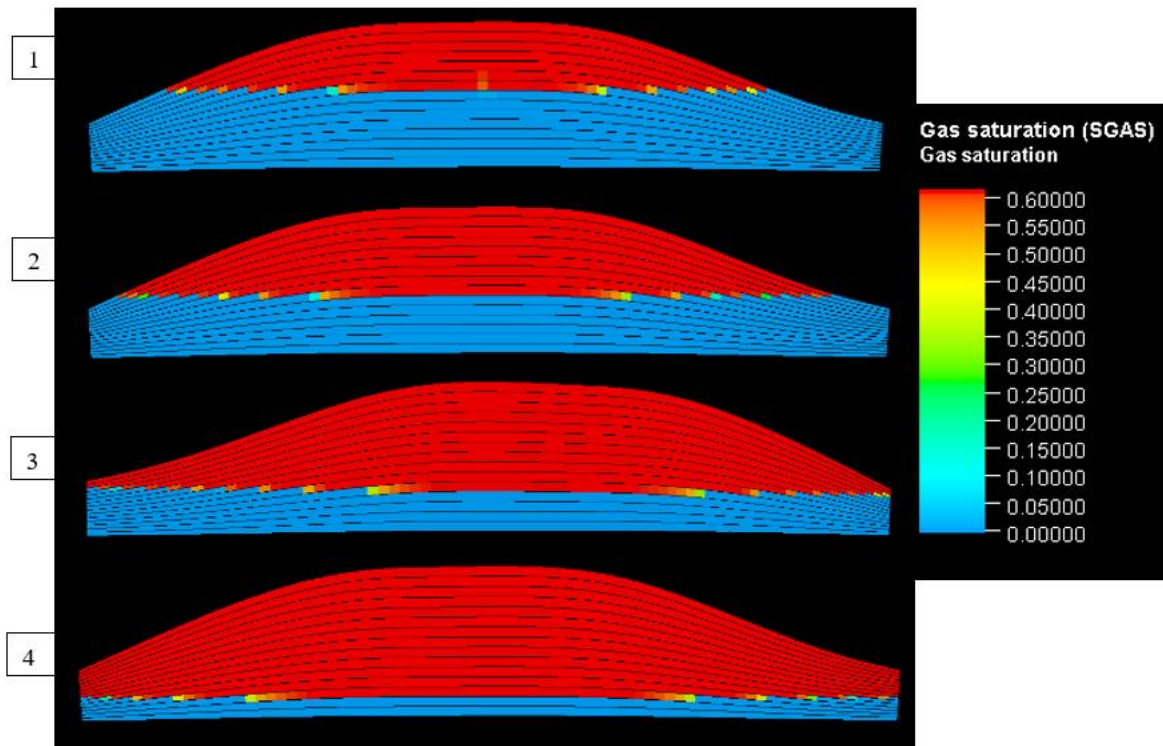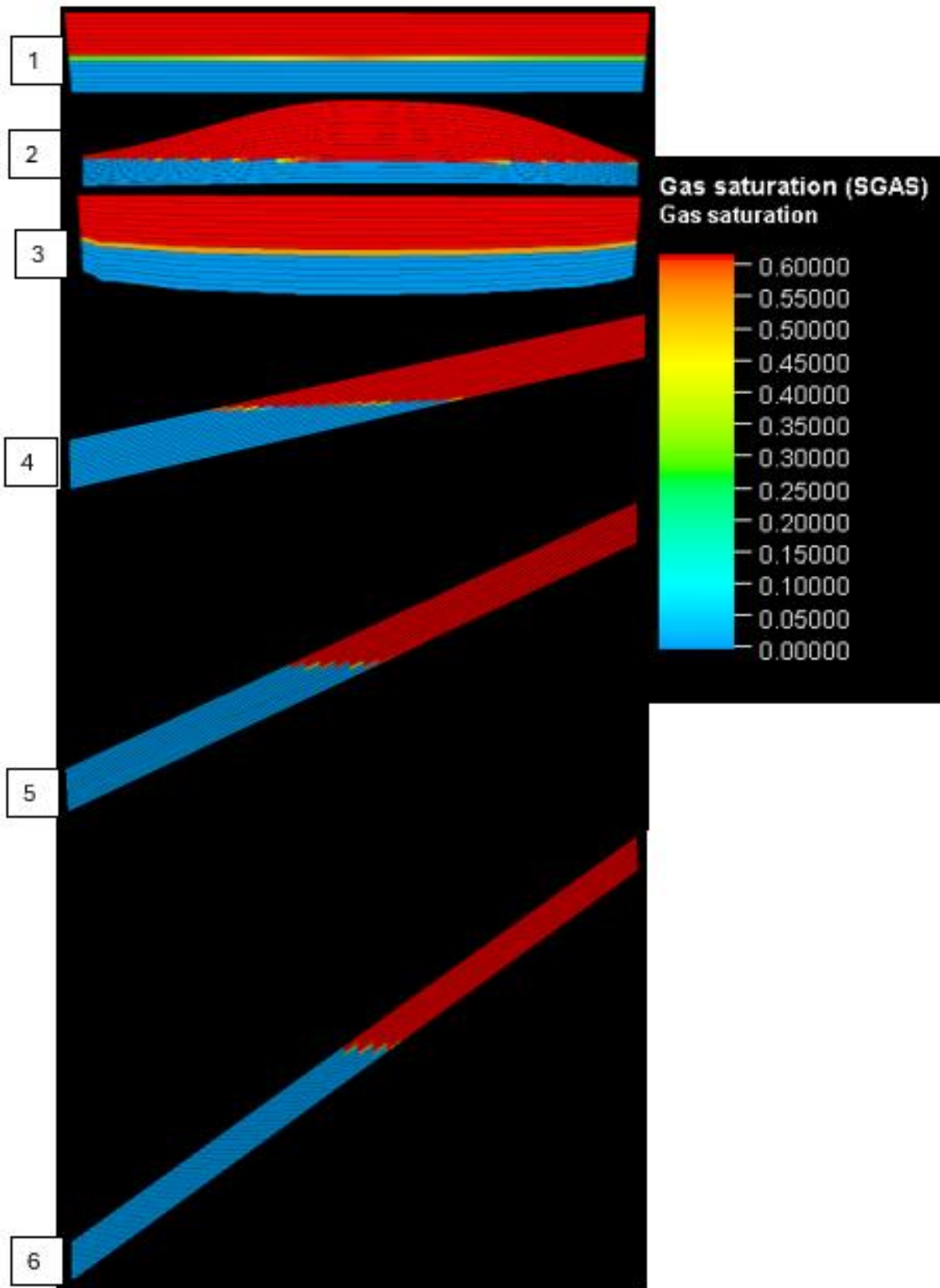
Figure 5-28: Showing Effect of structural shape on plume distribution in the anticline structure after four hundred and seventy six years (year 2500) of injection, where notation 1 depicts plume distribution in rectangular structure with no dip, 2 depicts plume distribution in anticline structure, 3 depicts plume distribution in radial structure, 4 depicts plume distribution in rectangular structure having 10 dip angle, 5 depicts plume distribution in rectangular structure having 25 dip angle, and 6 depicts plume distribution in rectangular structure having 40 dip angle.
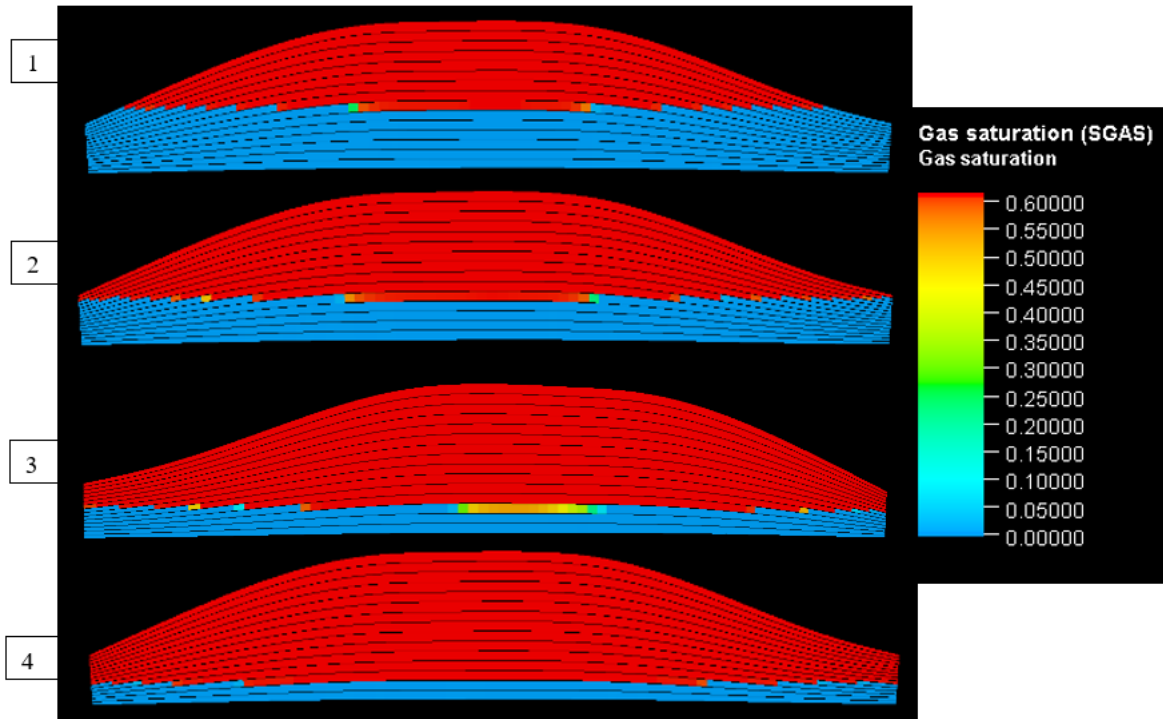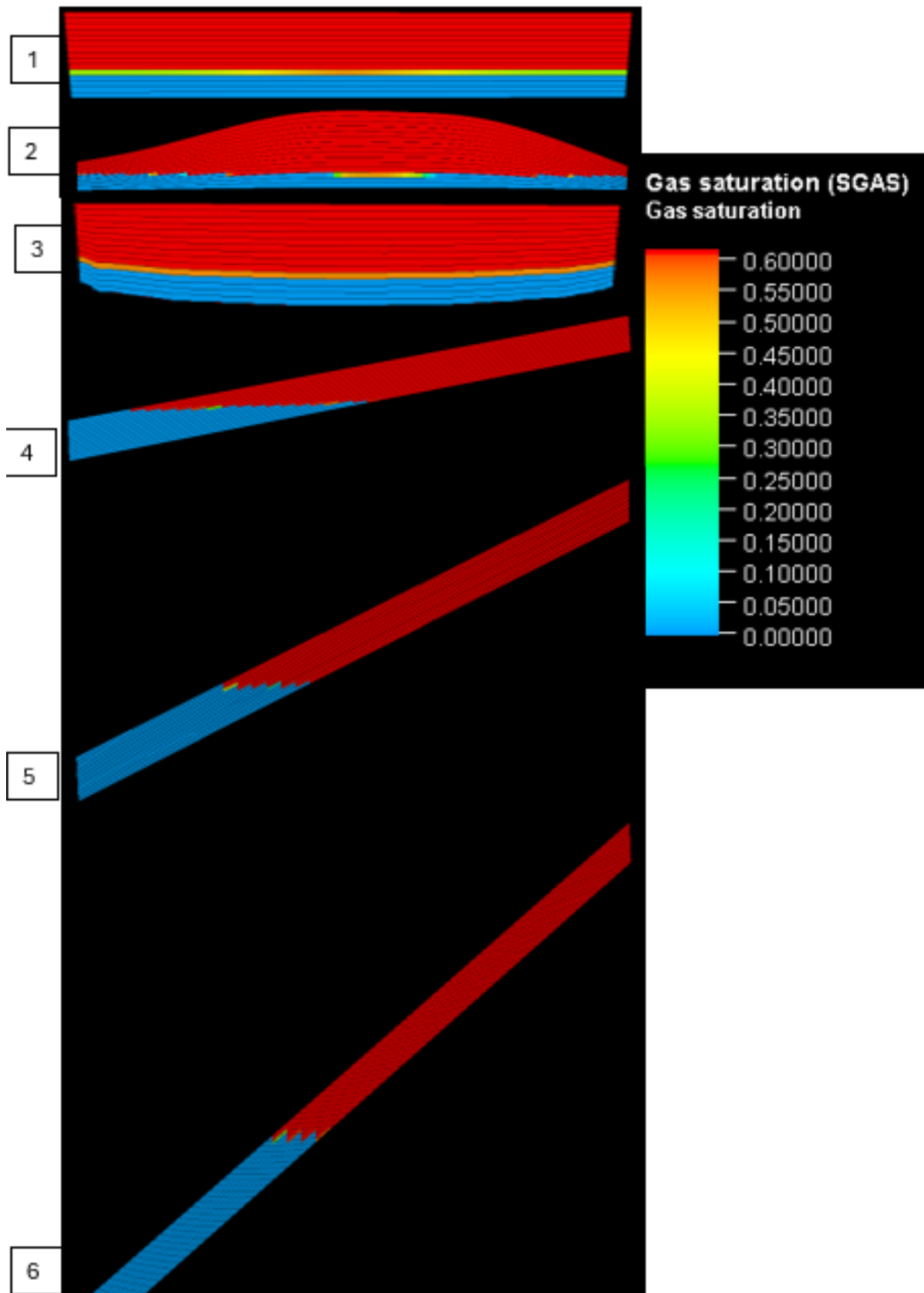
Figure 5-29: Showing Effect of structural shape on plume distribution in the anticline structure after fifty years (year 2950) of post injection, where notation 1 depicts plume distribution in rectangular structure with no dip, 2 depicts plume distribution in anticline structure, 3 depicts plume distribution in radial structure, 4 depicts plume distribution in rectangular structure having 10 dip angle, 5 depicts plume distribution in rectangular structure having 25 dip angle, and 6 depicts plume distribution in rectangular structure having 40 dip angle.

54

In rectangular dip angular structures, gravity segregation is more pronounced making the CO_2 which is less dense than brine to migrate upwards along the dip leading to more efficient displacement of brine in the higher dip structures and creating more efficient storage capacity, this is captured in the Figure 5-26 to Figure 5-29 above where plume distributions seen for different geological shapes at different injection intervals. Though buoyancy flow dominates in all the structures but due to the dip angles, more CO_2 tends to accumulate structurally in dip structures.

Observing from charts in Figure 5-30 and Figure 5-31 below, where the CO_2 capacity versus injection period were plotted for storage region (region-1) and spill regions (region-2) respectively, steeper dip angular structures have more volume of CO_2 accumulated compared to no dip structures. At the base injection rate of 2 million sm3/day, CO_2 plume will not breakthrough to the spill region for 25 degrees and 40 degrees dip rectangular structures throughout the injection period, while it took 800 years of injection for CO_2 plume to reach the spill point in the 10 degrees dip rectangular structure. Anticline structure shows to have shortest time to spill point of 290 years. CO_2 plume reaches the spill point after 540 years in the no dip rectangular structure while circular structure recorded 619 years before plume breakthrough to the spill point. See Table 5-5 for the amount of CO_2 to be stored by each geological structures before the spill point was reach.
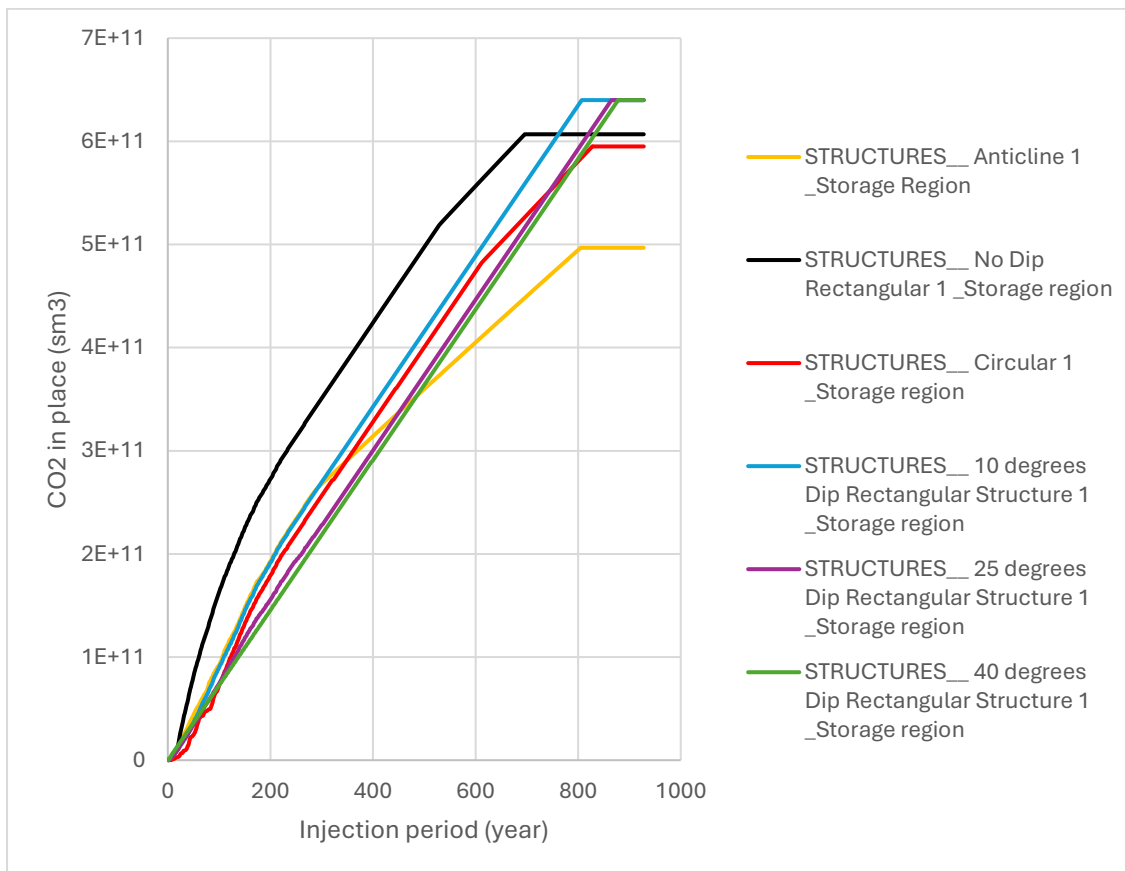
Figure 5-30: Effect of different geological shapes on the Storage capacity of the saline aquifer.
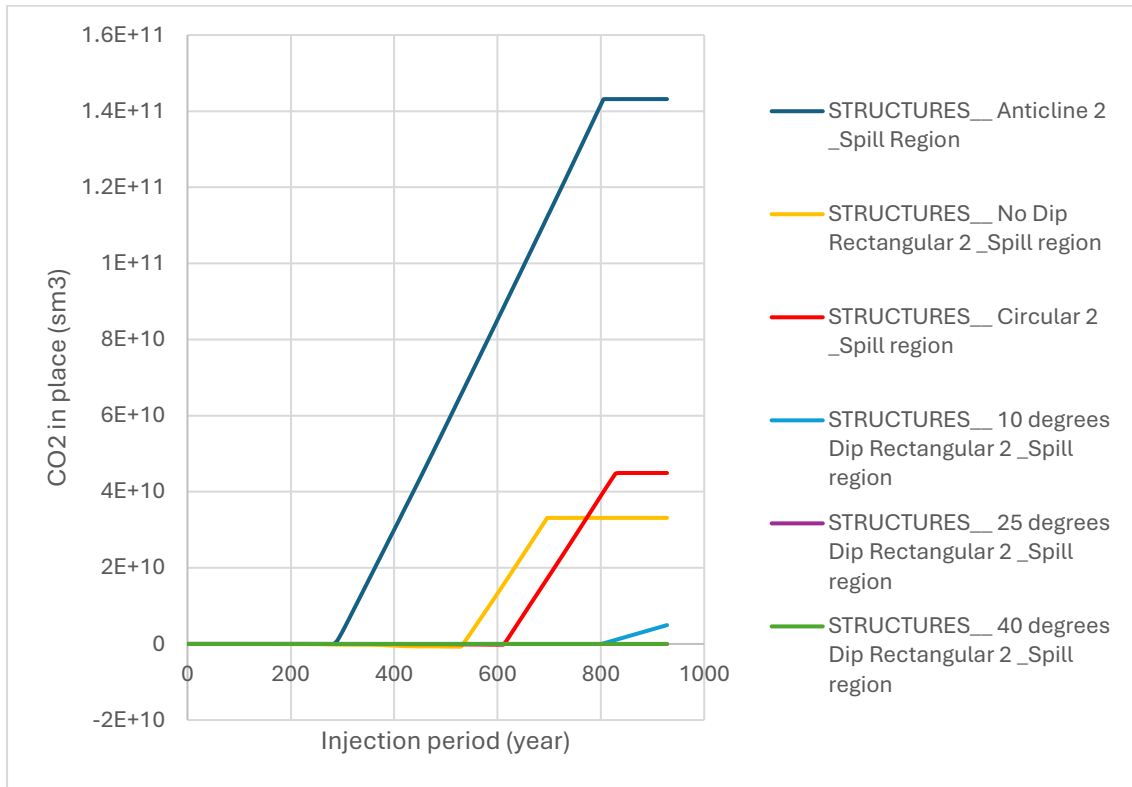
Figure 5-31: Effect of different geological shapes on the Spill time of the saline aquifer.

Table 5-5: Storage capacity of different geological structures before the spill point.

Structure	CO2 storage capacity before spill point	Time to spill point
No dip rectangular	525.220 billion sm3 (983.5 Mt)	2024 - 2564 (540 years)
Anticline	257.866 billion sm3 (482.9 Mt)	2024 - 2314 (290 years)
Circular (radial)	460.216 billion sm3 (861.8 Mt)	2024 - 2643 (619 years)
10 degrees dip rectangular	637.772 billion sm3 (1194.2 Mt)	2024 - 2824 (800 years)
25 degrees dip rectangular	> 639.918 billion sm3 (1198.3 Mt)	> 876 years
40 degrees dip rectangular	> 639.918 billion sm3 (1198.3 Mt)	> 876 years

In conclusion, the reservoir dip angle plays an important role in the preferential rise and lateral spreading of CO_2 plumes during storage. Gravity driven flow and structural trapping will be facilitated by high dip angles but if the spill point is located at higher level (top of structure), the plume will migrate to the spill spot easily. Steeper dips may result in lateral migration with little pore space occupied, but lower dip angles promote a more evenly distributed use of the reservoir and make horizontal migrations worth considering. 40 degrees dip angle used in our model is high for a structural dip, it is theoretical rather than realistic value. Injection and well placement will have to be tailored and monitored according to the dip angle of storage reservoirs, as well as the geology. All the structures have 9.6 billion cubic meters reservoir volume with 67 % of the volume designated for the storage region (Region-1) and the remaining 33 % assigned as the spill region (Region-2). The CO2 injector is placed at the middle of all the models within Region-1 and above Region-2, with 50 m perforation. Anticline structures can be good candidates for structural trapping but because the buoyant CO2 plume spread laterally from the top seal, an anticline with spill points at the upper edges will record a rapid plume breakthrough to such unintended region if compared to when the spill point is at lower edge of the structure

5.6. Analysing the Pressure Build up in the Anticline structure.

To evaluate reservoir pressure buildup in the anticline structure during injection, we assumed a closed boundary, high pressure saline aquifer condition and took effort in ensuring the pressure buildup does not facilitate the seal entry pressure or exceed the fracture pressure by using a well pressure constraint of 500 bars which is ninety percent of the reservoir fracture pressure. Taking this step allowed us to determine the optimal injection rate that will not facilitates the seal entry pressure or exceed the fracture pressure of anticline structure in a normal pressure condition. Also, since our sensitivity studies indicated that porosity has greater impact on the storage capacity, we decided to evaluate how porosity in homogenous reservoir affect the reservoir pressure buildup during injection. Figure 5-32 and Figure 5-33 depict the changes in pressure accumulation over time as the consequences of varying porosity and rates of injection respectively. The plots indicate the pressure build-up in the reservoir during CO2 injection period for arbitrary period of year 2024 to 2950. Starting point represents year 2024 while 950 years indicates year 2950 which is the end of simulation interval.
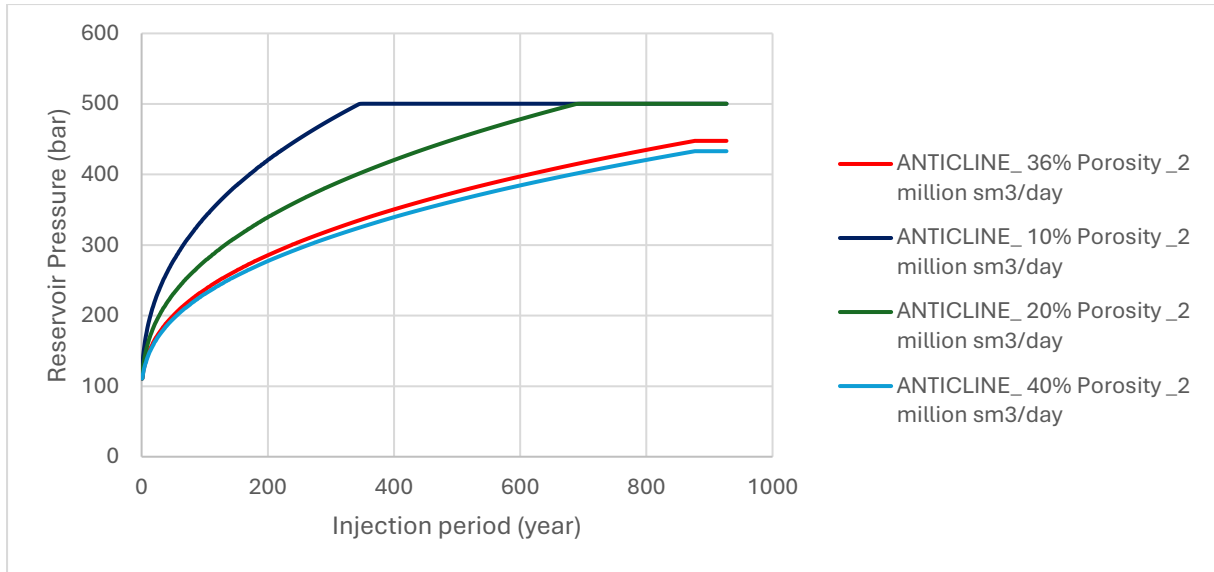
Figure 5-32: Plot of Reservoir pressure versus injection period on different porosity values for a closed boundary condition under 500 bar pressure constraint with constant injection rate of 2 million sm3/day in the anticline saline aquifer.

The higher the porosity, the better for storage capacity and pressure buildup. 40 % porosity value indicated a maximum pressure build-up of 425 bars while 36 % porosity indicated 445 bars of pressure build-up during the whole injection period. In the low porosity value of 10 %, the reservoir pressure reached the constraint value of 500 bars within 350 years of injection while 20 % porosity reached the constraint pressure value within 680 years of injection. This validated the storage capacity evaluation criteria contained in Table 3-4 which stipulates that higher porosity of greater than 10% is better.

To investigate the optimal injection rate suitable not to facilitates the seal entry pressure or exceed the fracture pressure, we kept the base parameters constant while we vary the injection rates.

Out of the four injection rates we considered, we observed that it is only five hundred thousand standard cubic meters per day of CO2 can be injected in the anticline structure to avoid excessive reservoir pressure buildup which can compromise sealing structures in a normal pressure saline aquifer.
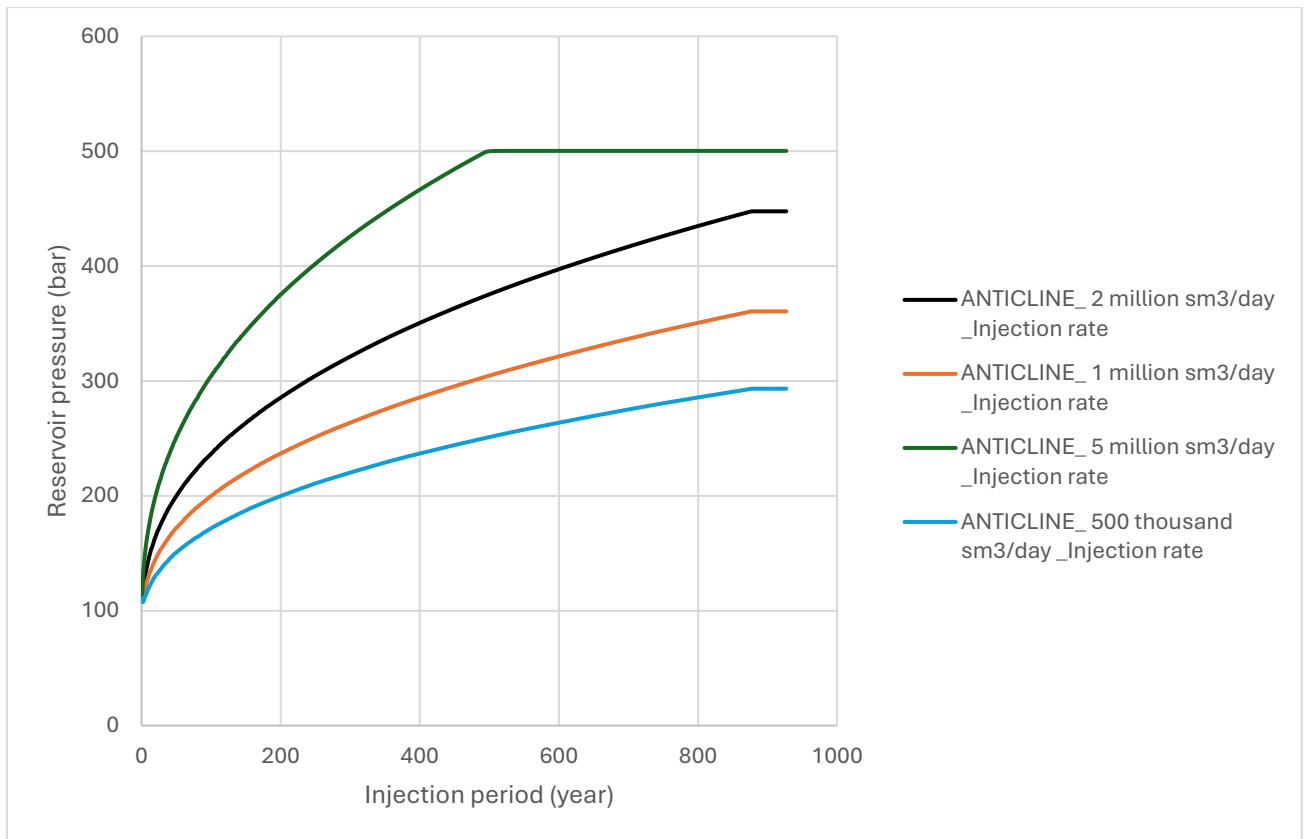
Figure 5-33: Plot of Reservoir pressure versus injection for a closed boundary reservoir conditions under 500 bar pressure constraint with different injection rates in the anticline saline aquifer.

In summary, both pressure and injection rate are important factors affecting dynamic storage capacity of CO2 in saline reservors because the injection rate determines how fast the pressure is buildup in a reservoir. Increased injection rates cause CO2 to enter the reservoir more quickly, causing a faster rise in pressure within the reservoir. On the other hand, slower injection rates cause a slow pressure buildup. Since we have to keep the reservoir at a pressure below it fracture pressure, there will be interplay on the capacity of CO2 to be stored at a given time in the aquifer. In this context, proper monitoring and management of these parameters ensure optimum storage capacity, reservoir integrity are paramount among other benefits for handling of CO2 storage capacity for a good reservoir containment security in the successful implementation of carbon sequestration projects.

6. Conclusion and Recommendations

These sensitivity tests offer useful insights for evaluating dynamic CO_2 storage capacity before spill sites. The recommendation for optimising dynamic CO2 storage capacity, findings of the many parameters assessed, and the conclusion are presented in this chapter.

6.1. Result summary and Conclusion

- Porosity:

Results: A high porosity reservoir provides more pore space hence it offered greater potential for CO2 storage. This in turn enhances CO_2 plume migration and distribution efficiency with improved injection stability that has broader immediate-storage tendencies as well as an advantageous long-term storage capacity eco-profile. The storage space of low porosity reservoirs is small. Lower pore space in closed boundary formation led to lower cumulative CO_2 injection rates, increase required injection pressures and risked exceeding assumed fracture pressure.

- Permeability:

Results: Good permeability aids in rapid addition of CO2 and spreading it out over larger areas by the reservoir. While this allows for a more optimal use of the available storage capacity, it also reduced breakthrough time to the spill point at constant injection rate. The low permeability where CO_2 is stored also slows the flow of CO_2; as a result, it requires higher injection pressures and the time for plume migration increases. This can be used to provide more stable trapping over time, although it requires very good control otherwise the increased pressure build-up and correspondingly hazards.

- Injection Rate:

Results: Higher injection rates decrease the fill up time of storage region. Plume was observed to spread horizontal away from the injector before gravity flow dominated.The vertical to horizontal permeability ratio (k_v/k_h):

The ratio of vertical to horizontal permeability (k_v/k_h) affects the CO2 migration pattern and can significantly affect the shape of the plume and influences capture by trapping systems.

Results: A high (k_v/k_h) ratio means higher value of vertical permeability, which made the CO_2 plume move upward faster till it reaches the top seal. This enhanced structural trapping and led to concentrate plumes from top seal and laterally displacing brine top-down while a low (k_v/k_h) ratio means reduced vertical permeability. Lower values decrease vertical migration and causes a lateral spreading of the CO_2 plume before reaching the top seal. The structurally trapping of higher values are more pronounced that the lower values.

- Geological Shape:

Result: The structural traps as anticlines and dip-traps which useful to contain the CO_2 plume. It facilitates structural trapping as CO_2 migrates to the top of these structures where they naturally accumulate at higher elevations.

In summary, sensitivity studies on porosity, permeability and (k_v/k_h) show that the dynamic CO_2 storage capacity is very sensitive to these parameters together with injection rate, geological shapes. This porous nature often maximizes storage volume and efficiency but requires careful pressure management. These are used to define the optimal injection rates, a compromise between efficiency and safety - but also such as Kv/Kh ratio that is decisive for controlling vertical or horizontal plume which then affect trapping. The geological form help containment and detectable shape of plumes during distribution but need wise knowledge to optimum storage, this is contrast to the static CO2 dynamic capacity evaluation which does not take into account the shape of the storage structure in determining the storage capacity as expressed in the Equation (3.1(3.4 of volumetric and compressibility static approach to CO2 capacity calculation.

Conclusion: In this thesis we have shown that dynamic CO_2 storage capacity in saline aquifers is highly dependent on the most important reservoir parameters. Greater porosity and permeability provide for higher storage capacity and plume distribution at the cost of appropriate pressure management to prevent overpressure with potential formation damage. Vertical and lateral plume behaviour and trapping efficiency are directly influenced by the CO_2 migration patterns, which in turn is largely controlled by the kv/kh ratio An optimal injection rate is necessary to balance storage efficiency and safety, without causing unacceptable pressure build-up while maintaining efficient usage of reservoir capacity. It is necessary that geological structures like anticlines provide a seal for the CO_2 which allows us to take advantage of structural trapping.

This requires site-specific CO2 geological storage injection protocols to be coupled with detailed monitoring plans in order for the sequestration process to occur both efficiently and securely. Follow-up work is needed to fine-tune these parameters and evaluate more complicated geologic settings with greater precision, in order to improve carbon capture and storage predictions and maximize the practice. This study provides insights for enhancing our understanding of the CO_2 sequestration process and reveals new challenges that have to be taken into consideration in reservoir characterization ans management strategies.

6.2. Recommendations to enhance the accuracy and applicability of dynamic CO2 storage capacity.

These findings combined with observation in this thesis lead to the following recommendations for future research, so as deepen understanding of dynamic CO2 storage capacity in saline reservoirs and possibility oil and gas reservoir.

- **Examining Spill Point Regions:** Further analyses of various spill point regions as a way to generate new knowledge on the dynamic CO2 storage capacity. While in some situations i.e. uncertain spill points, this variability will allow us

to investigate the influence of where a CO2 plume spills on storage potential and capacity.

- **Research CO2 Enhanced Oil Recovery (EOR) Prospects:** Expand the evaluation to incorporate potential of using a different technology called Carbon Dioxide enhancement oil recovery- EOR that not only stores carbon in reservoirs but also improves economic and energy return if enhanced oil encompasses significant untouched areas on reservoir. As the gravity flow plays impact in plumes distribution during injection, one possible approach could be to use horizontal well as oil producer and locate it at lower level of reservoir; then place CO2 injector above this producing point. This introduces a buoyancy-driven process whereby CO2 can accumulate in the top-most part of the reservoir layer by driving oil down and into producer well. In parallel, the producer well serves as a pressure relief to protect the overlying cap rock and confining layer from puncturing due to reservoir over pressurisation.

- **Repeat the second recommendations:** This time exclude the effect of CO2 dissolution in oil and assume oil as brine to relate the studies to saline aquifer conditions.

- **Complex Geological Features:** Though this study demonstrates the dynamic CO2 storage capacity from saline aquifers by BOM in Petrel, there are several other limitations that need to be addressed in future studies. The most debilitating limitation of the study is that it does not account for more intricate geological phenomena like faulting, fractures and reservoir heterogeneity. More importantly, these features can have strong impacts on CO2 storage patterns and were neglected in this study. Excluding such complex geological features in dynamic models may compromise final conclusions about accuracy and reliability. Actual reservoirs are seldom homogenous and simple; diverse geological discontinuity and heterogeneities can distort fluid flow under various conditions. Failing to account for these complexities may result in an over- or under-prediction of the CO2 storage capacities and could result a biased evolution of plume migration trends. Reservoir Heterogeneity in porosity, permeability and other reservoir properties also plays a very significant role when accounting for CO2 storage. Modelling these heterogeneities could improve the estimates of CO2 storage capacity and plume distribution in both reservoir performance simulation as well as risk-assessment. It is important to include more complicated geological features in the model for a better simulation of CO2 storage behaviour, similar to those occurring within real reservoirs. Further studies need to target these areas if CO2 storage models are meant to be accurate and applicable for diverse geologies.

- **Carryout comparative analysis on the static and dynamic CO2 storage capacity:** Comparison of static and dynamic CO2 storage capacity can

identify major methodological differences as well as potential knowledge gaps. The static approach looks at initial conditions without any kind of fluid dynamics and pressure changes over that long period of geologic time. These more advanced dynamic CO2 storage approach is able to include these elements, and therefore present a higher description of how CO2 will behave in the subsurface. Through such comparisons researchers can detect important variables and circumstances in which one or the other of these models performs better, providing guidance for where improvements in dynamic modelling is required. This would allow a comparative analysis to isolate the conditions and parameters that have reasonably large effects on storage predictions. This knowledge can thus contribute to improve the robustness and reliability of dynamic models. Critical evaluation of factors related to porosity, permeability pressure and fluid properties have therefore substantial value in refining this dynamic approach.

- **Model creation:** Developing dynamic models that simulates how porosity and permeability is changing over time due to the chemical reactions between CO2, brine and rock minerals. This will help with forecasting long-term storage capacity and stability.

Appropriate consideration of these recommendations in future research may help to increase the accuracy and reliability of dynamic CO2 storage capacity assessments, furthering successful implementation for cost-effective carbon sequestration strategies as well as enhanced oil recovery techniques.

References

Alnes, H., Eiken, O., & Stenvold, T. (2008). Monitoring gas production and C O2 injection at the Sleipner field using time-lapse gravimetry. *GEOPHYSICS*, *73*(6), WA155–WA161. https://doi.org/10.1190/1.2991119

AlRassas, A. M., Vo Thanh, H., Ren, S., Sun, R., Le Nguyen Hai, N., & Lee, K.-K. (2021). Integrated static modeling and dynamic simulation framework for CO2 storage capacity in Upper Qishn Clastics, S1A reservoir, Yemen. *Geomechanics and Geophysics for Geo-Energy and Geo-Resources*, *8*(1), 2. https://doi.org/10.1007/s40948-021-00305-x

Anthonsen, K. L., Aagaard, P., Bergmo, P. E. S., Gislason, S. R., Lothe, A. E., Mortensen, G. M., & Snæbjörnsdóttir, S. Ó. (2014). Characterisation and Selection of the Most Prospective CO2 Storage Sites in the Nordic Region. *Energy Procedia*, *63*, 4884–4896. https://doi.org/10.1016/j.egypro.2014.11.519

Bachu, S., Bonijoly, D., Bradshaw, J., Burruss, R., Holloway, S., Christensen, N. P., & Mathiassen, O. M. (2007). CO2 storage capacity estimation: Methodology and gaps. *International Journal of Greenhouse Gas Control*, *1*(4), 430–443. https://doi.org/10.1016/S1750-5836(07)00086-2

Bachu, S., Gunter, W. D., & Perkins, E. H. (1994). Aquifer disposal of CO2: Hydrodynamic and mineral trapping. *Energy Conversion and Management*, *35*(4), 269–279. https://doi.org/10.1016/0196-8904(94)90060-4

Benson, S. M., & Cole, D. R. (2008). CO2 Sequestration in Deep Sedimentary Formations. *Elements*, *4*(5), 325–331. https://doi.org/10.2113/gselements.4.5.325

Bickle, M., Chadwick, A., Huppert, H. E., Hallworth, M., & Lyle, S. (2007). Modelling carbon dioxide accumulation at Sleipner: Implications for underground carbon storage. *Earth and Planetary Science Letters*, *255*(1–2), 164–176. https://doi.org/10.1016/j.epsl.2006.12.013

Carbon Capture and Sequestration Technologies @ MIT. (n.d.). Retrieved 13 May 2024, from https://sequestration.mit.edu/tools/projects/sleipner.html

Chadwick, R. A., Kirby, G. A., Holloway, S., Gregersen, U., Johannessen, P. N., Zweigel, P., & Arts, R. (2002). *Saline Aquifer CO2 Storage (SACS2). Final report, geological characterisation of the Utsira Sand reservoir and caprocks (Work Area 1)* [Publication - Report]. British Geological Survey. https://nora.nerc.ac.uk/id/eprint/511461/

Chang, Y.-B., Coats, B. K., & Nolen, J. S. (1998). A Compositional Model for CO2 Floods Including CO2 Solubility in Water. *SPE Reservoir Evaluation & Engineering*, *1*(02), 155–160. https://doi.org/10.2118/35164-PA

Class, H., Ebigbo, A., Helmig, R., Dahle, H. K., Nordbotten, J. M., Celia, M. A., Audigane, P., Darcis, M., Ennis-King, J., Fan, Y., Flemisch, B., Gasda, S. E., Jin, M., Krug, S., Labregere, D., Naderi Beni, A., Pawar, R. J., Sbai, A., Thomas, S. G., ... Wei, L. (2009). A benchmark study on problems related to CO2 storage in geologic formations.

Computational Geosciences, *13*(4), 409–434. https://doi.org/10.1007/s10596-009-9146-x

Frailey, S. (2009). Methods for Estimating CO(2) Storage in Saline Reservoirs. *Energy Procedia*, *1*, 2769–2776. https://doi.org/10.1016/j.egypro.2009.02.048

Frailey, S., & Finley, R. (2009). Classification of CO 2 Geologic Storage: Resource and Capacity. *Energy Procedia*, *1*, 2623–2630. https://doi.org/10.1016/j.egypro.2009.02.029

Gibson-Poole, C. M., Svendsen, L., Underschultz, J., Watson, M. N., Ennis-King, J., Van Ruth, P. J., Nelson, E. J., Daniel, R. F., & Cinar, Y. (2008). Site characterisation of a basin-scale CO2 geological storage system: Gippsland Basin, southeast Australia. *Environmental Geology*, *54*(8), 1583–1606. https://doi.org/10.1007/s00254-007-0941-1

Gopalakrishnan, M., Punitha, V., & Saravanan, D. (2019). 8—Water conservation in textile wet processing. In S. S. Muthu (Ed.), *Water in Textiles and Fashion* (pp. 135–153). Woodhead Publishing. https://doi.org/10.1016/B978-0-08-102633-5.00008-7

Gunter, W. D., Bachu, S., & Benson, S. (2004). The role of hydrogeological and geochemical trapping in sedimentary basins for secure geological storage of carbon dioxide. *Geological Society, London, Special Publications*, *233*(1), 129–145. https://doi.org/10.1144/GSL.SP.2004.233.01.09

Hansen, H., Eiken, O., & Aasum, T. O. (2005). Tracing the Path of Carbon Dioxide From a Gas/Condensate Reservoir, Through an Amine Plant and Back Into a Subsurface Aquifer – Case Study: The Sleipner Area, Norwegian North Sea. *All Days*, SPE-96742-MS. https://doi.org/10.2118/96742-MS

Hatzignatiou, D. G., Riis, F., Berenblyum, R., Hladik, V., Lojka, R., & Francu, J. (2011). Screening and evaluation of a saline aquifer for CO2 storage: Central Bohemian Basin, Czech Republic. *International Journal of Greenhouse Gas Control*, *5*(6), 1429–1442. https://doi.org/10.1016/j.ijggc.2011.07.013

INSTITUTE OF MARINE RESEARCH (NORWAY), 11.05.2010. (n.d.). Havforskningsinstituttet. Retrieved 26 June 2024, from https://www.hi.no/hi/nettrapporter

Juanes, R., Spiteri, E. J., Orr, F. M., & Blunt, M. J. (2006). Impact of relative permeability hysteresis on geological CO 2 storage. *Water Resources Research*, *42*(12), 2005WR004806. https://doi.org/10.1029/2005WR004806

Kumar, A., Ozah, R., Noh, M., Pope, G. A., Bryant, S., Sepehrnoori, K., & Lake, L. W. (2005). Reservoir Simulation of CO2 Storage in Deep Saline Aquifers. *SPE Journal*, *10*(03), 336–348. https://doi.org/10.2118/89343-PA

Lindeberg, E. (n.d.). *Saline Aquifer CO2 Storage*.

Lindeberg, E. (2000). *Saline Aquifer CO2 Storage*. https://www.sintef.no/globalassets/project/ik23430000-sacs/formal-reports/sacs1_wa2_finalreport_longnew.pdf

Lindeberg, E., & Wessel-Berg, D. (1997). Vertical convection in an aquifer column under a gas cap of CO2. *Energy Conversion and Management*, *38*, S229–S234. https://doi.org/10.1016/S0196-8904(96)00274-9

Lindgren, H., & Springer, N. (2006). *Springer: Caprock properties of the Nordland Shale... - Google Scholar*. https://scholar.google.com/scholar_lookup?title=Caprock%20properties%20of%20the%20Nordland%20shale%20recovered%20from%20the%2015%2F9-A11%20well%2C%20the%20Sleipner%20area&author=N.%20Springer&author=H.%20Lindgren&publication_year=2006&journal=GHGT-8%20Abstract&volume=&pages=

Lothe, A., & Bergmo, P. (2014). Characterisation and Selection of the Most Prospective CO2 Storage Sites in the Nordic Region. *Energy Procedia*. https://www.academia.edu/20887249/Characterisation_and_Selection_of_the_Most_Prospective_CO2_Storage_Sites_in_the_Nordic_Region

Metz, B., Davidson, O., de Coninck, H., Loos, M., & Meyer, L. (2005). IPCC Special Report on Carbon dioxide Capture and Storage. *Policy Stud*.

Metz, B. & Intergovernmental Panel on Climate Change (Eds.). (2005). *IPCC special report on carbon dioxide capture and storage* (1. publ). Cambridge Univ. Press.

Muggeridge, A., Abacioglu, Y., England, W., & Smalley, C. (2004). Dissipation of anomalous pressures in the subsurface. *Journal of Geophysical Research: Solid Earth*, *109*(B11), 2003JB002922. https://doi.org/10.1029/2003JB002922

National Energy Technology Laboratory—Carbon Storage FAQs. (n.d.). Netl.Doe.Gov. Retrieved 26 June 2024, from https://netl.doe.gov/carbon-management/carbon-storage/faqs/carbon-storage-faqs

Netto, S. L. A., Schiozer, D. J., Ligero, E. L., & Maschio, C. (2003). History Matching Using Uncertainty Analysis. *Canadian International Petroleum Conference*. Canadian International Petroleum Conference, Calgary, Alberta. https://doi.org/10.2118/2003-145

Nordbotten, J. M., Celia, M. A., & Bachu, S. (2005). Injection and Storage of CO2 in Deep Saline Aquifers: Analytical Solution for CO2 Plume Evolution During Injection. *Transport in Porous Media*, *58*(3), 339–360. https://doi.org/10.1007/s11242-004-0670-9

Oldenburg, C. M., Cihan, A., Zhou, Q., Fairweather, S., & Spangler, L. H. (2014). Delineating Area of Review in a System with Pre-injection Relative Overpressure. *Energy Procedia*, *63*, 3715–3722. https://doi.org/10.1016/j.egypro.2014.11.400

Pickup, G. E. (2013). CO 2 storage capacity calculation using static and dynamic modelling. In *Geological Storage of Carbon Dioxide (CO2)* (pp. 26–44). Elsevier. https://doi.org/10.1533/9780857097279.1.26

Pruess, K., & Zhang, K. (2008). *Numerical Modeling Studies of The Dissolution-Diffusion-Convection ProcessDuring CO2 Storage in Saline Aquifers* (LBNL-1243E, 944124; p. LBNL-1243E, 944124). https://doi.org/10.2172/944124

Ringrose, P., Nordahl, K., & Wen, R. (2005). Vertical permeability estimation in heterolithic tidal deltaic sandstones. *Petroleum Geoscience*, *11*(1), 29–36. https://doi.org/10.1144/1354-079303-614

Rochelle, C. A., Czernichowski-Lauriol, I., & Milodowski, A. E. (2004). The impact of chemical reactions on CO_2 storage in geological formations: A brief review. *Geological Society, London, Special Publications*, *233*(1), 87–106. https://doi.org/10.1144/GSL.SP.2004.233.01.07

Singh, V., Cavanagh, A., Hansen, H., Nazarian, B., Iding, M., & Ringrose, P. (2010). Reservoir Modeling of CO2 Plume Behavior Calibrated Against Monitoring Data From Sleipner, Norway. *All Days*, SPE-134891-MS. https://doi.org/10.2118/134891-MS

Suekane, T., Nobuso, T., Hirai, S., & Kiyota, M. (2008). Geological storage of carbon dioxide by residual gas and solubility trapping. *International Journal of Greenhouse Gas Control*, *2*(1), 58–64. https://doi.org/10.1016/S1750-5836(07)00096-5

Tucker, M. E., & Wright, V. P. (1990). *Carbonate Sedimentology* (1st ed.). Wiley. https://doi.org/10.1002/9781444314175

Voormeij, D., & Simandl, G. (2004). Geological, Ocean, and Mineral CO2 Sequestration Options: A Technical Review. *Geoscience Canada*, *31*(1), 11–22.

Weibel, G. L., & Ober, C. K. (2003). An overview of supercritical CO2 applications in microelectronics processing. *Microelectronic Engineering*, *65*(1), 145–152. https://doi.org/10.1016/S0167-9317(02)00747-5

Yang, Y., & Aplin, A. C. (2004). Definition and practical application of mudstone porosity–effective stress relationships. *Petroleum Geoscience*, *10*(2), 153–162. https://doi.org/10.1144/1354-079302-567

Zhang, D., & Song, J. (2014). Mechanisms for Geological Carbon Sequestration. *Procedia IUTAM*, *10*, 319–327. https://doi.org/10.1016/j.piutam.2014.01.027

Zhou, Q., Birkholzer, J., Rutqvist, J., & Tsang, C. (2007). Sensitivity study of CO2 storage capacity in brine aquifers withclosed boundaries: Dependence on hydrogeologic properties. *Sixth Annual Conference on Carbon Capture and Sequestration - DOE/NETL, May*.

Zhou, Q., Birkholzer, J. T., Tsang, C.-F., & Rutqvist, J. (2008). A method for quick assessment of CO2 storage capacity in closed and semi-closed saline formations. *International Journal of Greenhouse Gas Control*, *2*(4), 626–639. https://doi.org/10.1016/j.ijggc.2008.02.004

Zweigel, P., Arts, R., Lothe, A. E., & Lindeberg, E. B. G. (2004). Reservoir geology of the Utsira Formation at the first industrial-scale underground CO_2 storage site (Sleipner

area, North Sea). *Geological Society, London, Special Publications*, *233*(1), 165–180. https://doi.org/10.1144/GSL.SP.2004.233.01.11

ZWEIGEL, P., HAMBORG, M., Arts, R., Lothe, A., Sylta, Ø., & Tømmerås, A. (2000). *Prediction of migration of CO2 injected into an underground depository: Reservoir geology and migration modelling in the Sleipner case (North Sea)*.

Appendix

Appendix A1 – Sleipner CO2 storage site layer 9 model input parameters assumptions modified from (Singh et al., 2010).

Formation properties	Units	Assumed reference case properties	Range	References and comments
Seabed temperature	C	7	6.1 – 7.2	(*INSTITUTE OF MARINE RESEARCH (NORWAY), 11.05.2010, n.d.*)
Geothermal gradient	C/km	35.6		(Lindeberg, 2000)
Hydrostatic gradient	Mpa/km			Assumed hydrostatic equilibrium
Lithostatic gradient	MPa/km	17		Assumed lithostatic gradient based on typical values (poro=0.36, rho=2700 kg/m3)
Total Utsira Fm area	Km2	26100		(Chadwick et al., 2002)
Total reservoir thickness	m	255	50 - 300	Assumed value derived from well log 15/9-A16 (CO2 injector); Range:(ZWEIGEL et al., 2000)
L9 model area	Km2	18		Defined as model area (3 x 6 km)
Top L9 depth	m TVD SS	817.3	802.2 – 840.5	Defined by seismic depth map
L9 thickness	m	11.3	3.5 – 26.3	Defined by seismic depth map

Intrashale thickness	m	6.5		Intrashale between layer 8 and 9
Caprock porosity	%	35	34 - 36	(Lindgren & Springer, 2006)
Caprock permeability	md	0.0010	0.00075 – 0.0015	(Lindgren & Springer, 2006)
Caprock threshold pressure	MPa	1.7		(Lindgren & Springer, 2006)
Utsira porosity	%	36	27 - 40	(Lothe and Zweigel, 1999, Holloway et al. 2000.)
Utsira permeability	md	2000	1100 - 5000	(Lindeberg et al. 2000)
Utsira anisotropy	[/]	0.1		Assumed based on general petroleum reservoir analogue data, e.g. (Ringrose et al., 2005)
Shale porosity	%	34	31 - 38	(Yang & Aplin, 2004; Zweigel et al., 2004) Porosity in shales is very uncertain and controlled by clay content and effective stress.
Shale permeability	md	0.0010	0.00075 – 0.0015	Assume same as caprock but has a large uncertainty, Springer and (Lindeberg, n.d.)
Assumed coordinates of L9 injection point	[/]	x: 438516; y: 64712e+06		Z: bottom of layer 8 (L89 model) or layer 9 (L9 model)
Injection perforation length	m	38		(Hansen et al., 2005)
Depth to top perforation	m TVD MSL	1010.5		(Hansen et al., 2005) Interval is

				1010.5 – 1013 m TVD MSL
Critical gas saturation	[/]	0.02		
Connate water saturation	[/]	0.89		
Residual gas saturation	[/]	0.21		
Interfacial tension factor	[/]	0.0625		IFT factor at the top of the model. Fluid conversion factor = IFT (hw) x Cos / IFT(ma)*cos, where hw is hydrocarbon water interface, and is wetting angle for the respective systems
CO2 viscosity	mPas	6.00E-02		
CO2 density	Kg/m3	760		(Alnes et al., 2008)
Porewater salinity	ppm	33500		
Porewater viscosity	Pas	8.00E-04	0.00079 – 0.000875	CREWES fluid property calculator. Assumed salinity of 33500 ppm and pressure of 8.1 MPa. Temperature taken from PVT range: 31 and 37 deg C
Porewater density	Kg/m3	1020		(Bickle et al., 2007)

Appendix A2 - Corey functions and end points fitted to laboratory measurements used in the simulation cases extracted from (Singh et al., 2010).

Water relative permeability end point: 0.54

CO2 relative permeability end point: 0.75

Critical water saturation: 0.386

Connate water saturation: 0.11

Critical CO2 saturation: 0.02

Connate CO2 saturation: 0.0

Water Corey exponent: 2.8
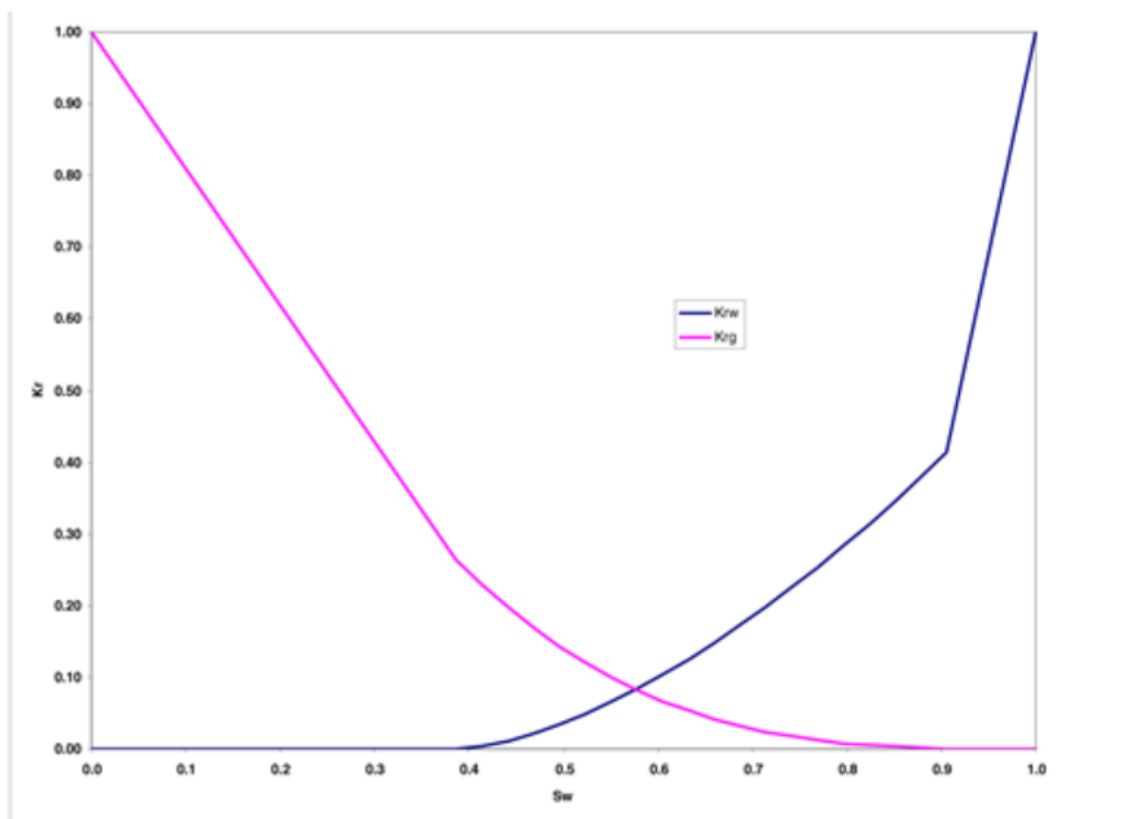
CO2 Corey exponent: 2.8

Figure A2 – Corey fit curves to the laboratory relative measurements (Singh et al., 2010)

Appendix A3 – Conversion factors.

1 year = 365 days.

1000 kg = 1 tonne

534 sm3 = 1 tonne

1E+06 tonnes = 1 million tonnes.

1 bar = 1E+05 Pa

1 cp = 1E-03 Pa.s

1 dyne = 1E-02 mN

2.831 ft3 = 1E-02 m3

6.895 psi = 1E+00 kPa